POLITECNICO
MILANO 1863

School of Civil, Environmental and Land Management Engineering
Master of Science in Environmental and Land Planning Engineering

# Strategic dam planning in the Mekong River Basin accounting for GHGs emissions and river sediment connectivity

Master Thesis by:
**Federico Sala**
Matr. 953288

Advisor:
**Prof. Andrea Francesco Castelletti**

Co-Advisor:
**Dr. Rafael J. P. Schmitt**
**Dr. Marco Tangi**

Academic Year 2020 – 2021

# Ringraziamenti

Con questa tesi si concludono questi lunghi anni di università al Politecnico di Milano, tappa fondamentale della mia vita in cui ho imparato tanto e sono cresciuto molto, sia come ingegnere, che come uomo.

Vorrei innanzitutto ringraziare il Professor Castelletti, Marco Tangi e Rafael Schmitt, che hanno reso possibile la realizzazione di questa tesi, aiutandomi e guidandomi durante la sua realizzazione.

Ringrazio anche tutti i professori e compagni di università, con cui ho condiviso questo faticoso ma splendido viaggio.

Ringrazio tutta la mia famiglia e tutti i miei amici, per l'affetto e il supporto che mi hanno sempre dimostrato.

Infine, ringrazio Sara, mia compagna di vita da ormai più di nove anni, che è sempre stata al mio fianco e non ha mai smesso di sostenermi.

# Abstract

In a global context in which the need for contrasting Climate Change is increasingly evident, hydropower represents one of the most important alternatives to electricity generation by fossil fuels. We analyzed the case study of the Mekong River Basin, denominated the "Battery of South-East Asia" for its large hydropower potential. Due to its relatively recent hydropower development, the Mekong River Basin is characterized by problems of data availability and high uncertainty. We developed a framework for strategic dam planning in which we used the "Borg" Multi-Objective Evolutionary Algorithm to solve a 3-objective optimization problem: maximize hydropower production, maximize sediment supply to the delta, and minimize GHGs emissions from reservoirs. We used the "CASCADE" model to simulate the sediment transport within the basin and empirical formulas to estimate the GHGs emissions of each dam. To deal with uncertainty and seek robust solutions, we performed a Sensitivity Analysis on GHGs emissions and river sediment connectivity input data. We could identify some regions characterized by robust results (e.g., the Lancang River Basin and the Tonle Sap Basin), and some regions with results affected by high uncertainty (e.g., the 3S Basin), in which there is an urgent need to increase the efforts on data collection and carry out in-depth researches. The goal of this work of thesis consists in giving a contribution to the scientific literature regarding the topic of strategic dam planning, essential to allow sustainable hydropower development. The novelty of our approach consists in considering simultaneously hydropower production, river sediment connectivity, and GHGs emissions, to better understand the cumulative impacts of dam construction at a basin scale in a context characterized by high uncertainty, such as the Mekong River Basin.

# Riassunto

In un contesto globale in cui la necessità di contrastare i cambiamenti climatici è sempre più evidente, l'energia idroelettrica rappresenta una delle più importanti alternative alla produzione di energia elettrica basata sui combustibili fossili. Abbiamo analizzato il caso di studio del bacino del fiume Mekong, denominato la "Batteria del sud-est asiatico" per il suo grande potenziale idroelettrico. A causa del suo relativamente recente sviluppo idroelettrico, il bacino del fiume Mekong è caratterizzato da problemi di disponibilità dei dati ed elevata incertezza. Abbiamo sviluppato un framework per la pianificazione strategica delle dighe in cui abbiamo usato l'algoritmo evolutivo multi-obiettivo "Borg" per risolvere un problema di ottimizzazione a tre obiettivi: massimizzare la produzione idroelettrica, massimizzare l'apporto di sedimenti al delta e minimizzare le emissioni di gas serra. Abbiamo utilizzato il modello "CASCADE" per simulare il trasporto dei sedimenti all'interno del bacino e formule empiriche per stimare le emissioni di gas serra di ogni diga. Per affrontare l'incertezza e cercare soluzioni robuste, abbiamo eseguito un'analisi di sensitività sui dati riguardanti le emissioni di gas serra e i sedimenti fluviali. Abbiamo potuto individuare alcune regioni caratterizzate da risultati robusti (ad esempio, il bacino del fiume Lancang e il bacino del Tonle Sap) e alcune regioni con risultati caratterizzati da un'elevata incertezza (ad esempio, il bacino 3S), in cui vi è l'urgente necessità di aumentare gli sforzi per la raccolta dei dati ed effettuare ricerche approfondite. L'obiettivo di questa tesi consiste nel dare un contributo alla letteratura scientifica sul tema della pianificazione strategica delle dighe, essenziale per consentire uno sviluppo idroelettrico sostenibile. La novità del nostro approccio consiste nel considerare contemporaneamente le emissioni di gas serra e la connettività dei sedimenti fluviali, al fine di comprendere meglio gli impatti cumulativi della costruzione di dighe alla scala di bacino in un contesto caratterizzato da elevata incertezza, come quello del fiume Mekong.

# Contents


**1 Introduction** **1**

1.1 Climate Change and renewable energy . . . . . 1

1.2 Hydroelectric power . . . . . 2

1.2.1 Dams impacts . . . . . 4

1.2.2 Sediment trapping process, consequences and possible solutions . . . . . 7

1.2.3 GHGs emissions from reservoirs . . . . . 14

1.3 Strategic dam planning . . . . . 21

1.4 Motivation and goals of the study . . . . . 24

**2 Case Study: the Mekong River Basin** **27**

2.1 Location and geography . . . . . 27

2.2 Natural resources and biodiversity . . . . . 31

2.3 Geopolitical situation and the Mekong River Commission . . . . 35

2.4 Hydropower development in the Mekong River Basin . . . . . 37

2.5 Previous studies on dam sediment trapping and GHGs emissions 40

**3 Materials and Methods** **45**

3.1 Available dam data . . . . . 45

3.2 GHGs emissions estimates . . . . . 47

3.2.1 Time horizon of the analysis . . . . . 48

3.3 River sediment connectivity estimation . . . . . 49

3.3.1 CASCADE model and framework . . . . . 49

3.3.2 CASCADE and sediment available data . . . . . 51

3.4 The optimization problem: finding Pareto Optimal dam portfolios 53

3.4.1 Indicator for sediment supply to the delta . . . . . 54

3.4.2 Indicator for hydropower production . . . . . 55

3.4.3 Indicator for GHGs emissions from reservoirs . . . . . 55

3.5 Borg Multi-Objective Evolutionary Algorithm . . . . . 56

3.5.1 Borg parameters setting . . . . . 61

3.5.2 Borg simulation modes . . . . . 62
3.6 Sensitivity Analysis on GHGs emissions and sediment connectivity parameters . . . . . 63
3.6.1 Perturbing GHGs emissions . . . . . 64
3.6.2 Perturbing sediment connectivity parameters . . . . . 67
3.6.3 Statistics to elaborate Sensitivity Analysis outcomes . . . . 69

**4 Results** **71**
4.1 Pareto-Optimal dam portfolios . . . . . 71
4.2 Sensitivity Analysis on GHGs emissions . . . . . 73
4.2.1 "Dams with High Uncertainty" . . . . . 78
4.3 Sensitivity Analysis on GHGs emissions and sediment connectivity parameters . . . . . 79
4.3.1 "Dams with Very High Uncertainty" . . . . . 81
4.4 "Lost Opportunities" . . . . . 82
4.5 Current basin dam portfolio and the actual planning possibilities 84

**5 Discussion and conclusions** **89**
5.1 Main findings . . . . . 89
5.2 Limitations and future developments . . . . . 94

**Bibliography** **99**

# List of Figures


1.1 Hydropower installed capacity growth since 1900. . . . . 3
1.2 Hydropower installed capacity of the top 20 hydropower producers and the rest of the world in 2020. . . . . 4
1.3 The river channel can be viewed as a "conveyor belt" for sediment. 8
1.4 The Brune Curve. . . . . 9
1.5 Schematic representation of sediment bypassing. . . . . 12
1.6 Schematic representation of sediment sluicing. . . . . 12
1.7 Schematic representation of sediment flushing. . . . . 13
1.8 Schematic representation of turbidity current venting. . . . . 13
1.9 Landscape transformation from a river to a reservoir. . . . . 16
1.10 Main pathways for GHGs emissions from hydropower plants. . . 17
1.11 Reservoir GHGs fluxes by trophic status. . . . . 19

2.1 Mekong River Basin with the political boundaries of the different countries. . . . . 28
2.2 Topography and geographic regions of the Mekong River Basin. . 29
2.3 Map of the "3S Basin". . . . . 30
2.4 Major factors driving fish production in the Mekong River Basin. 32
2.5 Main floodplains areas of the Lower Mekong River Basin. . . . . 33
2.6 Commissioned, committed, and potential hydropower projects in the Lower Mekong River Basin. . . . . 38
2.7 Current hydropower development in the Mekong River Basin. . . 39

3.1 Spatial distribution of all the dams in the Mekong River Basin subdivided by status and country. . . . . 46
3.2 Key concepts and steps behind the CASCADE modeling framework. . . . . 51
3.3 The Mekong River Basin subdivided into nine "Geomorphic Provinces". . . . . 53
3.4 General example of optimization by means of an MOEA. . . . . 58

3.5 Flowchart of the Borg main loop. . . . . 59
3.6 2D example showing how $\epsilon$-progress is measured. . . . . 60
3.7 Flowchart of the Borg restart logic. . . . . 61
3.8 "Jenks natural breaks" clustering for GHGs emissions values. . . 65
3.9 2D comparison between a Sobol sequence and a random sequence. 66
3.10 Map of the dams for which sediment flushing would be effective in the Mekong River Basin. . . . . 68

4.1 Objective space in which Pareto-Optimal solutions of the decision problem are displayed. . . . . 72
4.2 Map of all dams colored according to their annual GHGs emissions. The Sambor dam is highlighted with a red circle. . . . . 73
4.3 Map of all dams subdivided according to their Mean Probability of Inclusion (MPoI). . . . . 74
4.4 Map of all dams with the associated value of IQR. . . . . 75
4.5 The "triangular pattern" of uncertainty. . . . . 76
4.6 The link between uncertainty and GHGs emissions. . . . . 77
4.7 The link between uncertainty and hydropower production. . . . 77
4.8 "Dams with High Uncertainty": map of the basin and "IQR vs MPoI" plot. . . . . 79
4.9 Comparison between the "Dams with High Uncertainty" on the "IQR vs MPoI" plot for the Sensitivity Analysis on GHGs emissions and for the Sensitivity Analysis on GHGs emissions and sediment connectivity parameters. . . . . 80
4.10 "Dams with Very High Uncertainty" in the 3S Basin. . . . . 81
4.11 Map of the "Lost Opportunities" in the Mekong River Basin. . . . 83
4.12 "Actual" hydropower development scenario: map of all planned dams subdivided according to their Mean Probability of Inclusion (MPoI). . . . . 85
4.13 Comparison between the "Dams with High Uncertainty" on the "IQR vs MPoI" plot for the "pristine" scenario (a) and the "actual" scenario (b). . . . . 86
4.14 "Dams with High Uncertainty" in the 3S Basin for the "actual" hydropower development scenario. . . . . 88

# List of Tables

3.1 The nine "Geomorphic Provinces" of the Mekong River Basin and the corresponding sediment yield. . . . . 52
3.2 $\epsilon$ values and objectives values for all-dams and no-dams scenarios, for each indicator. . . . . 62

4.1 Mean "GHGs emissions per year" and mean "annual hydropower production" calculated for all the dams in the basin and only for the "Dams with High Uncertainty". . . . . 78
4.2 Mean "GHGs emissions per year" and mean "annual hydropower production" calculated for all the dams in the basin and only for "Lost Opportunities". . . . . 84
4.3 Mean "GHGs emissions per year" and mean "annual hydropower production" calculated for all the dams in the basin and only for the seven "Dams with High Uncertainty" in the 3S Basin. . . . . 88

# Acronyms

| | |
|---|---|
| **GHG** | Greenhouse Gas |
| $CO_2$ | Carbon dioxide |
| $CH_4$ | Methane |
| $N_2O$ | Nitrous oxide |
| **IEA** | International Energy Agency |
| **IHA** | International Hydropower Association |
| **WCD** | World Commission on Dams |
| **DM** | Decision-Maker |
| **MRB** | Mekong River Basin |
| **MRC** | Mekong River Commission |
| **SEA** | Strategic Environmental Assessment |
| **NGO** | Non-Governmental Organization |
| **JEM** | Joint Environmental Monitoring |
| **PMFM** | Procedures for the Maintenance of Flows on the Mainstream |
| **GWP** | Global Warming Potential |
| **CASCADE** | CAtchment Sediment Connectivity And DElivery |
| **DEM** | Digital Elevation Model |
| **PO** | Pareto-Optimal |
| **MOEA** | Multi-Objective Evolutionary Algorithm |
| **NFE** | Number of Function Evaluations |
| **CI** | Carbon Intensity |
| **TE** | Trapping Efficiency |
| **PoI** | Probability of Inclusion |
| **MPoI** | Mean Probability of Inclusion |
| **IQR** | Interquartile Range |

# 1 Introduction

## 1.1 Climate Change and renewable energy

Climate Change is surely one of the biggest challenges of our times (*European Environmental Agency (EEA)*, 2022). In 2015, the United Nations Member States declared that "taking urgent action to combat Climate Change and its impacts" was one of the so-called "Sustainable Development Goals" included in the "2030 Agenda for Sustainable Development", a plan of action to achieve a better and more sustainable future for people and the planet. (*United Nations (UN)*, 2015). Negative effects of Climate Change include, among others, rising atmospheric temperature, increasing frequency and intensity of many extreme events, melting glaciers, increasing mean sea level, and ocean acidification (*European Environmental Agency (EEA)*, 2022; *Pachauri et al.*, 2014). The causes are to be found in the increase of anthropogenic Greenhouse Gases (GHGs) emissions since the pre-industrial era, driven largely by economic and population growth, which has led to atmospheric concentrations of carbon dioxide ($CO_2$), methane ($CH_4$) and nitrous oxide ($N_2O$) that are unprecedented in at least the last 800,000 years (*Pachauri et al.*, 2014).

Recent data confirm that consumption of fossil fuels (coal, oil, and natural gas) accounts for the majority of global anthropogenic GHGs emissions (*Edenhofer et al.*, 2011). According to *Pachauri et al.* (2014), emissions of $CO_2$ (which is the primary GHG emitted through human activities) from fossil fuel combustion and industrial processes contributed about 78% of the total GHGs emissions increase from 1970 to 2010. For these reasons, it is increasingly evident

the key role of renewable energy sources and technologies in Climate Change mitigation. Currently, despite continuous improvements, the situation is far from satisfactory. In fact, as reported by *Qazi et al.* (2019), renewable energy sources contributed only 26.5% to worldwide electricity production in 2017.

Renewable energy comprises a wide and varied class of resources, each one with different characteristics and advantages. The most important and popular technologies include hydropower, bioenergy, direct solar energy (photovoltaics and concentrating solar power), wind energy, geothermal energy, and ocean energy (*Edenhofer et al.*, 2011). Hydroelectric power will be the focus of the present study and it will be discussed in detail in the next section.

## 1.2 Hydroelectric power

Hydropower has always been considered one of the most important alternatives to electricity generation by fossil fuels, making it of major importance in tackling Climate Change. It represents a reliable, versatile, low-cost, and low-carbon energy source (*International Hydropower Association (IHA)*, 2021). As Fig. 1.1 shows, hydropower has experienced rapid growth over the last century, coming to currently represent the largest source of renewable energy in the electricity sector, constituting around 60% of the global renewable electricity generation. In the last few years, this growth has become even steeper. In fact, in 2020, the hydropower sector generated a record 4,370 TWh of electricity (up from the previous record of 4,306 TWh in 2019), and the overall hydropower installed capacity reached 1,330 GW (*International Hydropower Association (IHA)*, 2021). Moreover, in the "Net Zero by 2050" scenario defined by the International Energy Agency (IEA), which explores how the global energy sector can successfully decarbonize by 2050, the global hydropower capacity will also need to double its value to fulfill this purpose (*Bouckaert et al.*, 2021).

As reported in Fig. 1.2, China (370 GW), Brazil (109 GW), the USA (102 GW), Canada (82 GW), and India (50 GW) make up the five world leaders in respect of total hydropower installed capacity in 2020. In particular, China and Brazil are the countries characterized by the steepest increasing trends in hydropower production in the last decades (*International Hydropower Association (IHA)*, 2021). Nevertheless, by the end of 2017, the total hydropower installed capacity of China accounted for only 18% of overall China's electricity generation (*Sun et al.*, 2019), with a large theoretical hydropower potential yet to be explored. A similar argument could be made for Brazil, where, despite more than two-thirds of the energy supply coming from hydropower (*Winemiller et al.*, 2016), there is still a large unused potential that can be exploited

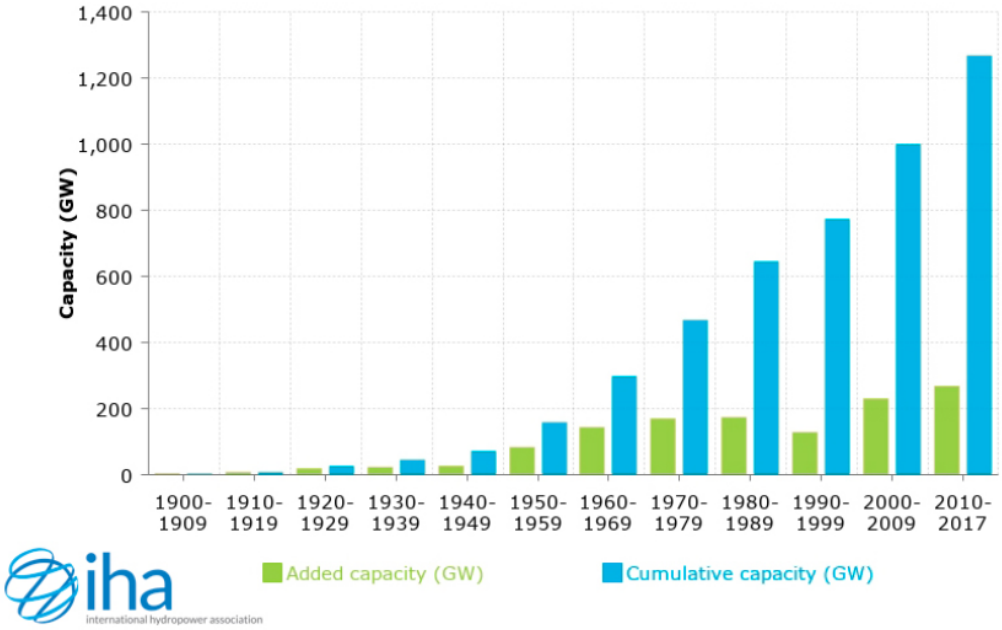


**Figure 1.1:** *Hydropower installed capacity growth since 1900. (International Hydropower Association (IHA), 2019)*

(*Almeida et al.*, 2019).

The construction of many hydropower dams is currently planned all over the world, especially in countries with developing economies, to fulfill the increasing energy demand derived from the human population growth, economic development, and Climate Change (*Zarfl et al.*, 2015). Furthermore, the exploitation of a high-efficiency renewable energy resource ensures energy security and other social aspects of nations' development (*Jadoon et al.*, 2020). As reported by *Abadie et al.* (2020), a future decrease in the number of fossil fuel power stations will lead to fewer baseload plants and higher intermittent generation, increasing the risk that the energy supply will be unable to meet the electricity demand. On the other hand, flexible management of hydro resources, operating in combination with other non-dispatchable technologies (e.g., solar and wind power), can alleviate this risk by adjusting peak power generation and providing baseload energy, also thanks to its large storage capacity.

Despite all these positive aspects, hydropower production can hide several drawbacks, very often underestimated. It has been observed that a non-strategic development and the lack of in-depth studies can lead to serious impacts on the environment, both at a local and global scale. These impacts are described in detail hereafter.

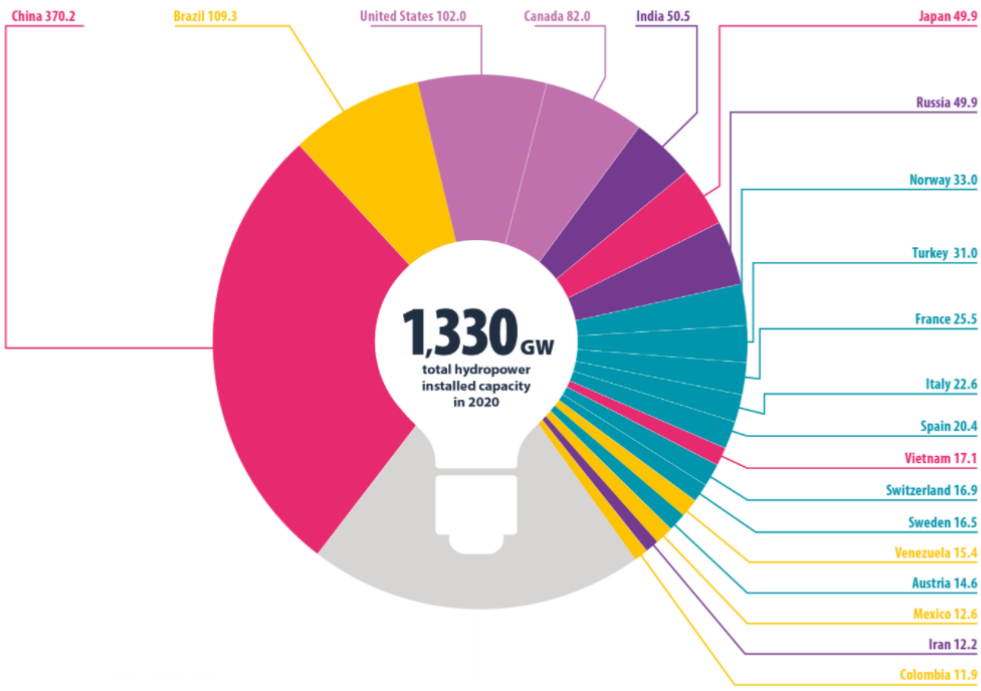


**Figure 1.2:** *Hydropower installed capacity (GW) of the top 20 hydropower producers and the rest of the world in 2020. (International Hydropower Association (IHA), 2021)*

### 1.2.1 Dams impacts

Hydropower production technologies include dams with reservoirs, "run-of-river" and "in-stream" projects, covering a wide range of project scales (*Owusu and Asumadu-Sarkodie*, 2016). Impoundment facilities use a dam to store river water in a reservoir and produce electricity by releasing it through turbines. They are by far the most common type of hydroelectric power plant and, since this work of thesis only focuses on them, they will be the only ones taken into account from now on.

Dams and impoundments have been built for thousands of years for various purposes (*Lehner et al.*, 2011). Only a minority of the world's dams are built for hydropower, with the majority used for irrigation, water supply, flood and drought control, and other purposes (e.g., recreation, fish breeding, navigation) (*International Hydropower Association (IHA)*, 2021). A large number of dam projects are indeed multipurpose. For this reason, it is always important to remember that the decision on whether to build, remove or improve a dam should always be taken considering all its possible multiple uses.

As anticipated, hydroelectric power often represents the main substitute for non-renewable energy sources for both developed and developing countries. The decrease in Greenhouse Gases (GHGs) emissions and the high reliability

are among the main advantages of this technology (*International Hydropower Association (IHA)*, 2021). However, various studies have brought to light several negative impacts of dam construction; some of which are more obvious, others less so. A global overview of dam-based impacts on large river systems showed that over half of them, including the most bio-geographically diverse, now present at least one dam (*Nilsson et al.*, 2005). Since dams have impacts on both upstream and downstream ecosystems, the consequences are multiple, varied, and complex. Therefore, it is extremely difficult to predict all the repercussions that dam construction will have for any particular river ecosystem, especially in the absence of large amounts of data (which is the case of the majority of projects to date) (*McCartney et al.*, 2001). Nevertheless, some common traits can be identified. In general, some of the main potential impacts associated with dams are as follows:

- alteration of river system equilibrium, natural flow regime and water quality;
- interruption of longitudinal fish migration;
- blockage of sediment and nutrient transport;
- inundation of upstream terrestrial environment;
- GHGs emissions from the degradation of large stocks of organic matter.

Dam construction can therefore affect both upstream and downstream ecosystems, and lead to both natural and social impacts. These will be further examined hereafter.

Balancing hydropower and biodiversity in a river system is surely a complicated task, since the alteration of its equilibrium will endanger the ecosystems, the flora, and the fauna of the area. *Richter et al.* (2010) estimated that about 472 million river-dependent people live downstream of large dams. Despite the benefits of the latter (e.g., irrigation, flood, and drought protection), negative impacts on ecosystems are far more common than are usually thought. In fact, by changing the natural flow patterns and blocking the movement of fish and other animals, large dams can severely disrupt natural riverine production systems, especially fisheries, flood-recession agriculture, and dry-season grazing. Moreover, by delaying and attenuating seasonal flood pulses, large dams reduce fish access to floodplain habitats that are essential nursery areas and feeding grounds (*Winemiller et al.*, 2016; *Baran and Myschowoda*, 2009). In addition, the water storage process alters the physico-chemical characteristics of the water flow, reducing the natural ability of rivers for transportation and

dilution of pollutants and water purification (*Brismar*, 2002; *Schmutz and Sendzimir*, 2018).

It is quite obvious that the physical presence of dams can remarkably compromise river connectivity, blocking the upstream migration routes used by fish and preventing them to complete their life cycles. This may be particularly devastating to tropical river fisheries, where many high-value species migrate hundreds of kilometers in response to seasonal flood pulses and a large part of the population relies on this food source (*Winemiller et al.*, 2016; *Richter et al.*, 2010). Furthermore, also the location of dams in the river basin influences this phenomenon. Dams built downstream near the sea and floodplain habitats presumably have the most significant impacts (*Baran and Myschowoda*, 2009). On the other hand, dams are usually built in correspondence of high-gradient reaches, where rapids and waterfalls boost hydropower potential. Unfortunately, these are crucial spots for many unique species of fish adapted for life in fast water (*Winemiller et al.*, 2016).

As well as for fish, dams infrastructures also constitute physical obstacles for sediment and nutrient transport. When the fast-moving water of the river enters the quiet water of the reservoir, the difference between the two velocities causes a hydrodynamic energy drop. Consequently, a significant amount of the transported sediments are deposited in the impoundment and upstream the reservoir in the reaches influenced by backwater (*Kondolf*, 1997). This may lead to consequences such as channel incision ("downcutting"), coarsening of bed material, loss of spawning habitats for salmonids (e.g., salmon and trout), channel narrowing, and coastal erosion (see Section 1.2.2). Furthermore, as we will explain in Section 1.2.3, the accumulation of sediments in dams reservoirs can also boost GHGs emissions (*Sobek et al.*, 2012; *Maeck et al.*, 2013).

Downstream ecosystems are not the only ones to be affected by the construction of a dam, since the creation of an impoundment necessarily implies the flooding of the upstream terrestrial environment, impacting all the flora and the fauna currently living there. As further explained in Section 1.2.3, decomposition of flooded vegetation and soil organic matter are also potentially an important source of GHGs in hydroelectric reservoirs (*Barros et al.*, 2011; *Song et al.*, 2018; *Abril et al.*, 2005). Depending on the type of vegetation, the flooding could result in the loss of a sink of atmospheric $CO_2$ and $CH_4$ (*St. Louis et al.*, 2000). Moreover, the social impacts of dam construction are also to be taken into account, especially for large dam projects. In 2000, the World Commission on Dams (WCD) estimated that the number of people forcibly displaced by large dams between 1950 and 2000 could range from 40 to 80 million people (*World Commission on Dams (WCD)*, 2000). According to current esti-

mates regarding the decade 2011-2020, the number of people resettled due to infrastructure projects (including hydropower) exceeds 20 million a year, or 200 million over the decade (*Hay et al.*, 2019). Other social impacts of large dam projects concern changes in land use patterns, rural economy and employment structure, repercussions on infrastructure and housing, worsening of human health and gender relations, and impacts on non-material or cultural aspects of life (*Nilsson et al.*, 2005; *Tilt et al.*, 2009). For a variety of reasons, many of the burdens associated with resettlement are borne by women and children, and disproportionately affect poor families (*Tilt et al.*, 2009; *Schulz and Adams*, 2019). Additionally, even if sometimes the consequences of these dam-induced impacts were largely overcome within a decade, in other cases they persisted through multiple generations (*Richter et al.*, 2010).

Lastly, a growing number of recent studies have even questioned the assumption that hydropower is a carbon-free source of energy. In fact, several initially underestimated phenomena contribute to GHGs emissions, in addition to the impacts related to the construction, operation, maintenance, and decommissioning phases (*Song et al.*, 2018). To date, many studies have tried to provide the most accurate estimates of GHGs emissions from hydroelectric reservoirs, often achieving conflicting results. According to *Prairie et al.* (2018), this uncertainty can be attributed to both the difficulties in measuring these highly variable fluxes and the lack of a clear accounting methodology. Due to the fact that direct measurements are, in many aspects, practically impossible, several reservoir characteristics have been used to estimate GHGs emissions. The topic of GHGs emissions from reservoirs will be further analyzed in Section 1.2.3.

### 1.2.2 Sediment trapping process, consequences and possible solutions

Hydropower is certainly an important renewable energy resource, but the right assessment of the trade-offs between the benefits and the environmental impacts of dam construction is crucial for sustainable development. One of the key impacts of dams is the trapping of sediments which are transported by rivers from high elevation areas to sea level.

*Schmitt et al.* (2016) defined sediment connectivity as the set of processes that describe the transfer of sediment between multiple sources and sinks. Many aspects influence sediment connectivity in fluvial networks, such as the distance between a source and a sink, source grain size and sediment supply, network topology and topography, and hydrologic forcing. Dam construction changes the natural sediment connectivity, affecting the river ecosystems and accelerat-

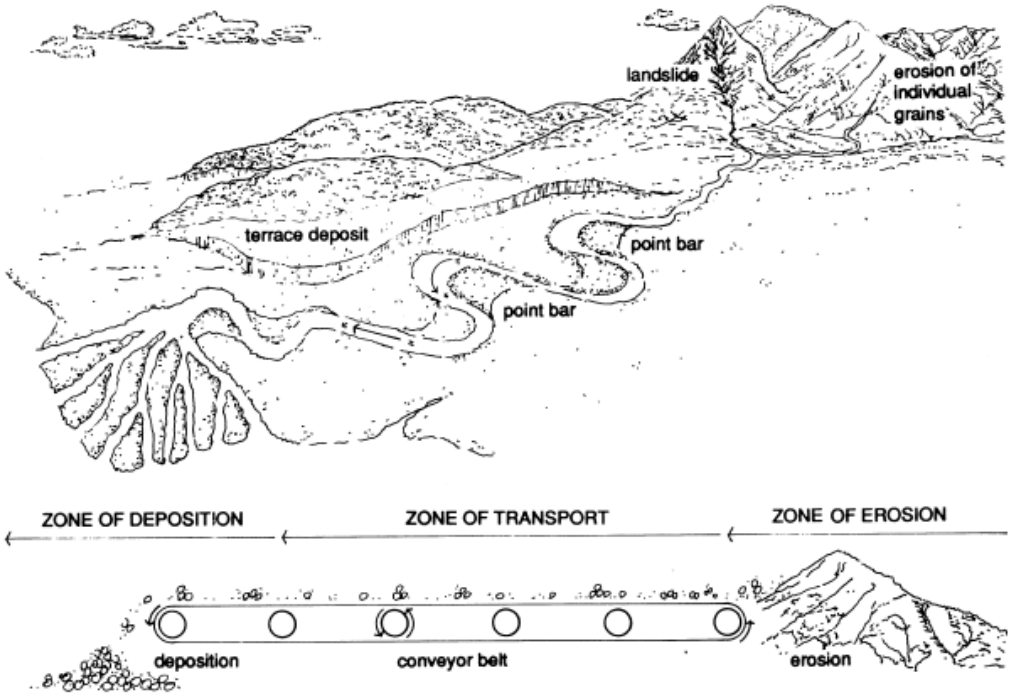


**Figure 1.3:** *The idealized watershed can be divided into three zones: that of erosion, transport, and deposition. The river channel can be viewed as a "conveyor belt" for sediment. (Kondolf, 1997)*

ing the subsidence of river deltas (*Schmitt et al.*, 2018a).

*Kondolf* (1997) illustrated how the idealized watershed can be divided into three zones (Fig. 1.3): that of erosion (steep, rapidly eroding headwaters), transport (through which sediment is moved more or less without net gain or loss), and deposition (e.g., river deltas). Hence, the river channel in the zone of transport can be viewed as a "conveyor belt", which carries the sediments produced by erosion in uplands downstream to the ultimate depositional areas near sea level. Depending on the grain size and river flow properties, sediment can be transported as suspended load, floating in the water column due to turbulence, or as bed load, which is transported by rolling, sliding, and bouncing along the riverbed. Although a relatively small part of the total load, coarse sediments constitute the "architecture" of most riverbeds, as the material that compose the channel bed, bars, riffles, and often banks. Nonetheless, even fine-grained sediment is very important for the structure of some riverine forms, such as floodplains and estuarine mudflats (*Kondolf et al.*, 2014a).

Dam construction interrupts the longitudinal continuity of the river system and interferes with the action of the "conveyor belt" of sediment transport. *Vörösmarty et al.* (2003) estimated that more than 53% of the global sediment flux in regulated basins is potentially trapped in reservoirs (or 28% if con-

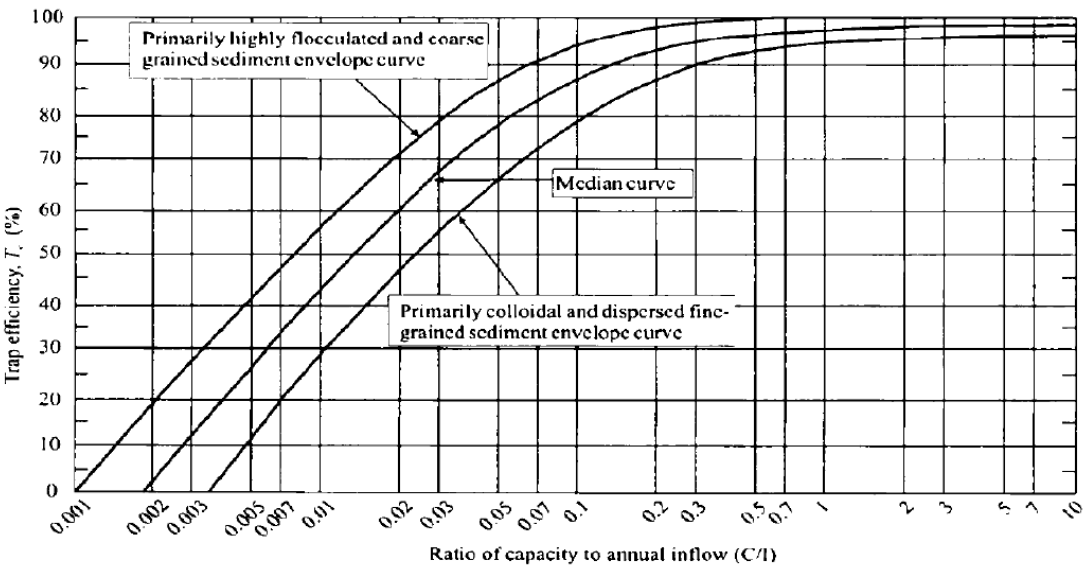


**Figure 1.4:** *The Brune Curve expresses the relation between dam trapping efficiency and reservoir capacity-inflow ratio (C/I). (Brune, 1953)*

sidering all river basins). Sediment deposition in reservoirs takes place as a consequence of the hydrodynamic energy drop that the fast-moving water of the river undergoes when enters the quiet water of the impoundment. As described by *Kondolf et al.* (2014a), since gravel moves through river channels as bed load, it is virtually certain to be trapped by dams (only small dams on steep channels can be capable of passing bed load). Sand can overcome many smaller dams on steep streams with turbulent flow, but typically not large reservoirs. Silt and clay (often called "wash load") are always transported as suspended load and are thus characterized by the lowest sedimentation rates. *Brune* (1953) estimated that the percentage of suspended sediment trapped by a reservoir (also known as "trapping efficiency") increases with the water residence time, and generally increases with the ratio of total reservoir storage to inflow. This relation is expressed by the well-known Brune curve (Fig. 1.4), widely used in many applications. Furthermore, in absence of sediment management strategies, the clear water released from the dam possesses the energy to move sediment while having little or no sediment load. *Kondolf* (1997) referred to this sediment-starved water as "hungry water", which is prone to erode the river bed and banks even for many hundreds of kilometers downstream (*Richter et al.*, 2010).

One of the repercussions of the reduced supply of coarse sediment downstream of dams is the channel incision. This phenomenon, also known as "downcutting", consists in a vertical erosion of the river bed, which leads to

a decrease in the channel bed elevation and a consequent alteration in the natural flow pattern (*Kondolf*, 1997).

Channel incision is frequently accompanied by a change in particle size on the bed, as gravels and finer materials are more easily transported downstream by the "hungry water", leaving a bottom layer mostly composed of large gravel, cobbles, and boulders. Since salmonids use freshwater gravels to incubate their eggs, bed coarsening can threaten the success of spawning of these species, as the grain size can increase to such an extent that the fish can no longer move the gravel (*Kondolf*, 1997).

By storing water coming from the upstream river, many reservoirs (especially those of large size) reduce flood peaks. Downstream of the dam, riparian vegetation can rapidly grow and invade some sections of the active channel in response to a reduction in flood peaks and sediment deposition. Channel narrowing has been greatest below reservoirs that are large enough to contain the river's largest floods. In some cases, the reduction in peak floods and their flushing ability can lead to the accumulation of fine sediment on the river bed, potentially affecting aquatic habitats (*Kondolf*, 1997).

Very often, the impacts of dams may extend for great distances (sometimes, even for many hundreds of kilometers), until reaching the river delta and coastal areas (*McCartney et al.*, 2001; *Kondolf et al.*, 2018; *Richter et al.*, 2010).

Coastal areas that rely on riverine sediment supply are particularly vulnerable to impacts of reduced sand delivery. As a consequence, sand-starved beaches may shrink or disappear, accelerating erosion of coastal cliffs (*Kondolf et al.*, 2014a). Paradoxically, by trapping sediment and reducing peak flows, the flood control effect of dams can result in reducing property damage along rivers while contributing to property damage along the coast by decreasing sand supply to the protective beaches (*Kondolf*, 1997). *Syvitski et al.* (2005) estimated that more than 37% of the world's population lived within 100 km of a coastline (and approximately 44% if considering 150 km), highlighting the major implications of coastal erosion for human habitat.

River deltas deserve particular attention since they are impacted cumulatively by all disturbances in the basin upstream (*Kondolf et al.*, 2018; *Lehner et al.*, 2011; *McCartney et al.*, 2001). Dam construction, especially considering the combined effects of several dams at the scale of the entire basin, can have significant impacts on river deltas. For instance, many of them are sinking due to the reduced sediment delivery (together with sea level rise and land-use change caused by Climate Change), thus increasing the vulnerability of local inhabitants who depend on fishing activities, floodplain agriculture, and navigation (*Lehner et al.*, 2011; *Anderson et al.*, 2018; *Kuenzer et al.*, 2013).

As explained by (*Kondolf et al.*, 2014a), reservoirs themselves are impacted by sediment trapping, since the accumulation of sediment implies the loss of reservoir capacity over time and the consequent compromise of dam functions. In some extreme cases, reservoirs have already filled with sediments, not only making useless the dam infrastructure, but posing safety hazards as well. Fortunately, sediment trapping by dams is not inevitable, and some techniques may be applied to partially prevent and/or solve this problem.

*Maeck et al.* (2013) described how sediment accumulation also correlates with $CH_4$ emissions in reservoir, since certain deposition zones (e.g., dam forebays) can easily become methane emission hot-spots (see Section 1.2.3 for more details). All the impacts described above have the possibility to severely disrupt natural and human ecosystems throughout the whole river basin, and the situation is further aggravated by sand and gravel mining practices, not rarely out of control (*Kondolf*, 1997).

Therefore, it is increasingly evident the need for reservoir sediment management strategies that both prolong reservoir life and benefit downstream reaches by mitigating the sediment starvation that results from sediment trapping.

Fig. 1.5 shows two similar configurations of sediment bypassing. The approach displayed in Fig. 1.5.b consists in diverting part of the incoming river waters to an off-channel reservoir during times of clear flow, and avoiding diversion when suspend sediment concentrations are high. A variant of this approach is shown in Fig. 1.5.c, in which sediment-laden river waters are diverted at a weir dam upstream of the reservoir into a diversion channel (or tunnel), which conveys the sediment-laden waters downstream of the dam, where they rejoin the river. Typically, the weir diverts during high flows, when sediment loads are high, but once sediment concentrations decrease, water is allowed into the impoundment. The ideal geometry corresponds to a relatively short reservoir and a river that makes a sharp turn between the point of water diversion and the point of sediment reintroduction, minimizing the length of the bypass channel (or tunnel) and taking advantage of the steep gradient for gravity flow (*Kondolf et al.*, 2014a).

Fig. 1.6 presents the "sediment sluicing" (or "drawdown routing") strategy, which is performed by lowering the reservoir pool before high-discharge sediment-laden floods. The objective is to discharge high flows through the dam during periods of high inflows to the reservoir, in order to permit the sediment to be transported downstream of the reservoir as rapidly as possible, minimizing sedimentation. Even if some previously deposited sediment may be scoured and transported, the main effect consists in reducing incoming sediment trapping. This approach requires relatively large capacity outlets, placed

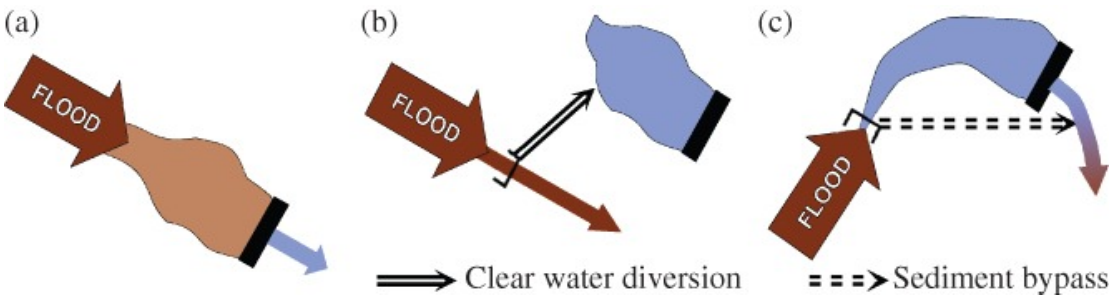


**Figure 1.5:** *Schematic representation of sediment bypassing. (a) Conventional configuration, where the reservoir traps the incoming sediment. (b) Part of the river water is diverted to an off-channel reservoir during times of clear flow. (c) Sediment-laden river waters are redirected upstream of the reservoir to a diversion channel (or tunnel), passing around the impoundment and flowing into the downstream reach. (Kondolf et al., 2014a)*

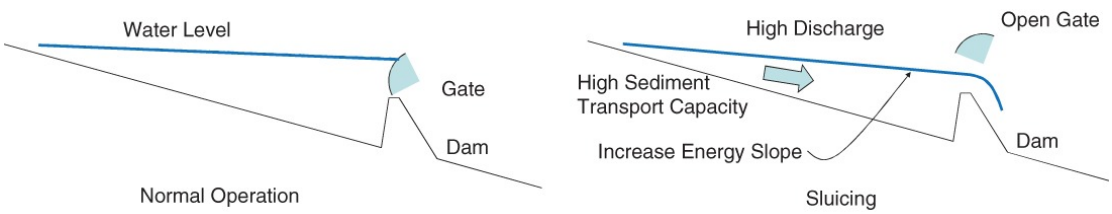


**Figure 1.6:** *Schematic representation of sediment sluicing. (Kondolf et al., 2014a)*

not at the very bottom of the dam, in order to discharge large flows while maintaining low water levels and the required velocities and transport capacity. The "drawdown and sluicing" strategy can be employed at reservoirs of all sizes, but the duration of sluicing depends on the watershed size and the time scale of flood events. For instance, for dams of small watersheds with rapidly rising floods, the reservoir may be drawn down only for a period of hours. In other cases, the reservoir may be held at a low level for most of the flood season to maximize sediment passing through, and use only late-season flows to fill the impoundment (*Kondolf et al.*, 2014a).

Fig. 1.7 shows the "sediment flushing" strategy, whose goal is to scour and re-suspend deposited sediment and transport it downstream. This approach involves the complete emptying of the reservoir through low-level gates that are large enough to let the flushing discharge pass through the dam without upstream impounding, so that the free surface of the water is below the gate. The best scenario for flushing is to establish river-like conditions through the reservoir upstream of the dam, which can be more easily obtained with small, long, and narrow reservoirs, and on rivers with strongly seasonal flow patterns. A secondary, but potentially very significant effect of drawdown flushing consists in releasing sediment to the downstream reach at a timing that may be different from that of the sediment inflow into the reservoir. Especially during

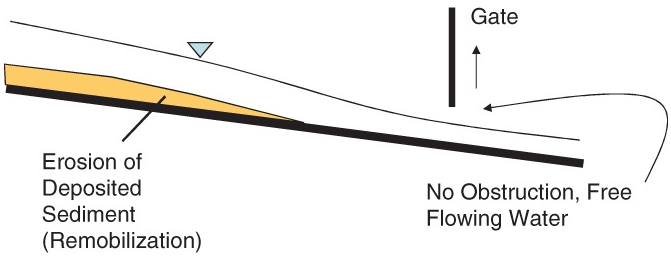


**Figure 1.7:** *Schematic representation of sediment flushing. (Kondolf et al., 2014a)*

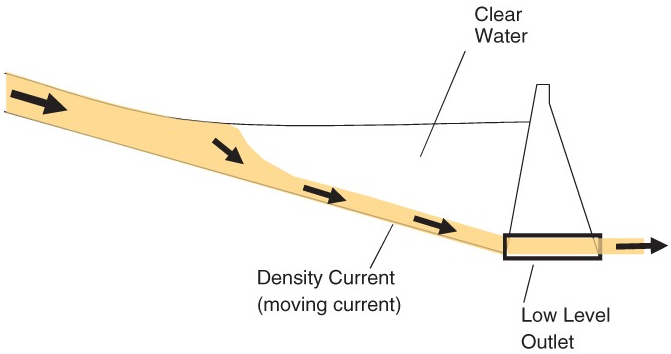


**Figure 1.8:** *Schematic representation of turbidity current venting. (Kondolf et al., 2014a)*

the non-flood season, increasing the release of coarse-grained sediment otherwise buried in the impoundment can considerably enhance the environmental quality of downstream ecosystems. Additionally, flushing can provide a large amount of discharge water during low-flow periods, when the river is unlikely to have sufficient eroding energy, avoiding the accumulation of grained sediments, and preventing the encroachment of riparian vegetation and the narrowing of the active channel. On the other hand, off-season sediment-rich floods could alter excessively the system equilibrium, resulting in negative consequences (e.g., channel incision, fish death by smothering). Hence, in-depth studies on downstream ecosystems are needed to assess the potential positive or negative impacts. Sediment flushing is more effective the lower is the ratio of reservoir storage to mean annual flow is, because with larger storage the reservoir cannot be easily drawn down. The main challenge is to find the best trade-off between frequent flushing, with its frequent power losses, and less frequent flushing operations, associated with high hydropower production (*Kondolf et al.*, 2014a).

Fig. 1.8 displays the so-called "turbidity current venting" technique. Turbidity (or "density") currents form when inflowing waters with high sediment concentrations create a distinct, higher-density current that flows along the bottom of the reservoir toward the dam without mixing with the overlying, lower-density waters. The strategy consists in allowing this dense, sediment-laden

water to pass through dam outlets and it is feasible only where the turbidity currents have sufficient velocity and turbulence to maintain particles in suspension, in order to travel all the way to the dam as a distinct flow (*Kondolf et al.*, 2014a).

Accumulated sediments can be removed by suction using hydraulic pumps, but, since dredging is expensive, it is most often used to extract sediments from specific, critical areas. If a reservoir is completely drawn down (or remains dry for parts of the year), accumulated sediments can be mechanically removed using scrapers, dump trucks, and other heavy equipment. While still costly, mechanical removal is commonly less expensive than hydraulic dredging and more effective on coarser sediments (*Kondolf et al.*, 2014a).

Some projects attempted to artificially replenish gravel below dams, trying to partially restore the natural river ecosystem. While this strategy can provide short-term habitat, the amount of gravel added was just a small fraction of the bed load deficit and it was still largely washed out during high flows. This required the continuous addition of more imported gravel, often with unsustainable costs (*Kondolf*, 1997).

As stated by *Kondolf et al.* (2014a), all the techniques here presented have been proven by several studies, but are still not enough implemented where they could be. Moreover, considering that their implementation after the dam construction is often highly expensive or even impossible, it is clear the need to consider these solutions during the design phase.

Choices in the siting, design, and operation of dams determine their ability to pass sediment. This highlights the absolute need to apply a strategic dam planning approach, in which a larger spatial and temporal context is taken into account (*Schmitt et al.*, 2019). This concept will be expanded in Section 1.3.

### 1.2.3 GHGs emissions from reservoirs

Hydropower is traditionally considered a "clean" source of renewable energy. Although most hydropower plants have a "carbon intensity" (i.e., total GHGs emissions per unit of produced electricity) comparable to other types of renewable energy (e.g., solar energy, wind energy), certain conditions could lead to values close to or even higher than fossil fuel power stations. Indeed, it is estimated that about 10% of the world's hydroelectric facilities, mainly located in tropical regions, emit as many GHGs per unit of energy as conventional fossil-based power plants (*Almeida et al.*, 2019; *Song et al.*, 2018).

One of the biggest problems related to the early estimates of GHGs emissions from reservoirs consisted in considering exclusively the situation after

the dam construction, thus only the "gross" emissions, without taking into account the pre-impoundment conditions. On the contrary, the actual effect of dam construction and impoundment (in simple words, what the atmosphere truly "sees") should be measured as the net difference between GHGs fluxes before and after flooding, i.e., the "net" emissions (*Prairie et al.*, 2018; *St. Louis et al.*, 2000). The latter deeply depend on the kind of pre-flood landscape. In fact, the entire reservoir area, or a part of it, could have previously been either a carbon sink (e.g., soils, forests, agricultural lands) or a carbon source (e.g., rivers, lakes, peatlands, swamps) (*Song et al.*, 2018; *Demarty and Bastien*, 2011; *Hertwich*, 2013).

Therefore, the "net" emissions should be measured as follows:

$$\begin{aligned} \text{"net" emissions} \;=\; & \text{"gross" emissions} \;+ \\ & + \text{previous uptake from sinks} \;- \\ & - \text{previous emissions from sources} \end{aligned}$$

Hence, disentangling preexisting (natural) and new (anthropogenic) GHGs sources is crucial to allocate correctly the part of GHGs emissions that can be legitimately attributed to the creation of the reservoir itself (*Prairie et al.*, 2018).

However, the resulting calculation is still incomplete because it neglects the critical questions of how much of these "net" emissions would have occurred regardless of the presence of the reservoir, how much may have been displaced elsewhere and what is the temporal evolution of the post-impoundment emissions (*Prairie et al.*, 2018).

Fig. 1.9 shows an example of landscape transformation following an impoundment, from a river to a reservoir. Although a large fraction (about 75% over a 100-year time horizon, according to *Almeida et al.* (2019)) of diffusive $CO_2$ emissions occurring at the reservoir surface can be considered natural (green arrows), the fraction emanating from the degradation of flooded organic matter is new and induced by the impoundment (blue arrows). In contrast, essentially all $CH_4$ emissions can be considered anthropogenic (*Prairie et al.*, 2018).

*Demarty and Bastien* (2011), *De Faria et al.* (2015), and *Maeck et al.* (2013) identified four major pathways (illustrated in Fig. 1.10) through which GHGs are released into the atmosphere after the reservoir creation:

- diffusion of dissolved $CO_2$, $CH_4$, and $N_2O$ at the air-water interface;
- $CH_4$ bubble emissions;
- degassing at turbines and spillways;
- downstream of dam emissions.

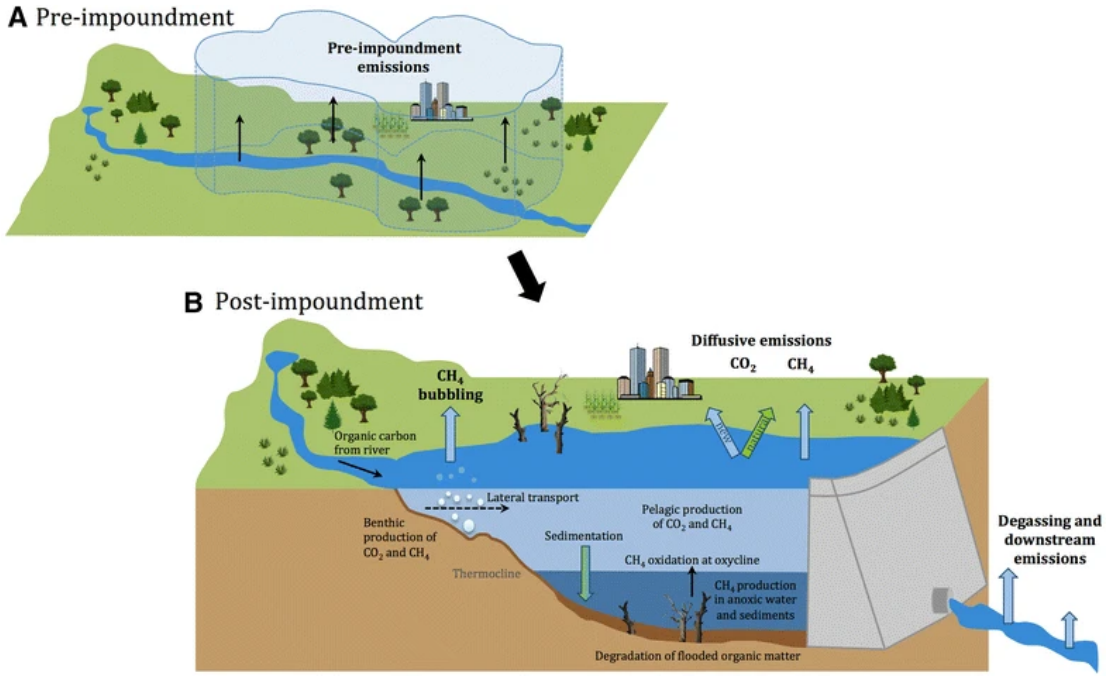


**Figure 1.9:** *Landscape transformation from a river to a reservoir. (A) Pre-impoundment conditions: the area delimited by the dashed line coincides with the future reservoir, where the GHGs balance needs to be accounted for. (B) Post-impoundment conditions: multiple processes and pathways for $CO_2$ and $CH_4$ emissions are indicated by arrows; green arrows represent natural emission fluxes, while blue arrows represent the emissions induced by the impoundment. (Prairie et al., 2018)*

Diffusive GHGs emissions (mainly $CO_2$, $CH_4$ and $N_2O$) are caused by the difference in gas concentrations at the air-water interface and depend on several local weather conditions such as air and water temperatures, wind speed, and rainfall (*Demarty and Bastien*, 2011; *Hertwich*, 2013). They originate from microbial decomposition of flooded organic matter present in the reservoir (e.g., vegetation, soils, algae) or entering the system from the terrestrial landscapes they drain (close proximity to human activities is likely to increase the delivery of organic matter and nutrients from land to water) (*Räsänen et al.*, 2018; *Deemer et al.*, 2016).

Reservoir stratification occurs as a consequence of thermal differentials in the water column that prevent vertical water from mixing (*De Faria et al.*, 2015). This phenomenon results in the formation of an anoxic bottom layer (hypolimnion), fueling methanogenesis from the anaerobic decomposition of organic matter in the sediments (*Sobek et al.*, 2012). $CH_4$, released as bubbles due to its low solubility ("bubbling"), can either rapidly reach the surface and be released into the atmosphere or undergo oxidation and be emitted as $CO_2$ (*DelSontro et al.*, 2011; *Demarty and Bastien*, 2011; *Barros et al.*, 2011).

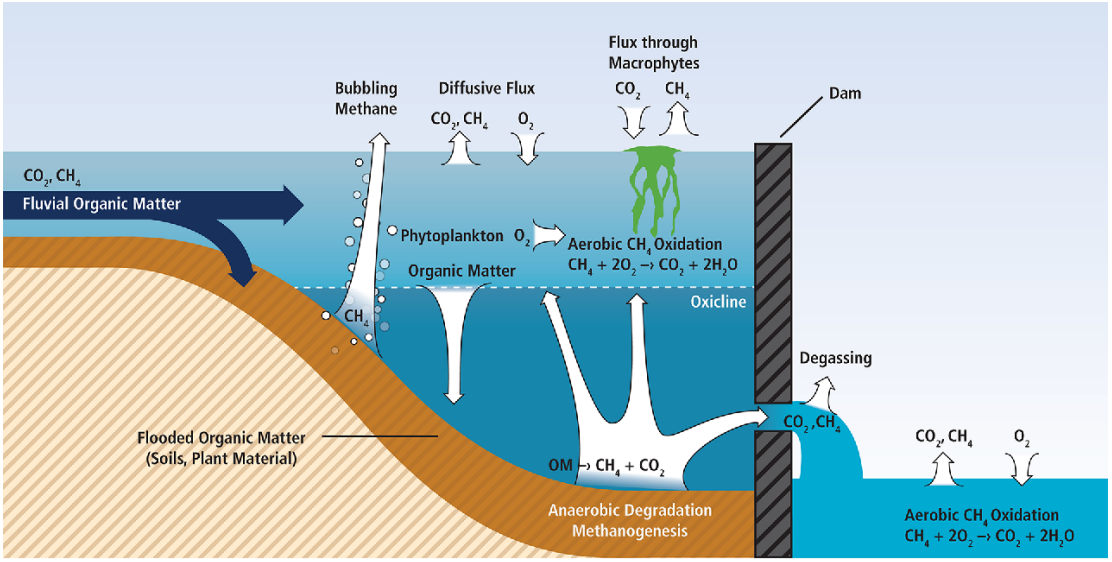


**Figure 1.10:** *Main pathways for GHGs emissions from hydropower plants. (Hertwich, 2013)*

Degassing emissions from turbines and spillways derive from the rapid depressurization, aeration, and temperature change of discharge flows just after low-level outlets (*Deemer et al.*, 2016; *De Faria et al.*, 2015).

GHGs that remain in solution after the water passes through a dam can be emitted into the atmosphere by either diffusive or ebullitive fluxes in the downstream river segment (*Song et al.*, 2018; *Hertwich*, 2013).

Currently, despite the well-established knowledge of the phenomena responsible for GHGs emission from reservoirs, their estimates present a high uncertainty among the different studies, caused by both the complexity of the measurements and the lack of a shared methodology (*Prairie et al.*, 2018). For this reason, several reservoir characteristics have been used for GHGs estimates.

According to *Almeida et al.* (2019), diffusive emissions are proportional to the impoundment surface. In fact, the authors pointed out that "power density" (i.e., the electricity generation per unit of flooded area) represents a key parameter in evaluating the performance of a dam project. They noted that lowland dams in the Amazon basin, with their typically larger reservoir areas, presented significantly higher carbon intensities with respect to upland dams, where the steeper topography of high-elevation regions favors hydroelectric production.

Moreover, carbon emissions are negatively correlated to both reservoir age and latitude (*Barros et al.*, 2011). Indeed, the maximum values are recorded in the first 2 to 3 years after the impounding due to the decomposition of the newly flooded biomass (*Abril et al.*, 2005); the latter still remains the main

source of carbon for the first 10 to 15 years (*Deemer et al.*, 2016; *Barros et al.*, 2011), declining exponentially over time (*St. Louis et al.*, 2000; *Teodoru et al.*, 2011). For what concerns the influence of latitude, *Song et al.* (2018) observed huge differences between carbon intensities of dams located in boreal and temperate regions (3 - 70 $kg\,CO_2eq/MWh$) compared to dams dams located in tropical and equatorial regions (8 - 6647 $kg\,CO_2eq/MWh$). The main reasons are to be found in the higher water and sediments temperature of tropical reservoirs, along with larger biomass quantities and higher average biomass carbon contents (*Barros et al.*, 2011; *Demarty and Bastien*, 2011).

GHGs emissions are also negatively correlated to the reservoir depth: since methane is primarily produced in the sediments, a longer distance to the surface both increases the fraction of $CH_4$ that is oxidized and reduces the fluxes by ebullition and through vegetation (*Barros et al.*, 2011; *DelSontro et al.*, 2011).

*Song et al.* (2018) also put in evidence that the depth of the reservoir from which the water passing the turbines is drawn is relevant; especially in stratified systems, deeper water corresponds to higher pressure, lower temperature, and higher solubility and concentration of GHGs, resulting in higher emissions when the supersaturated water passes through the turbines.

Furthermore, as stated by *Prairie et al.* (2018) and *Weissenberger et al.* (2010), one of the most significant hydrological changes induced by the impoundment of a river is the increased water residence time, and, since the fraction of the organic matter that is mineralized within the system is known to increase with it, the net result is higher carbon emissions. However, according to *Prairie et al.* (2018), at least a part of these emissions would have taken place regardless of the creation of the impoundment, although distributed at a location downstream, including the sea. This means that these emissions are not new, but simply displaced in space. Nevertheless, *De Faria et al.* (2015) tried to estimate GHGs emissions from future Amazonian hydroelectric plants and found out that reservoirs with high residence time presented higher simulated carbon intensities compared to thermal power plants.

As already mentioned in Section 1.2.2, the sediment trapping efficiency of a dam is linked to $CH_4$ emissions within the reservoir. *Maeck et al.* (2013) noticed that sediment accumulation in certain deposition zones (e.g., dam forebays) creates methane emission hot-spots, where high organic loads rise the ebullition rate. Small reservoirs are particularly susceptible to intense sedimentation. The authors estimated that over 90% of the $CH_4$ emissions from the entire 96-$km$ portion of the River Saar (Germany) considered in the study are from the reservoir sections which cover only about 16% of the total surface area. The creation of an impoundment also increases the sedimentation rate, supplying reactive

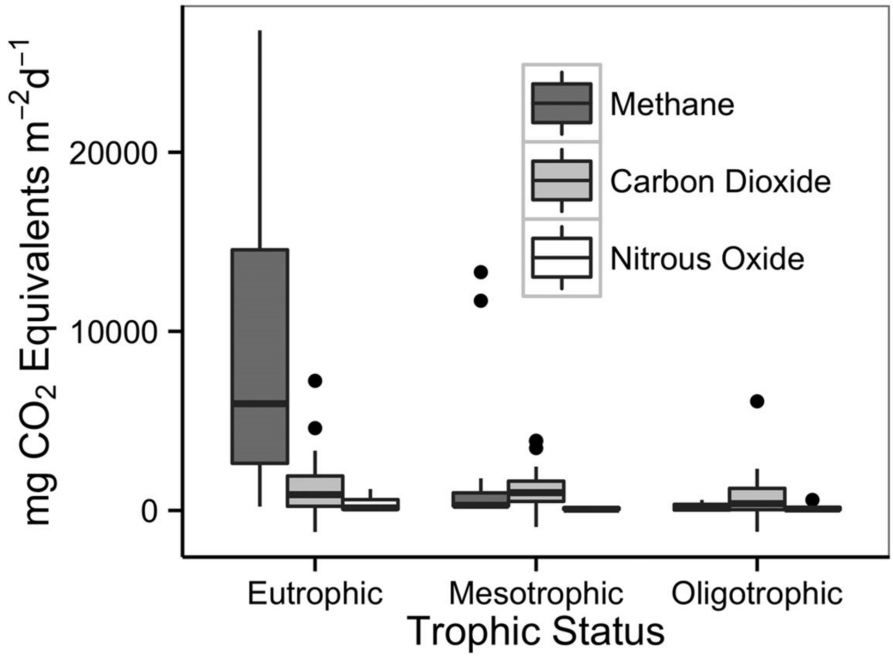


**Figure 1.11:** *Reservoir GHGs fluxes by trophic status. The lines within the boxes indicate median fluxes. The boxes demarcate the 25th and 75th percentiles, the whiskers delineate the 95% confidence intervals, and the dots represent data outside this range. (Deemer et al., 2016)*

organic matter to the deep, anoxic layers and fueling methanogenesis (*Sobek et al.*, 2012; *Lohrberg et al.*, 2020).

*Deemer et al.* (2016) paid instead special attention to net primary production. In particular, this study reported that methane emissions were best predicted by chlorophyll *a* concentrations; eutrophic systems, due to low oxygen and high dissolved organic carbon conditions, emitted approximately an order of magnitude more $CH_4$ than oligotrophic ones (Fig. 1.11).

Lastly, as anticipated, carbon emissions are also correlated to the pre-flood landscape. In the study made by *Teodoru et al.* (2011) on the Eastmain Reservoir in Northern Quebec (Canada), the authors observed that surface $CO_2$ fluxes were spatially heterogeneous. However, at least part of this spatial heterogeneity could be traced to the pre-flood landscape that underlies the different portions of the reservoir. In particular, surface emissions appeared to be linked to the total carbon stocks associated with each type of landscape, with significant differences between former wetlands and forest areas. Indeed, *De Faria et al.* (2015) suggested that vegetation clearing before reservoir flooding supports a significant reduction in GHGs emissions in all the projects in which it was implemented.

Due to the high variability of the characteristics of the reservoirs, in situ measurements are extremely complex. However, an upgrade in measuring

technologies and tools can surely help to improve GHGs emissions estimates. As described by *Hertwich* (2013), diffusive emissions can be directly measured using surface water chambers or derived from boundary layer models, while ebullitive fluxes are usually measured using bubble capturing funnels or, more recently, echosounders; degassing emissions can be calculated from the difference in gas concentrations upstream and downstream of the dam and the turbine discharge (*Abril et al.*, 2005). Nevertheless, water bodies can be very extended and remarkably different from each other, making measurements highly expensive and/or uncertain, as well as quite difficult to generalize or to apply directly to other case studies (*Song et al.*, 2018).

In addition, the scientific literature on this topic shows a lack of a shared methodology (*Prairie et al.*, 2018). For example, methane bubble emissions are often underestimated or not even considered due to the stochastic nature of ebullition and the consequent problems in measurements (*Hertwich*, 2013; *Lohrberg et al.*, 2020). According to *Deemer et al.* (2016), $CH_4$ bubble emissions can constitute up to about 99% of total methane flux; hence, excluding them from the calculations can severely compromise the quality of the estimates. The studies made by *Teodoru et al.* (2011), *DelSontro et al.* (2011) and *DelSontro et al.* (2010) on reservoir from both tropical and temperate regions put in evidence the spatial heterogeneity of both diffusive and ebullitive emissions, adding even more uncertainty to global results.

As stated by *Deemer et al.* (2016), drawdown emissions are another phenomenon often poorly considered. They occur when fluctuating water levels create zones that are periodically dry and then inundated. Drawdown areas are usually shallow and characterized by rapid regrowth of vegetation, thus significantly contributing to systemwide GHGs emissions (*Barros et al.*, 2011; *St. Louis et al.*, 2000). In general, drops in hydrostatic pressure during water level drawdowns can enhance $CH4$ bubbling rate in the whole reservoir (*Deemer et al.*, 2016).

As well as improving the quality of the estimates, global GHGs emissions from hydropower reservoirs can be reduced by encouraging a basin-wide strategic development of dam projects, for example by favoring the construction of hydroelectric plants characterized by high energy densities (*Almeida et al.*, 2019). The next section will expand this fundamental concept.

## 1.3 Strategic dam planning

It is now clear how hydropower is simultaneously a very important option of electricity production from a renewable energy source and a potential threat to the ecosystems where the plants are built, both at the local and basin scale. So, how can these negative impacts be reduced to guarantee sustainable hydropower development?

River networks are very complex and interconnected systems, and the decision of where, when, and if construct a dam should not be taken only considering the local surroundings, ignoring the impacts that can occur downstream and upstream of the plant site. The traditional approach was mainly based on uncoordinated project-by-project planning, without a strategic analysis of cumulative dam impacts and benefits, which very often resulted in sub-optimal trade-offs between hydropower production and consequences on ecosystem goods, services, and processes (*Schmitt et al.*, 2019). Strategic planning considers instead a larger spatial scale (at best, even the whole hydrographic basin), taking into account the heterogeneity of river networks and favoring sustainable hydropower development. Obviously, strategic planning will not eliminate the impacts of future dams, but it has the potential to identify better tradoffs between dam impacts and benefits, set limits for sustainable development, and finally improve hydropower outcomes (*Schmitt et al.*, 2018a).

*Soncini-Sessa et al.* (2007) underlined the necessity to reverse the "top-down" approach of the standard planning methodology in favor of a "bottom-up" participatory and integrated planning procedure, in which the stakeholders are not just informed or consulted, but also involved in the design and evaluation of the alternatives and ideally even in the final choice. The principle of integration in the decision-making process should manifest itself at many levels, among the different parts that compose the system, among the stakeholders and the political decision-makers (DMs), and among the stakeholders themselves, particularly between those who benefit and those exposed to negative impacts. As stated by *Giuliani et al.* (2012), the presence of multiple, distributed, and institutionally-independent, but physically-interrelated, decision-makers (DMs), as well as many conflicting stakeholders, is a major challenge to the optimal planning and management of water resources, especially in large-scale systems. For this reason, a multi-agent approach can provide a promising and feasible alternative to the traditional centralized, mostly uncoordinated methodology. In particular, the authors focused their attention on upstream-downstream relationships among different agents of water systems, evaluating several degrees of cooperation and information sharing. They concluded that,

for instance, increasing the degree of information exchange without imposing constraints on the agents' decisions allows downstream agents to better adapt to the upstream behaviors, thus incurring lower costs.

As highlighted by *Richter et al.* (2010), dam designs, operational plans, and potential impacts need to be assessed by interdisciplinary teams, including natural, physical and social scientists, in order to address the full spectrum of ecological and social values. In addition, the authors mentioned the importance of including a program of monitoring, evaluation, and adjustment (commonly referred to as "adaptive management") in every dam project, supported by continuous data collection. They also pointed out that all these measures would be far easier, less expensive, and more politically acceptable if integrated into dam development plans at the very earliest stage. Nevertheless, *Brismar* (2002) noticed that, despite the introduction of national laws and regulations and international conventions to protect environmental interests, many dam projects continued to be planned and implemented without proper attention to the ecological impacts.

*Jager et al.* (2015) attempted to define general spatial design principles for sustainable hydropower development in river basins. In particular, the authors tried to find out what could be the best way to arrange dams within the river network by answering these questions:

- *Is it better to build fewer mainstem dams or more tributary dams?*
- *Should dams be clustered or distributed among distant subbasins?*
- *Where should dams be placed along a river?*
- *At what spatial scale should decisions be made?*

The answers to these questions should not be interpreted as universal solutions which would be valid in every context, but rather as general guidelines that can be used as a starting point for every strategic dam siting problem.

Regarding the first question, the authors reported that building fewer large mainstem dams is generally more cost-effective than building more dams on smaller rivers due to the high capital cost of dams and associated infrastructure construction. Energy potential is also reliably higher in rivers draining large areas because flows are higher and more consistent than those in smaller tributaries. On the other hand, mainstem dams can have larger ecological impacts, especially on sediment and fish connectivity, than a larger number of smaller dams within tributaries. This results in a trade-off between energy and ecological values. In some cases, both objectives can be satisfied by avoiding the

placement of mainstem dams characterized by low energy densities (*Almeida et al.*, 2019).

Considering now the second question, the authors advanced the hypothesis that concentrating dams within a subset of tributary basins can lead to higher ecological benefits than distributing dams across all tributary basins with a lower density of dams in each basin. Secondly, distributing freshwater reserves among the remaining tributary basins can allow to reduce spatially autocorrelated exposure to risks and preserve upper portions of migration corridors. Moreover, even if clustering dams within fewer tributary basins seems to be an energy-neutral decision, this allows infrastructure to be shared, thus reducing construction costs. However, this configuration is also more vulnerable to power shortages related to drought, which can be buffered by spreading dams across sub-basins with different weather and flow patterns.

For what concerns the third question, placing dams in series is desirable from the hydropower production point of view, since the same amount of water can be used to generate electricity at each dam. On the other hand, adding more dams to the same river can induce cumulative negative ecological effects. In any case, the length of the undammed reach between the dams is a crucial parameter to verify if this section can sustain a population of a given species.

Finally, regarding the fourth question, the authors pointed out how decisions are often made taking into account political boundaries, while government entities and stakeholders should instead consider watershed boundaries that are relevant to aquatic biota. In general, expanding the project scale leads to solutions with higher ecological value and with a broader range of choices, enabling a more sustainable hydropower development.

To date, the relevance of strategic planning in river networks has been recognized by several studies. *Winemiller et al.* (2016) put efforts into finding a balance between tapping hydropower potential and preserving the biodiversity of large tropical rivers. *Ziv et al.* (2012) evaluated trade-offs between hydropower, fish biodiversity, and food security in the Mekong River Basin. Strategic planning can even be applied to dam removal projects, in which multi-objective optimization is used to balance hydropower production, sediment and fish connectivity, habitat restoration, and economic losses (*Kuby et al.*, 2005; *Zheng et al.*, 2009; *O'Hanley et al.*, 2013).

Recently, advanced analyses have been made regarding sediment connectivity in large river systems (*Schmitt et al.*, 2018b,a, 2019). The innovative framework applied by the authors in the Mekong River Basin (in particular, the CASCADE modeling framework described in Section 3.3.1) allowed to make significant progress in this area of study. The latest addition to the topic is repre-

sented by GHGs emissions from hydroelectric reservoirs, which have indeed been considered only by very recent studies. *Almeida et al.* (2019), in their study on the Amazon River Basin, demonstrated how strategic dam planning could minimize aggregate carbon intensity as hydropower generation expands. This work of thesis will focus on the research of trade-offs between hydropower production, sediment connectivity of the river system, and GHGs emissions from reservoirs, simultaneously considered.

## 1.4 Motivation and goals of the study

In the scientific literature, there are many studies that highlight the importance of strategic dam planning for sustainable hydropower development. However, many of them are just based on the maximization of hydropower production. Sometimes, the strategic dam planning approach is applied accounting for hydropower and one environmental objective. For example, *Schmitt et al.* (2019) analyzed how to find the best trade-offs between hydroelectric production and river sediment connectivity in the Mekong River Basin. Moreover, studies that include GHGs emissions from reservoirs, such as the one of *Almeida et al.* (2019) on the Amazon River Basin, are very rare.

In this work of thesis we developed a framework for strategic dam planning accounting for both river sediment connectivity and GHGs emissions. In detail, we asked ourselves these research questions:

- *Which combinations of dams give the best trade-offs between hydropower production, river sediment supply, and GHGs emissions?*
- *How much the optimization problem results are robust to uncertainty in the estimations of input data related to sediment and GHGs?*
- *Which are the dams characterized by the most uncertainty?*
- *What is the consequence of the project-by-project planning approach?*
- *Considering the current basin dam portfolio, what are the actual planning possibilities?*

To answer these questions, we started from the work of *Schmitt et al.* (2019), and, adding the findings of *Almeida et al.* (2019), we formulated an optimization problem with three objectives: maximize hydropower production and sediment supply, while minimizing GHGs emissions from reservoirs. We started by considering a pristine basin, where no dam has yet been constructed, to investigate the full spectrum of possibilities that the basin could have offered

before being altered by the current hydropower development. Then, we performed Sensitivity Analyses on GHGs emissions and river sediment connectivity input data, to assess the robustness of the outcomes. Lastly, we repeated these procedures considering the current basin dam configuration to evaluate the actual planning possibilities.

We organized this work of thesis into five chapters, the first of which is the present introduction. The other chapters can be briefly described as follows:

- Chapter 2 will give a general overview of the Mekong River Basin, which is the case study of this thesis;
- Chapter 3 will describe the methodology followed to perform the optimizations, from the available data to the models used to elaborate them;
- Chapter 4 will present step-by-step the results of all the optimizations;
- Chapter 5 will be dedicated to the conclusions, discussing the main findings shown in Chapter 4, the limitations of the study, and the possible future developments.

The goal of this work of thesis consists in giving a contribution to the scientific literature regarding the topic of strategic dam planning. The novelty of our approach consists in considering simultaneously hydropower production, river sediment connectivity, and GHGs emissions, in order to better understand the cumulative impacts of dam construction at a basin scale in a context characterized by high uncertainty, such as the Mekong River Basin. We claim that this methodology is essential to allow sustainable hydropower development in a global framework in which is increasingly of vital importance.

# 2

# Case Study: the Mekong River Basin

## 2.1 Location and geography

The Mekong River is the longest river in South-East Asia and the 8th longest river in the world. From its origins in the Tibetan Plateau in China at 5,160 *m* elevation, the Mekong River flows for about 4,909 *km* through Myanmar, Laos, Thailand, Cambodia, and Vietnam, where it finally discharges into the South China Sea (Fig. 2.1). With a mean annual discharge of 475 $km^3$, the Mekong River can be considered the 10th largest river in the world. Laos contributes some 35% of this water, followed by Thailand and Cambodia (18% each), China (16%), Vietnam (11%), and Myanmar (2%). The river basin drains a total land area of 795,000 $km^2$, 25% of which is located in Laos, 23% in Thailand, 21% in China, 20% in Cambodia, 8% in Vietnam, and 3% in Myanmar. The Mekong River Basin (MRB) is commonly divided into two sections: the Upper Mekong River Basin, which comprises the Tibet and Yunnan regions in China, and the Lower Mekong River Basin, which extends downstream the border between China, Laos, and Myanmar until the South China Sea (*Mekong River Commission (MRC)*, 2022; *CGIAR Research Program on Water, Land and Ecosystems (WLE)*, 2022).

The Upper MRB, where the Mekong River is known as Lancang River, makes up 24% of the total drainage area and contributes 15-20% of the water that flows into the Mekong River. The catchment here is characterized by very steep topography, through which the river rushes down narrow gorges. The tremendous altitude drop of approximately 4,500 *m* makes this part of the

**Figure 2.1:** *Mekong River Basin with the political boundaries of the different countries. (Paul, 2019)*

river particularly suitable for generating hydroelectric energy. On the other hand, soil erosion has been a major problem and about 50% of the sediment in the river comes from this section (*Paul*, 2019; *CGIAR Research Program on Water, Land and Ecosystems (WLE)*, 2022).

From North to South, the Upper MRB can be further subdivided into three zones: the Tibetan Plateau, the Three Rivers Area, and the Lancang Basin (see Fig. 2.2). The source of the Mekong is situated in the Tibetan Plateau, the most densely glaciated region on earth. Then, the river continues its journey in the Three Rivers Area, where the Mekong flows closely in parallel with two of the region's other great rivers: the Salween River and the Yangtze River. In this mountainous stretch, there are no significant tributaries. Before leaving China, the Mekong runs through the Lancang Basin, a still relatively elevated highland

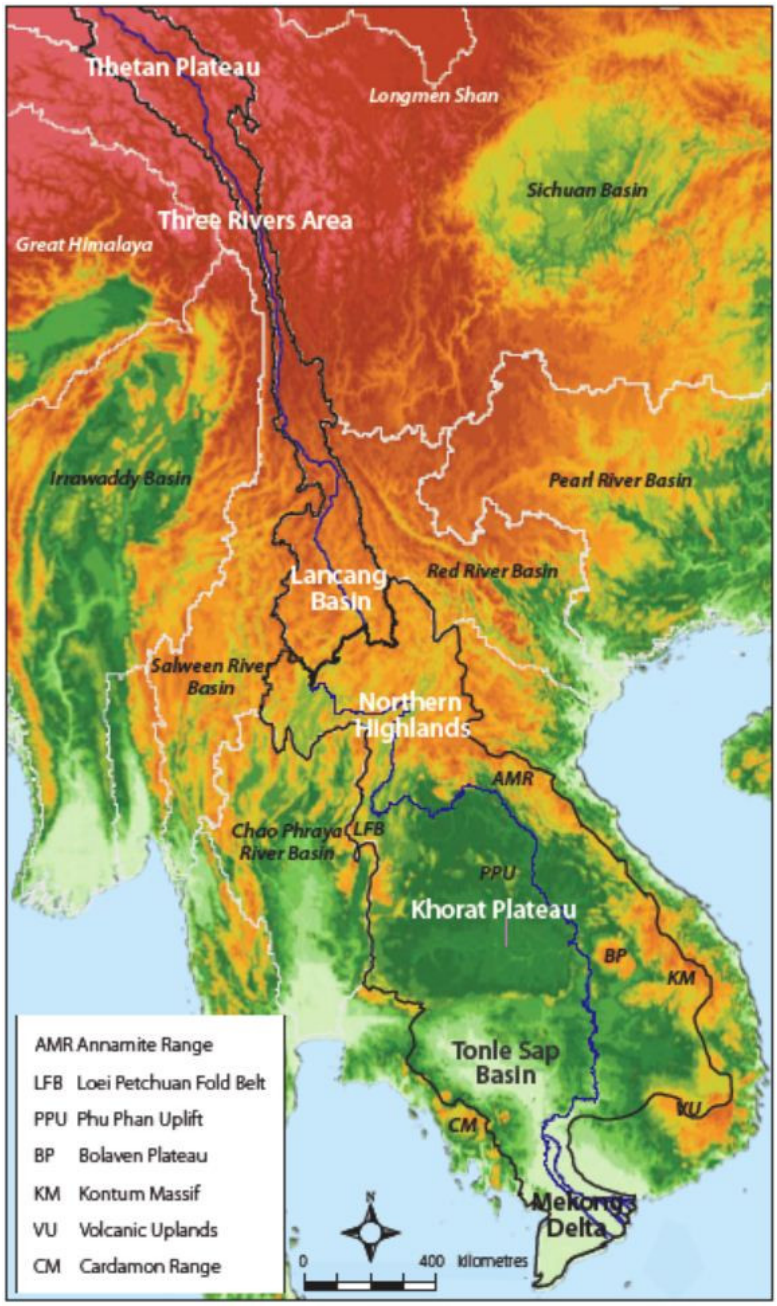


**Figure 2.2:** *Topography and geographic regions of the Mekong River Basin. (Mekong River Commission (MRC), 2022)*

and plateau area (2,000-3,000 *m* above sea level). Here, small tributary catchments drain into the river from both sides of the mainstream (*Mekong River Commission (MRC)*, 2022).

The Mekong continues its course downstream the Chinese border entering the Lower MRB, which is functionally subdivided into four geographic regions: Northern Highlands, Khorat Plateau, Tonle Sap Basin, and the Mekong Delta

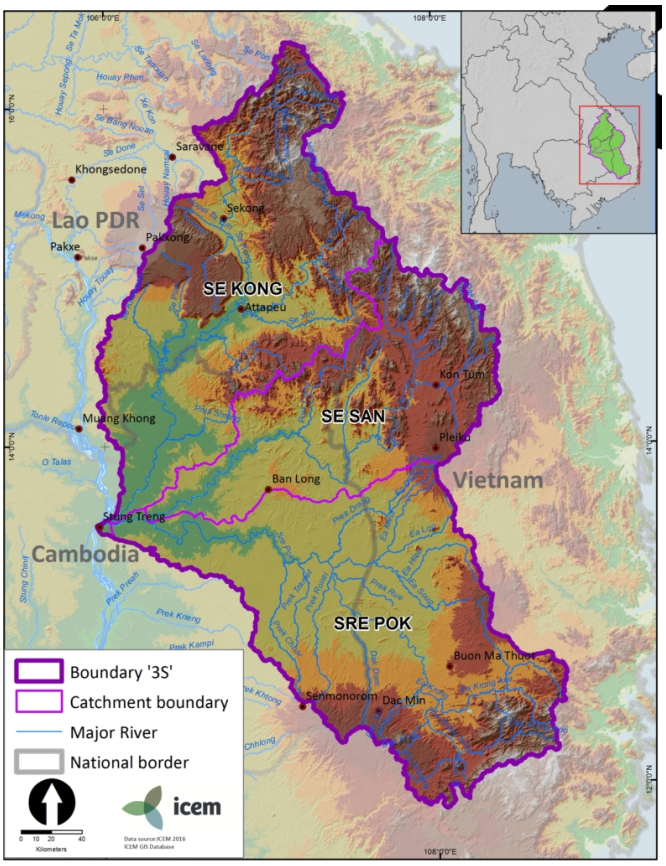


**Figure 2.3:** *Map of the "3S Basin". (International Centre for Environmental Managenment (ICEM), 2016)*

(see Fig. 2.2). As it flows through the Northern Highlands and the Khorat Plateau, the Mekong widens and the major tributary systems develop. Of particular relevance is the so-called "3S Basin", located in the south-eastern area of the Mekong River Basin (Fig. 2.3). It owes its name to the Se Kong, Se San, and Sre Pok tributaries, which are among the most important in the entire Mekong River Basin.

The Tonle Sap Basin is a large alluvial plain surrounded by hills, characterized by the presence of the Tonle Sap Lake (also known as "Great Lake") located in the Cambodian floodplains. The seasonal cycle of changing water levels of the Mekong River at Phnom Penh, the Cambodian capital, results in the peculiar "flow reversal" of water into and out of the lake: during the dry season, the Tonle Sap Lake drains into the Mekong River via the Tonle Sap River; during the wet season, the high flows in the Mekong River cause the Tonle Sap River to reverse its flow direction to flood the Tonle Sap Lake; and, at the end of the wet season, the flow of the Tonle Sap River reverts again to the downstream direction, draining excess water off the inundated floodplain surrounding the

Tonle Sap Lake.

Phnom Penh also marks the beginning of the Mekong Delta. Here, the Mekong River and the Bassac River, the Mekong's largest distributary river channel, branch off into numerous smaller watercourses and enter a large fertile plain in southern Vietnam. The wedge-shaped delta covers an area of 70,000 $km^2$ at elevations mostly below 3 $m$ above sea level and experiences regular annual flooding, essential to the preservation of local ecosystem goods and services (*Mekong River Commission (MRC)*, 2022; *CGIAR Research Program on Water, Land and Ecosystems (WLE)*, 2022; *Kuenzer et al.*, 2013).

## 2.2 Natural resources and biodiversity

The Mekong River Basin is characterized by a vast range of geographic and climatic zones. As a result, among the world's river basins, the Mekong River Basin is the second most biodiverse basin, since only the Amazon possesses a greater diversity of plants and animals (*Mekong River Commission (MRC)*, 2022). The water irrigates large tracts of forest and wetlands, serving as habitats for thousands of species, as well as providing food, medicines, and building materials to the 65-70 million people living in the basin (*Paul*, 2019; *Kondolf et al.*, 2018).

According to *Mekong River Commission (MRC)* (2022), about 40% of the people living in the Lower MRB are established within 15 $km$ of the Mekong River, most of them within 5 $km$ of the mainstream. For many of them, the river is of crucial importance in terms of food security, livelihood, and access to trade. In particular, the MRB is the site of the biggest inland fishery in the world, which produce around 2.5 million tonnes of protein every year (*Mekong River Commission (MRC)*, 2022; *Baran and Myschowoda*, 2009). An estimated 40 million rural people are involved in the fishery, two-thirds of the entire basin rural population (*CGIAR Research Program on Water, Land and Ecosystems (WLE)*, 2022). As anticipated, the MRB is also a biodiversity hot-spot for many fish species, most of them characterized by large-scale longitudinal migrations (*Ziv et al.*, 2012; *Poulsen et al.*, 2002).

As regards climate and hydrology, the Mekong River Basin is an extremely complex system with highly variable inter- and intra-annual flows. Given the considerable extension of the MRB, its climate ranges from high-altitude continental and temperate in the upper basin to tropical monsoonal in the lower basin. In particular, the climate of the Lower MRB is dominated by the Southwest Monsoon, which gives rise to wet and dry seasons of approximately equal length: the monsoon season lasts from June to November, with heavy rainfall in

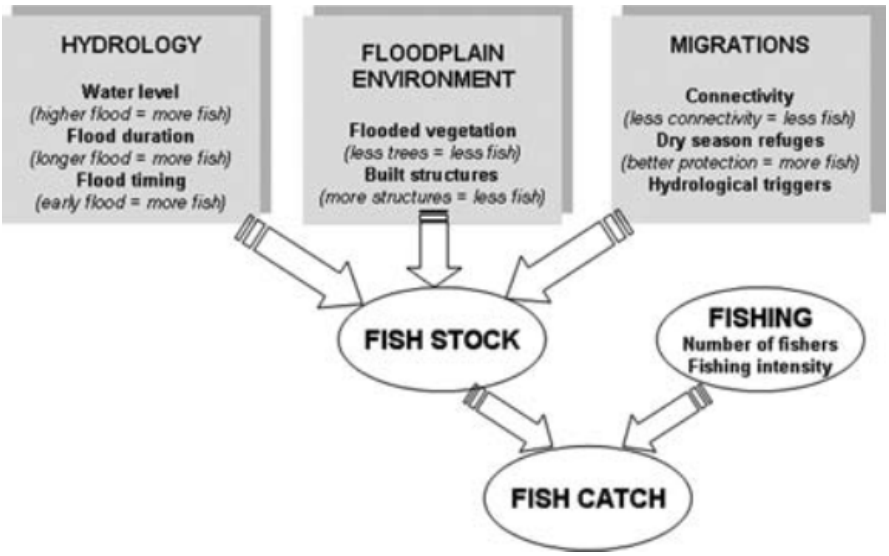


**Figure 2.4:** *Major factors driving fish production in the Mekong River Basin. (Baran and Myschowoda, 2009)*

most of the basin, while the dry season from December to May, with cooler temperatures and low rainfall in most areas, except for the Mekong Delta. Roughly 74% of the total annual flow is delivered to the Mekong River from tributaries in the Lower MRB, with the flood season contributing to approximately 70-80% of this amount (*Mekong River Commission (MRC)*, 2022). Indeed, many of the local ecosystems have developed as a result of seasonal flow variations. For example, as described by *Poulsen et al.* (2002) and *Baran and Myschowoda* (2009), there is an intimate link between fish life cycles, fish habitats, and hydrology.

Migrating fishes respond to hydrological changes and use hydrological events as indicators for the timing of their migrations (Fig. 2.4). In the Lower MRB there is no exception, and wetlands, generated and sustained by annual flooding events, are of fundamental importance (Fig. 2.5). During the dry season, fish migrate to deep pools in the mainstream to seek refuge; then, when the flood season starts, they migrate back to spawning and nutrient-rich feeding grounds on floodplains. Wetlands also play a vital role in supporting the livelihoods of local people, providing a productive environment for agriculture, fishery and tourism. In addition, wetlands offer several important indirect benefits, such as absorbing potentially disastrous floodwaters during the wet season and preventing erosion in the delta's coastal areas (*Mekong River Commission (MRC)*, 2022).

One of the most important floodplain complexes of the Lower MRB is associated with the Tonle Sap Lake system in Cambodia (*Poulsen et al.*, 2002). During the peak of the flood season, the lake's surface area increases from around

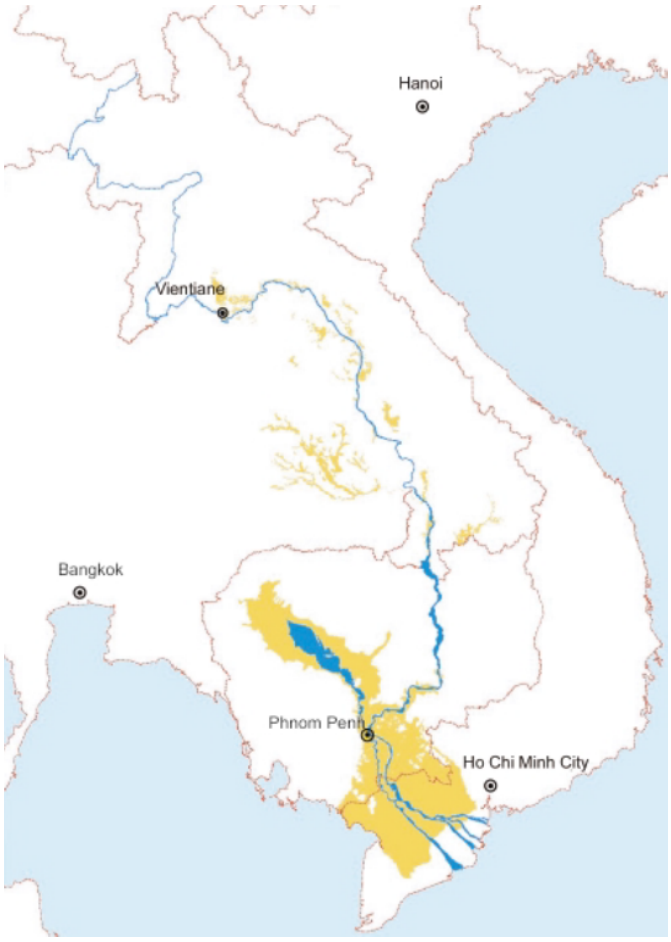


**Figure 2.5:** *Main floodplains areas of the Lower Mekong River Basin. (Poulsen et al., 2002)*

2,500 $km^2$ to around 15,000 $km^2$, and its volume increases from about 1.5 $km^3$ to about 60-70 $km^3$. This hydrological cycle, also characterized by the peculiar "flow reversal" phenomenon (see Section 2.1), supports the lake's rich biodiversity, including fish, wildlife, and plants on which many local communities rely for their livelihoods. For instance, 40% of the Cambodian population depends on the Tonle Sap Lake and its floodplains for both income and food supply (*Mekong River Commission (MRC)*, 2022). To further highlight the value of the wetlands of this region, *Kuenzer et al.* (2013) described how the fish yield in the Tonle Sap Lake system could be up to 850% higher than in the floodplains of, for example, the Amazon or the Brahmaputra.

Another region of great interest is the Mekong Delta, mostly situated within Vietnam. It is among the world's largest river deltas and its rich resources are of vital importance for the about 18 million Vietnamese living here, as they account for some 40% of agricultural production in the country, including 50% of rice harvest (2.5% of global production). Rice and fishery products contribute

significantly to export earnings and account for approximately 27% of the Gross Domestic Product (GDP). The socio-economic importance of the Mekong Delta is also underlined by the presence of the city of Ho Chi Minh (7.5 million inhabitants), which accounts for 17% of Vietnam's GDP and 25% of Vietnam's industrial output (*Paul*, 2019; *Kondolf et al.*, 2018; *Schmitt et al.*, 2019). Deltas are built, shaped, and sustained by the sediment and nutrients delivered from the entire upstream river basin. Thus, they are also impacted cumulatively by all the upstream disturbances. Since the Mekong Delta land surface is mostly below 3 $m$ above sea level, this region is particularly vulnerable to any human-induced changes in the river's hydrology and sediment transport regime, and in the delta's sediment budget. Global Climate Change and sea level rise, together with sand mining practices and dam construction, can severely put in danger this complex ecosystem and its inhabitants (*Kondolf et al.*, 2018; *Kuenzer et al.*, 2013).

In the last decades, the Mekong River Basin is experiencing an unprecedented boom in the construction of hydropower plants, and dam site selection matters greatly for conserving biodiversity, especially for large projects (*Winemiller et al.*, 2016). For example, fish diversity is inevitably reduced by dam construction, which physically blocks movements that connect populations and enable migratory species to complete their life cycle (see Section 1.2.1). Moreover, large dams attenuate seasonal flood pulses, reducing fish access to floodplains that are essential nursery areas and feeding grounds. Flood timing is another key factor for the sustainability of fish impacted by dam construction. Since the timing of fish migrations is "tuned" to the flood pulse, any variations in the natural flow regime can put at risk the success of seasonal breeding migrations.

Furthermore, as described in Section 1.2.2, damming also involves sediment trapping processes, which contribute to a loss of productivity for fisheries as well as for agriculture (*Baran and Myschowoda*, 2009; *Poulsen et al.*, 2002). As anticipated, ecological impacts of large dams are not limited to rivers: trapping sediment alters nutrient dynamics and other biochemical processes in deltas and other wetlands ecosystems, which in turn impact agriculture, fisheries, and human settlements. It is therefore clear the need for strategic and sustainable basin-wide dam planning. Without it, species extinctions, declines in fisheries, agriculture, and other ecosystem services are certain to accompany hydropower development in the Mekong River Basin (*Winemiller et al.*, 2016; *Ziv et al.*, 2012).

## 2.3 Geopolitical situation and the Mekong River Commission

As it flows from the Tibetan Plateau to the South China Sea, the Mekong River runs through six countries: China, Myanmar, Laos, Thailand, Cambodia, and Vietnam (Fig. 2.1). The Mekong River Basin is therefore shared among these riparian nations, both geographically and administratively. However, the great geomorphic and hydrologic heterogeneity, and the difficult political and social realities of the transboundary basin gave rise to an intricate and delicate situation (*Schmitt et al.*, 2019). In fact, each of the six countries has a complex history of power relations with its neighbors, which still influences their perceptions and dialogue.

Power distribution within the MRB is defined particularly by strategic position. Upstream development and behavior strongly influence downstream regions directly and indirectly, both in an environmental context of impacts on water flow, sediment availability, river ecology, and biodiversity, and in an economic context of electricity production, navigability, and monetary flow. Upstream locations provide considerable power, and China's additional power, especially in political, economic, and military terms, further complicates the situation. For the same reason, Vietnam, since it is the most downstream nation, it is also the most vulnerable. All this led to a rising need for a basin-wide debate on the balance between economic progress and ecological preservation. However, up to the present day, several border disputes remain unresolved (*Kuenzer et al.*, 2013).

As a consequence, hydropower development in the basin proceeded essentially "project-by-project", where each country tried to exploit its maximum hydropower potential without a strategic analysis of cumulative dam impacts and benefits. An attempt to improve this complex situation was made in 1995, when an agreement between the basin countries (except for Myanmar and China) gave birth to the Mekong River Commission (MRC) (*Schmitt et al.*, 2019). With the so-called "1995 Mekong Agreement", the four member countries established the goals and principles by which they intended to cooperate in matters of water management, sustainable development, and environmental protection (*Mekong River Commission (MRC)*, 2022). However, notifications about dam construction are almost never comprehensive, member countries often do not adhere to consultation procedures, and sharing of data (e.g., regarding hydrology, sediment, and water management policies) is almost always incomplete. To give a concrete example, although the "1995 Mekong Agreement" requires international consultations before constructing mainstem dams, tributary dams are within national jurisdiction and necessitate only a "notification" to the MRC

Joint Committee (*Ziv et al.*, 2012).

Additionally, China mostly acts as just an observer, and not as a member. Consequently, with its enormous political power and strategic position, China can exert considerable control over the hydrology of the whole Lower MRB, while participating neither in the consultation process nor in efforts for data and knowledge sharing. Despite some attempts to increase transboundary cooperation in recent years with projects such as the Lancang-Mekong Cooperation (2016), the situation remains far from being optimal (*Schmitt et al.*, 2019).

Nevertheless, the role of the Mekong River Commission in taking a step towards sustainability and cooperation should certainly not be underestimated. *Suhardiman et al.* (2015) demonstrated how the MRC, despite operating in a constrained political environment, has used Strategic Environmental Assessments (SEAs) as a way of providing political space and opening the discussion on dams to a wider public. The authors described how SEAs, even if often criticized for being just political means to justify already made decisions, can instead be exploited to shape governance alliances at both national and transboundary levels, and to a certain extent democratize decision-making processes. However, as a donor-funded project, SEAs are unable to override national decisions made by member countries and the MRC cannot force them to comply with the findings and recommendations of the assessment. At least, SEAs helped to shift the decision-making process from a top-down, elitist, sectoral-ministry-focused authority to a "soft space" with fuzzier governance boundaries and active involvement of NGOs, environmental ministries, civil society groups, and international agencies.

The MRC developed many other programs with the objective of establishing a more sustainable context in the Mekong River Basin, such as the "Joint Environmental Monitoring (JEM)" project and the "Procedures for the Maintenance of Flows on the Mainstream (PMFM)". The first aims to implement enhanced data collection and sharing about hydrology, water quality, ecosystems health, fisheries, and sediment (*Mekong River Commission (MRC)*, 2020a). The second set out a framework for how to maintain minimum or maximum levels of river flow of the Mekong mainstream and reverse flow of Cambodia's Tonle Sap River (see Section 2.1) (*Paul*, 2019). However, despite the important steps forward in recent years, one of the biggest issues on this topic is represented by the almost complete lack of data collection and research on GHGs emissions from dam reservoirs, being it a concern that has been raised only very recently.

## 2.4 Hydropower development in the Mekong River Basin

The transboundary Mekong River Basin remained pristine until relatively recently. Some dams were built in the 1960s in Thailand and Laos, but regional conflicts, political struggles, and wars delayed most of the basin's economic development until the mid-1990s, when the Manwan hydroelectric dam was built on the Lancang River, China (see Fig. 2.2). From the mid-1990s to the early 2000s, dam development accelerated in China and Vietnam, with the construction of a dense cascade of dams on the lower Lancang and tributary dams in the Vietnamese highlands (*Kondolf et al.*, 2018). Nowadays, the Mekong River Basin has been dubbed the "Battery of South-East Asia" for its large hydropower potential, estimated to be approximately 268,000 $GWh/year$, of which around half has been developed (*Schmitt et al.*, 2019).

According to *Mekong River Commission (MRC)* (2020b), as of 2019, there are 89 hydropower projects in the Lower MRB, with 12,285 MW total installed capacity. Of these, 65 are in Laos (8,033 $MW$ installed capacity), 7 in Thailand (1,245 $MW$ installed capacity), 2 in Cambodia (401 $MW$ installed capacity), and 14 in Vietnam (2,607 $MW$ installed capacity). By 2040, hydropower is estimated to generate more than 30,000 $MW$ (see Fig. 2.6). In the Upper MRB, China has constructed 11 hydropower dams, and another 11, each with an installed capacity of over 100 $MW$, are planned or under construction. The total production capacity is estimated to increase from 21,310 $MW$ to 31,606 $MW$. Although on a much smaller scale, hydropower is also starting to be developed in a tributary of the Upper MRB in Myanmar, with the first dam commissioned in 2017 and construction of further dams by both Chinese and Myanmar developers expected. Fig. 2.7 shows the current hydropower development at the scale of the entire Mekong River Basin.

As anticipated in previous sections, hydropower development brings both positive and negative consequences. On one hand, the increasingly rapid dam construction will help to meet the rising energy demand of the Mekong riparian countries, especially China, Thailand, and Vietnam. For instance, the energy demand of the Lower MRB is projected to grow at 6-7% annually. Moreover, the development of hydropower brings synergies with other water-related sectors (including expanding irrigation that is key to food security), provides access to electricity that is key to poverty reduction, contributes to navigation that enhances regional trade, and provides flood and drought management that is crucial to Climate Change adaptation and mitigation (*Mekong River Commission (MRC)*, 2020b; *Kuenzer et al.*, 2013). On the other hand, dam construction can have severe negative impacts on the environment and the livelihoods of the

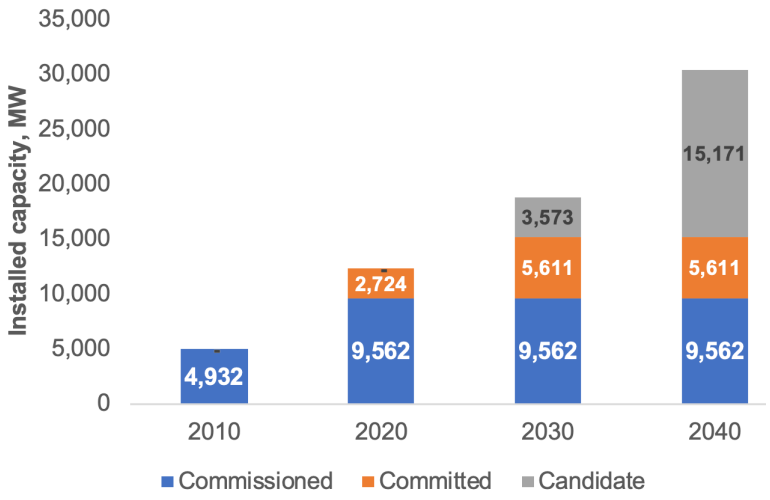


**Figure 2.6:** *Commissioned, committed, and potential hydropower projects in the Lower Mekong River Basin. (Mekong River Commission (MRC), 2020b)*

rural Mekong River population, mainly affecting water flow, sediment load, and GHGs emissions (see Section 1.2.1).

For example, since the Lancang Basin is estimated to contribute about 50% of the Mekong River's total sediment load, dams built in this area alone would reduce the Mekong's total sediment load by around 50%. This, together with hydrological alterations, will likely decrease the Lower MRB floodplains ecosystem's primary productivity by 34% (*Kondolf et al.*, 2018).

As stated by *Kondolf et al.* (2018), the ultimate effects regarding the Mekong Delta would even be more devastating: the construction of all dams of the entire MRB as planned would reduce the sediment delivery to the delta ranging from 60% to 96%. According to the authors, without concrete and effective measures, it is likely that nearly half of the Mekong Delta's land surface will be below sea level by 2100, with the remaining areas impacted by salinization and frequent flooding.

In addition, despite the economic gains from full hydropower development in the Lower MRB and in the Upper MRB are estimated at respectively US$ 160 billion and US$ 4 billion by 2040, potential costs can be extremely high as well. The decline of fisheries could cost nearly US$ 23 billion, the loss of forests and wetlands may cost up to US$ 145 billion, and rice growth along the Mekong River will be severely reduced. Although fish farms, irrigation schemes, and expanding agriculture could totally or partially compensate for these losses, they may not always be feasible and the results will be anyway uneven between countries (*Mekong River Commission (MRC)*, 2020b).

Unfortunately, because of the complex geopolitical situation, hydropower

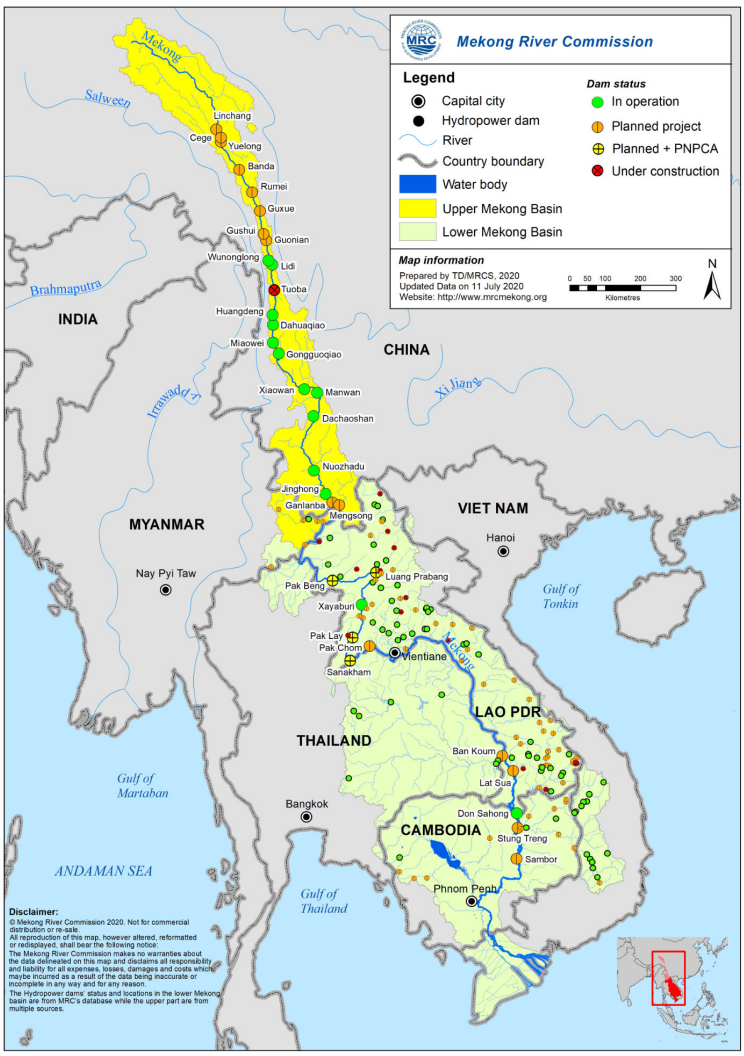


**Figure 2.7:** *Current hydropower development in the Mekong River Basin. (Mekong River Commission (MRC), 2020b)*

development in the Mekong River Basin has proceeded essentially "project-by-project", without a strategic analysis of cumulative dam impacts and benefits (see Section 2.3). This, together with the very low participation and integration of stakeholders, has led to concerns and objections from the local population. For instance, in Thailand, opposition to large-scale power plants was so strong that the government increasingly favored the importation of hydroelectric energy from neighbor countries (Laos and Myanmar), thus outsourcing social and environmental impacts.

Another thorny topic of discussion regards the large-scale transboundary impacts of the mainstem cascade of dams in Lancang Basin, which are held responsible for the alteration of the overall Mekong River flow, both in the

present and even more in the future. China has an optimistic vision of improving inter-annual flow regulation or attenuation. However, the downstream countries are against this perception. In fact, the latter are worried about a possible intensification of the inter-annual flow differences, which in the long-term may imply high environmental and social costs due to bank erosion, water shortage, increased irrigation challenges, and shifts in biodiversity. At the same time, it is often overlooked that the numerous mainstem dams also planned in Laos, Cambodia and Vietnam would certainly have similar regional (although different local) effects, further aggravating the situation at the scale of the whole MRB (*Kuenzer et al.*, 2013).

In addition, according to the study made by *Ziv et al.* (2012), the construction of all planned tributary dams, nearly all within Laos national borders, would have graver impacts on fish biodiversity basin-wide and on the Cambodian and Vietnamese floodplain's fish productivity, than the combined impacts of the six planned upper mainstem dams on the Lower MRB. In the light of all these possible negative consequences, the strong need for basin-wide strategic dam planning becomes evident (see Section 1.3).

## 2.5 Previous studies on dam sediment trapping and GHGs emissions

As anticipated in Section 1.4, this work of thesis will put particular emphasis on the matter of dam sediment trapping and GHGs emissions in the Mekong River Basin. This section will provide an overview of some of the most important recent findings.

A significant contribution related to the sediment budget of the Mekong River was given by *Kondolf et al.* (2018). The authors described how, since the Lancang Basin is estimated to contribute about 50% of the Mekong River's total sediment load, dams built in this area alone would reduce the Mekong's total sediment load by around 50%. However, the ultimate reduction of sediment to the Mekong Delta will strongly depend upon which dam portfolio (i.e., combination of dam sites) is developed in the mainstem and tributaries of the Lower MRB: the construction of all dams as planned would reduce the sediment delivery to delta ranging from 60% to 96%. Additionally, the results of this study consider the total sediment load, but the dams are more likely to trap coarser material, disproportionately passing the finer sediments; therefore, a total 50% total sediment reduction will likely translate into more than a 50% reduction in delta deposition, because the remaining sediment will be finer and thus more

easily transported to the sea. This research reports that a 57% sediment reduction is already evident at Chiang Saen (Thailand), the most upstream measurement station on the Lower MRB, since the construction of the Manwan dam in 1993. As proof of this, an analysis by *Koehnken* (2014) shows that the sediment load entering the Lower MRB from China has decreased from an average of 84.7 $Mt/year$ (1960-2002) to 10.8 $Mt/year$ at Chiang Saen. Downstream, at the measurement station of Pakse (in Laos, nearly 150 $km$ before Cambodia's border), this value has decreased from an average of 147 $Mt/year$ to 66 $Mt/year$.

Studies regarding improving trade-offs between hydropower production and sediment connectivity in the Mekong River Basin were performed considering first the Se Kong, Se San, Sre Pok ("3S") Basin (*Schmitt et al.*, 2018a,b), and then extending the analysis to the whole Mekong River Basin (*Schmitt et al.*, 2019). The 3S Basin, despite covering only around 10% of the total drainage area, contributes up to 25% of the basin's total sediment load (about 25 $Mt/year$ out of 100-160 $Mt/year$). Specifically, since the 3S Basin plays a crucial role as a source of sand for the Mekong Delta, *Schmitt et al.* (2018a,b) focused on the transport of sandy bed material rather than on total load. What they found is that, with strategic planning, 68% of the hydropower potential of the 3S Basin could have been developed while trapping 21% of the basin's sand load. Instead, the current dam portfolio resulting from project-by-project planning exploits 54% of the hydropower potential while trapping 91% of the sand load. The authors also described that the magnitude of sediment delivery from each tributary to the Mekong River is controlled by some specific reaches of low transport capacity (also named "bottlenecks").

These analyses highlighted the need to consider a basin scale perspective, since trade-offs improve at a larger planning scale. For this reason, *Schmitt et al.* (2019) extended the previous studies to the entire MRB compiling a database of 124 large dam projects in the six riparian countries. According to the authors, around 59,000 $MW$ capacity could be installed at these dam sites, which would result in a generation of around 268,000 $GWh/year$. In general, dams located in the lower Mekong mainstem have much less favorable trade-offs (i.e., high sediment trapping compared to their hydropower generation), than the dams located in the Upper MRB, due to the high gradient and large flow of the Lancang River. Some lower basin countries are thus limited to a portfolio of dam sites with unfavorable trade-offs between hydropower and sediment trapping. After the completion of all the projects under construction, the current dam portfolio will cumulatively reduce sediment supply to the delta from an estimated pre-dam load of 160 $Mt/year$ to 52 $Mt/year$ (corresponding to a 125,000 $GWh/year$ hydropower production). In addition, constructing all dams

would trap 95% of the transported sediment, reducing the sediment supply to the delta to around 9 $Mt/year$.

According to *Schmitt et al.* (2019), the hypothesis of implementing whole-basin-scale strategic planning is quite unrealistic due to the complex political situation. Nonetheless, limiting the research of the best trade-offs only to the scale of the Lower MRB could represent a valuable and more realistic alternative. In any case, the resulting dam portfolios alone do not yield information on how to sequence the development. The goal of dam sequencing is not only to derive optimal dam portfolios, but also to determine the sequence with which dams should be built to match a certain future hydropower demand. Hence, guidance on the development sequence can result in better trade-offs for whatever portfolio is lastly developed.

As regards of GHGs emissions from hydropower reservoirs in the Mekong River Basin, a massive contribution was given by the study made by *Räsänen et al.* (2018). The authors based their analysis on 119 existing and planned hydropower reservoirs in the basin, with a focus on atmospheric gross emissions through the reservoir water surface. They were found to have an emission range of 0.2-1994 $kg\,CO_2\,eq/MWh$ over a 100 year lifetime, with a median of 26 $kg\,CO_2\,eq/MWh$. 82% of hydropower reservoirs have GHGs emissions comparable to other renewable energy sources (<190 $kg\,CO_2\,eq/MWh$), while the rest can have emissions even higher than fossil fuel power plants (>380 $kg\,CO_2\,eq/MWh$). What can be immediately noticed by these results is the extremely high variability of the values of GHGs emissions (even of some orders of magnitude), which indeed depend on a large number of factors (see Section 1.2.3). Even if the authors themselves consider this work tentative, what is clear is that hydropower in the MRB cannot be considered categorically as low-emission energy. On the contrary, GHGs emissions from hydropower reservoirs should be carefully examined case-by-case, possibly together with other impacts on the natural and social environment.

Another important contribution regarding the topic of GHGs emissions from hydropower reservoirs comes from the study made by *Almeida et al.* (2019). In this case, the location of the research is not the Mekong River Basin, but instead the Amazon River Basin, one of the world's largest untapped hydropower frontiers. Despite the different study sites, many analogies can be found in the results. According to the authors, most of the proposed upland dams (92% for a 100-year time horizon and 60% for a 20-year time horizon) would likely result in carbon intensities below 80 $kg\,CO_2\,eq/MWh$, which is a reference value for sustainable electricity generation defined by the International Energy Agency (IEA) (*Bouckaert et al.*, 2021). On the contrary, only a mi-

nority of lowland dams would be expected to emit less than 80 $kg\,CO_2\,eq/MWh$ (36% for a 100-year time horizon and 14% for a 20-year time horizon). In fact, considering a 20-year time horizon, about 25% of the proposed lowland dams would likely be more carbon-intensive than coal-fired power plants. Since total GHGs emission is proportional to flooded area (see Section 1.2.3), lowland dams tend to have significantly higher carbon intensities due to their typically larger reservoir areas and innately lower power densities (i.e., electricity generation capacities per unit of reservoir flooded area), whereas the steeper topography of high-elevation regions favors hydropower projects with higher power densities. Building dams without basin-wide coordination has led to a current dam portfolio with a collective carbon intensity of about 90 $kg\,CO_2\,eq/MWh$ (100-year time horizon) and about 200 $kg\,CO_2\,eq/MWh$ (20-year time horizon). However, the authors claim that if future hydropower dams are selected optimally, it will be possible to develop approximately 80% (75 $GW$) of the total proposed electricity generation capacity while creating a portfolio of new dams with an aggregate carbon intensity below 80 $kg\,CO_2\,eq/MWh$ over a 100-year time horizon. By contrast, uncoordinated dam planning may result in portfolios of new dams with collective carbon intensities incompatible with sustainable energy goals.

All of these recent findings have contributed to making some important steps toward a more sustainable hydropower development, both in terms of sediment connectivity and GHGs emissions. This work of thesis, which presents a strategic dam planning approach that includes both the phenomena simultaneously, aims to take a further step in this direction.

# 3

# Materials and Methods

## 3.1 Available dam data

Hydropower in the Mekong River Basin has developed relatively recently, and consequently also scientific studies and data collection about it. For this reason, data on reservoir characteristics, sediment transport, and GHGs emissions are very often scarce.

The dam database used for this work of thesis comes from the study made by *Schmitt et al.* (2019), slightly modified and corrected. The authors collected information from published dam databases (*Mekong River Commission and others*, 2014; *International Rivers*, 2014; *Open Development Mekong*, 2014), assigning some key parameters to each dam site, such as location, mean annual flow ($m^3/year$), total storage ($m^3$), and mean annual hydropower generation ($GWh/year$). Unfortunately, even if some non-available data were estimated by interpolation from neighbor dam sites or global geospatial data, some values are still missing in the final dataset.

The resulting database used in this work of thesis is composed of 123 dams, 32 of which are Existent and already operating ("E"), 23 under Construction ("C"), and 68 Planned ("P"). The spatial distribution of all the dams in the basin subdivided by status is reported in Fig. 3.1.a. With the currently developed portfolio, the total electricity generation is around 88,000 $GWh/year$, while the total hydropower production that would result from the implementation of all projects is around 267,000 $GWh/year$ (corresponding to a total installed capacity of around 59,000 $MW$).

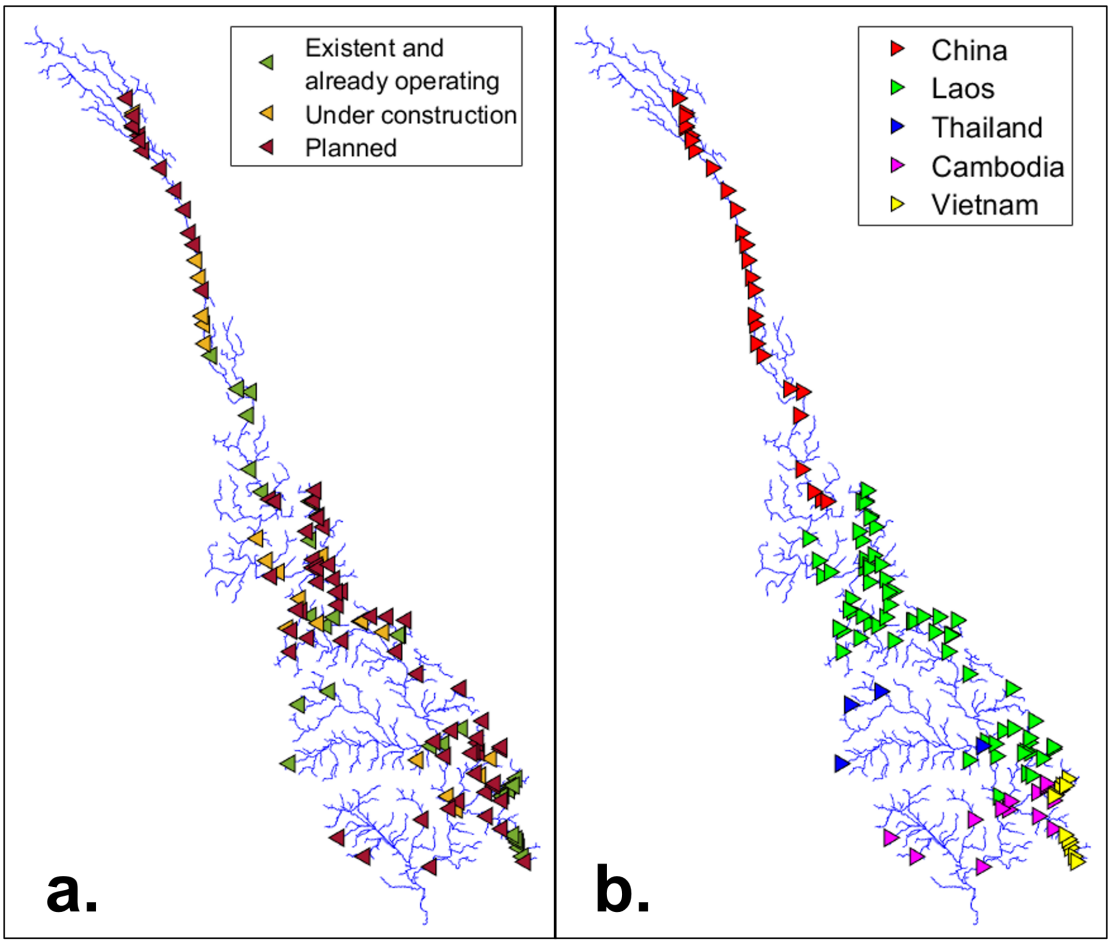


**Figure 3.1:** *(a) Spatial distribution of all the dams in the Mekong River Basin subdivided by status: Existent and already operating ("E"), under Construction ("C"), and Planned ("P"). (b) Spatial distribution of all the dams in the Mekong River Basin subdivided among the six riparian countries.*

The dams are distributed among the riparian countries as such: 27 in China (about 155,000 $GWh/year$ generation), 66 in Laos (about 77,000 $GWh/year$ generation), 4 in Thailand (about 750 $GWh/year$ generation), 13 in Cambodia (about 23,000 $GWh/year$ generation), and 13 in Vietnam (about 11,000 $GWh/year$ generation). To date, Myanmar has no listed existing or potential dams in the basin. Fig. 3.1.b shows the spatial distribution of all the dams in the basin subdivided by country.

In Section 3.2 we will explain how we estimated GHGs emissions for each dam included in the dataset. In order to simulate the sediment transport within the basin and the effects of dam construction, the dam database was then integrated within a river network model, described in Section 3.3.

## 3.2 GHGs emissions estimates

On-field measurements or reliable estimates are almost completely missing in the Mekong River Basin. To date, there exist published GHGs emissions measurements only for three reservoirs in Laos (*Räsänen et al.*, 2018). For this reason, the estimates of GHGs emissions from each dam reservoir were computed through empirical formulas and added to the dam database.

We followed the same procedure applied in the study made by *Almeida et al.* (2019) on the Amazon River Basin. The authors started from the work published by *Deemer et al.* (2016), which provided a global estimate of GHGs gross fluxes from reservoirs, taking into account both ebullition and diffusion phenomena (see Section 1.2.3). In particular, *Almeida et al.* (2019) considered only $CO_2$ and $CH_4$ fluxes, since $N_2O$ fluxes generally represent less than 5% of the total gross $CO_2\,eq$ emissions from reservoirs.

The total net GHGs emissions from each dam reservoir were computed as follows:

$$GHG_{net,tot}(d) = A(d) \times (net_{CO_2} \times F_{CO_2}(d) + net_{CH_4} \times F_{CH_4}(d) \times GWP_{CH_4}) \times \\ \times (1 + R_{downstream}) \tag{3.1}$$

where $GHG_{net,tot}(d)$ is the total net GHGs flux ($kg\,CO_2\,eq/day$) for each dam ($d$), $F_{CO_2}(d)$ and $F_{CH_4}(d)$ are respectively the gross $CO_2$ and $CH_4$ fluxes ($kg/km^2/day$), and $A(d)$ is the reservoir flooded area ($km^2$) (*Deemer et al.*, 2016). To convert $CH_4$ emissions into $CO_2\,eq$ emissions, the net methane flux has been multiplied by a $GWP_{CH_4}$ equal to 34 $kg\,CO_2\,eq/kg\,CH_4$, which is the conversion factor for the global warming potential of methane over a 100-year time horizon (*Myhre*, 2013). Since turbine intakes often draw methane-rich bottom waters, an extra amount of $CH_4$ is emitted downstream the dam (see Section 1.2.3). To account for this, a multiplier factor of $(1 + R_{downstream})$ has been applied to the calculation, where $R_{downstream}$ is a constant representing the ratio of downstream emissions to reservoir-surface emissions, estimated to be 17% (*Forsberg et al.*, 2017). Since $F_{CO_2}$ and $F_{CH_4}$ refer to gross fluxes, it has been necessary to convert these values to net GHGs emissions, in order to account only for the net (anthropogenic) change associated with reservoir creation. Correction factors has been applied according to the findings of *Prairie et al.* (2018). In absence of land cover information, the authors suggested to conservatively assume that 75% of the gross $CO_2$ emissions and 10% of the gross $CH_4$ emissions existed also in the pre-impoundment conditions. Hence, correction factors $net_{CO_2}$ and $net_{CH_4}$ has been respectively put equal to 0.25 and 0.90.

Then, the Carbon Intensity ($kg\,CO_2\,eq/MWh$) of each dam was calculated as follows:

$$CI(d) = \frac{GHG_{net,tot}(d)}{HPP_{day,tot}(d)} + CI_{construction} \tag{3.2}$$

where $HPP_{day,tot}(d)$ is the total hydropower production of a given dam over a day ($MWh/day$) and $CI_{construction}$ is a constant representing the Carbon Intensity associated with construction and infrastructure of hydropower dams, estimated to be equal to 19 $kg\,CO_2\,eq/MWh$ for a 100-year time horizon (*Edenhofer*, 2015).

As described in Section 1.2.3, GHGs fluxes are naturally affected by a large variability, making these Carbon Intensity estimates subjected to high uncertainty. For this reason, the GHGs fluxes data reported by *Deemer et al.* (2016) were re-sampled through a bootstrapping procedure with equal probability, combined, and summed 10,000 times. In this way, 10,000 values of total net GHGs emissions ($kg\,CO_2\,eq/day$) were obtained for each dam, and, by applying Eq. 3.2, the respective values of Carbon Intensity were calculated. Lastly, the ultimate Carbon Intensity value for each dam was computed as the average of the correspondent 10,000 values.

### 3.2.1 Time horizon of the analysis

As seen in the previous section, we used Eq. 3.1 to estimate the GHGs emissions from each dam reservoir. As one can notice, the selection of the time horizon is a very important choice, because of its influence on the $GWP_{CH_4}$ value.

Different GHGs have different warming potential and atmospheric residence times. Hence, in order to compare the radiative forcing effects of different GHGs, a Global Warming Potential (GWP) index is assigned to each of them. GWP is defined as the heat absorbed by any GHG in the atmosphere, as a multiple of the heat that would be absorbed by the same mass of carbon dioxide ($CO_2$). Therefore, by definition, GWP of $CO_2$ is equal to 1, while for all other gases it depends on the time horizon taken into account. The most widely used values are 100-year and 20-year. The choice of the latter instead of the first prioritizes GHGs with shorter lifetimes, since it ignores any impact that occurs after 20 years from the emission.

The atmospheric residence time of $CH_4$ is relatively short (around 12 years), but it has a very strong radiative forcing effect. Consequently, the GWP of methane on a 20-year time horizon (84 $kg\,CO_2\,eq/kg\,CH_4$) is much higher than the corresponding 100-year value, which is about equal to 34 $kg\,CO_2\,eq/kg\,CH_4$

(*Myhre*, 2013). In this work of thesis, we considered a 100-year time horizon, because it is a typical value for the lifespan of large infrastructures, such as dams. However, it is important to be aware that considering such a time horizon means to under-represent the high potential radiative forcing effect of dams over short timescales.

## 3.3 River sediment connectivity estimation

In this work of thesis, we implemented the CASCADE model to simulate the river sediment connectivity within the Mekong River Basin. In this section, we will provide a general framework of the CASCADE model (Section 3.3.1) and we will describe how the dam dataset was integrated within it (Section 3.3.2).

### 3.3.1 CASCADE model and framework

As anticipated in Section 1.2.2, sediment connectivity, which describes the transfer of sediment between multiple sources to sinks in terms of magnitude, transport time, and grain size, represents a key aspect in river networks, since it is directly linked to fluvial processes and ecosystem goods and services. One of the impacts of dam construction is the trapping of sediments that are transported by rivers throughout their basins (*Schmitt et al.*, 2016; *Tangi et al.*, 2019).

Modeling basin-scale sediment connectivity and its response to dam construction is a difficult task. A huge step forward in this regard was made with the study made by *Schmitt et al.* (2016), in which the authors presented for the first time the CASCADE (CAtchment Sediment Connectivity And DElivery) modeling framework. The model combines concepts of graph theory with empirical sediment transport formulas to quantify sediment transfers between many connected sediment sources and sinks in a river network. According to the authors, CASCADE should be considered a flexible, exploratory tool to project the local impacts on sediment connectivity onto a basin-wide scale. It is a 1D conceptual model, particularly suitable in situations where the lack of data, the case study scale, and the need to explore different development scenarios would not allow the implementation of 2D or 3D physically-based models.

In the CASCADE model, each sediment cascade establishes connectivity between a specific source and its multiple sinks. From a source perspective, the fate of sediment is controlled by its detachment and downstream transport capacity, resulting in a specific trajectory of transfer and deposition. From a sink perspective, CASCADE traces back all sediment inputs to their sources and de-

termines the total local sediment flux, the flux of each grain size, the spatial distribution of sources, and the connection times between sources and sinks. In this way, CASCADE is able to identify emerging patterns of sediment connectivity and the location of "bottlenecks", i.e., reaches where a large amount of sediment is deposited (*Schmitt et al.*, 2016).

Fig. 3.2 displays the key concepts and steps behind the CASCADE modeling framework. The real-life river network (Fig. 3.2.A) is converted into a directed acyclic graph (Fig. 3.2.B), which represents the network topology as a set of nodes and edges (Arabic numerals). Each edge (also named "reach"), which is the core modeling unit, represents a part of the river network with homogeneous geomorphic and hydraulic features. Each reach is assigned a set of hydromorphologic attributes related to sediment transport, such as discharge flow, grain size distribution, drainage area, and channel slope, length, width, roughness. Some of them are derived from a Digital Elevation Model (DEM), others from models, surveys, field data, or a mixture of those (*Tangi et al.*, 2019). Then, multiple sediment sources are identified in the river network (Roman numerals), each one with its specific grain size (dot size) and sediment supply (Fig. 3.2.C). In this step, also barriers (e.g., dams) are added to simulate sediment obstacles. Barriers are modeled using a simple representation of reservoir hydraulics, empirical formulas, or from observed trapping rates (*Tangi et al.*, 2019). The sediment from each source is transported along an individual sediment cascade. Therefore, the river graph is expanded to represent the attributes of each cascade separately (Fig. 3.2.D). After that, each cascade is assigned a specific transport capacity (line width) in each reach downstream of its source (Fig. 3.2.E). The calculated transport capacity does not yet consider the presence of multiple sediment cascades in the same reach. The more cascades that are present in a river reach, the less energy is available for each cascade. This competition for the available energy (Fig. 3.2.F) reduces the transport capacity for each cascade (compare line widths between Fig. 3.2.E and Fig. 3.2.F). The sediment routing associated with each cascade is determined as a function of sediment supply and the local competition-corrected transport capacity (Fig. 3.2.G). Sediment is deposited if the input to a reach exceeds the local transport capacity (downward arrows in Fig. 3.2.G). Sinks are defined as reaches where a cascade deposits sediment. Hence, a reach can act as a sink for multiple cascades. Finally, connectivity information of each reach (Fig. 3.2.H) can be derived from the assemblage of cascades connected to them, which defines sediment provenance (i.e., the location of the sources), connection time to each source, and the sorting and magnitude of the total sediment delivery to a reach (*Schmitt et al.*, 2016).

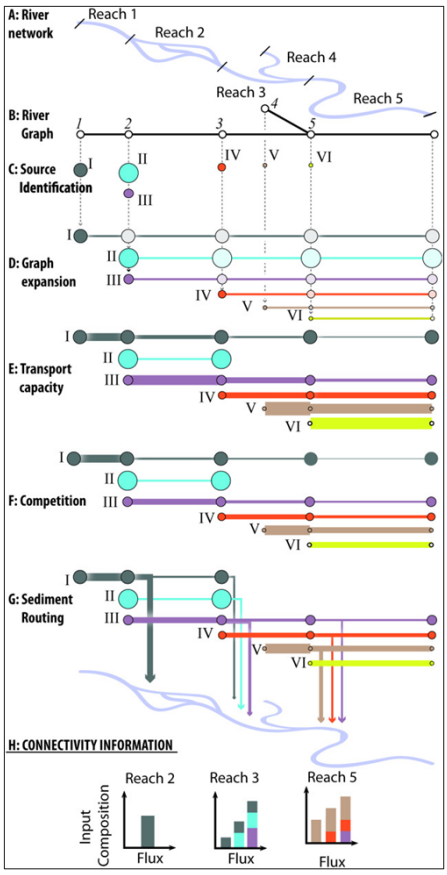


**Figure 3.2:** *Key concepts and steps behind the CASCADE modeling framework. (A) River network subdivision into reaches. (B) River graph representation by nodes and edges (Arabic numerals). (C) Identification of multiple sediment sources (Roman numerals), each one with its specific grain size (dot size) and sediment supply. (D) River graph expansion to represent attributes of each cascade separately. (E) Definition of the transport capacity for each reach (line width). (F) The competition for the available energy reduces the transport capacity for each cascade. (G) Cascade specific, edge-to-edge sediment routing. (H) Connectivity information of each reach can be derived from the assemblage of cascades connected to them. (Schmitt et al., 2016)*

In this work of thesis, the CASCADE modeling framework will be implemented in MATLAB environment in order to simulate the sediment transport and connectivity at the entire Mekong River Basin scale, and assess the impact of dam construction for several different portfolios.

### 3.3.2 CASCADE and sediment available data

All the information regarding the Mekong River network and sediment transport used in this work of thesis comes from the study made by *Schmitt et al.* (2019). The authors represented the natural sediment transport through the basin using a combination of the CASCADE framework (see Section 3.3.1) for sediment supply (*Schmitt et al.*, 2016) and distributed geomorphic estimates for

sediment yield in the Mekong River Basin (*Kondolf et al.*, 2014b). The procedure can be summarized as follows.

*Kondolf et al.* (2014b) divided the Mekong River Basin into nine "Geomorphic Provinces" based on topography, climate, tectonic history, and lithological parameters (Table 3.1 and Fig. 3.3), and assigned a specific sediment yield ($t/km^2/year$) to each geomorphic province such that the total load at the basin outlet matched an estimated value of 160 $Mt/year$. Then, *Schmitt et al.* (2019) derived the drainage area and the river network from a 250-$m$ resolution digital elevation model (DEM) (*CGIAR Consortium for Spatial Information (CSI)*, 2008). They assigned a sediment source to each reach in the network and computed the sediment supply rate of each source from the direct drainage area and the sediment yield of the geomorphic province in which a reach was located.

Lastly, the sediment trapping efficiency of each dam was calculated using the Brune model (Fig. 1.4), an empirical model based on the hydraulic residence time of each dam's reservoir (*Brune*, 1953). The Brune model was chosen because of its limited data demand, which makes it particularly suitable for data-poor settings, such as the Mekong River Basin. Originally, *Brune* (1953) conceived its model for suspended sediment only, while the Mekong River transports a relevant fraction of sandy bedload (*Bravard et al.*, 2013). Hence, the Brune trapping efficiency was corrected assuming that each reach transports 10% of the total load as sand, which is completely trapped behind dams (*Turowski et al.*, 2010).

| **Geomorphic Province** | **Sediment yield** |
|---|---|
| Lancang | 372 $t/km^2$ |
| Northern Highlands | 207 $t/km^2$ |
| Loei Fold Belt | 132 $t/km^2$ |
| Annamite Mountains | 165 $t/km^2$ |
| Mun-Chi Basin | 33 $t/km^2$ |
| Kon Tum Massif | 231 $t/km^2$ |
| Tertiary Volcanic Plateau | 240 $t/km^2$ |
| Tonle Sap | - |
| Delta | - |

**Table 3.1:** *The nine "Geomorphic Provinces" of the Mekong River Basin and the corresponding sediment yield. (Kondolf et al., 2014b)*

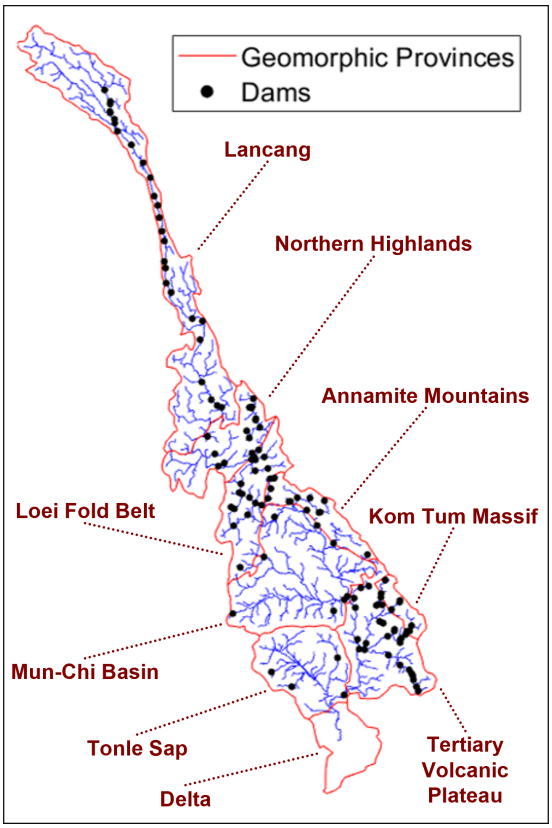


**Figure 3.3:** *The Mekong River Basin subdivided into nine "Geomorphic Provinces" based on topography, climate, tectonic history, and lithological parameters. (Kondolf et al., 2014b)*

## 3.4 The optimization problem: finding Pareto Optimal dam portfolios

To solve a strategic dam planning optimization problem means to find among different possible portfolios (i.e., combinations of dam sites), the ones that show the best trade-offs between some objectives defined "a-priori". In particular, in this work of thesis we considered simultaneously three objectives: maximize hydropower production and sediment supply to the delta, while minimizing GHGs emissions from reservoirs. Hence, the decision problem can be formulated as

$$\max_{u}(J_1(u), J_2(u), -J_3(u)) \tag{3.3}$$

in which $J_1$ is the indicator for sediment supply to the delta ($t/year$), $J_2$ is the indicator for hydropower production ($GWh/year$), $J_3$ is the indicator for GHGs emissions from reservoirs ($kg\,CO_2\,eq/year$), and $u$ is a binary decision vector which identifies a particular portfolio.

Note that, since the optimization problem was formulated as a maximization problem, the third objective indicator presents a minus sign in order to

be consistent with the other two. The decision vector $u$ consists of 123 binary decision variables (one for each dam site), which indicate whether a dam is included in the portfolio ("1") or not ("0"). The optimal solutions ($u^*$) of the decision problem consist of the "Pareto-Optimal portfolios" (PO portfolios), i.e., solutions that cannot be improved with respect to one objective without worsening at least one of the others. In the objective space, the set of all optimal solutions composes the Pareto front, i.e., all the portfolios which show the best trade-offs between the three objectives (*Soncini-Sessa et al.*, 2007). All the equations used to compute the three indicators are presented hereafter.

### 3.4.1 Indicator for sediment supply to the delta

The procedure followed to calculate the indicator for sediment supply to the delta derives from the study made by *Schmitt et al.* (2019). For further information regarding the methodology and data availability refer to Section 3.3. The CASCADE modeling framework was used to simulate sediment transport throughout the whole river network and the impact of dam construction under alternative dam development scenarios. We chose to consider the sediment supply value computed at the delta since the latter, in the specific case of the Mekong River Basin, is particularly vulnerable to the cumulative impacts of dam construction on sediment delivery (see Section 2.2).

The pristine sediment supply to the delta ($\Theta_{S,\Omega}$) is represented by the sediment flux in the most downstream reach (denoted as $\Omega$), and it was computed as

$$\Theta_{S,\Omega} = \sum_{\varsigma \in \Gamma_\Omega} \Theta^{\varsigma}_{S,\Omega} \tag{3.4}$$

where $\Theta^{\varsigma}_{S,\Omega}$ is the sediment supply from a specific source $\varsigma$ to the delta, and $\Gamma_\Omega$ is the set of all sediment cascades (i.e., of all processes delivering the sediment from all upstream sources to the basin outlet).

The pristine sediment supply to the delta can be reduced if one or more dams are included in a dam portfolio ($P$). The amount of sediment trapped by a dam ($d$) depends on its Trapping Efficiency ($TE_d$). The modified sediment supply ($\Theta^{\varsigma}_{S,\Omega}(P)^*$) from a specific source $\varsigma$ to the delta, due to the presence of dams included in the portfolio $P$, was computed as

$$\Theta^{\varsigma}_{S,\Omega}{}^{*}(P) = \left[ \prod_{d \in D_{\varsigma,\Omega,P}} (1 - TE_d) \right] \times \Theta^{\varsigma}_{S,\Omega} \tag{3.5}$$

where $D_{\varsigma,\Omega,P}$ is the set of dams that are added between the source $\varsigma$ and the

basin outlet $\Omega$ as part of the portfolio $P$.

Finally, the indicator of the first objective of the optimization problem ($t/year$) for a specific portfolio $P$ was computed as the total modified sediment supply from all sources to the delta:

$$J_1(P) = \sum_{\varsigma \in \Gamma_\Omega} {\Theta^{\varsigma}_{S,\Omega}}^{*}(P) \tag{3.6}$$

### 3.4.2 Indicator for hydropower production

Hydropower generation data were obtained from the dataset built by *Schmitt et al.* (2019) from tabulated data. Missing data on generation were interpolated from the tabulated installed capacity (see Section 3.1).

The indicator of the second objective of the optimization problem ($GWh/year$) for a specific portfolio $P$ was calculated as the sum of the mean annual hydropower production ($HPP$) of all dams ($d$) included in the portfolio ($P$):

$$J_2(P) = \sum_{d \in P} HPP(d) \tag{3.7}$$

### 3.4.3 Indicator for GHGs emissions from reservoirs

GHGs emission from dam reservoirs were computed starting from the values of Carbon Intensity ($kg\ CO_2\ eq/GWh$), obtained by applying Eq. 3.2 (for further information regarding the procedure and data availability refer to Section 3.2). The mean annual GHGs emissions ($GHG$) from each dam reservoir ($d$) were calculated as

$$GHG(d) = CI(d) \times HPP(d) \tag{3.8}$$

where $CI(d)$ is the Carbon Intensity of the dam $d$ and $HPP(d)$ is the mean annual hydropower production ($GWh/year$) of the same dam $d$ (see Section 3.4.2).

The indicator of the third objective of the optimization problem ($kg\ CO_2\ eq/year$) for a specific portfolio $P$ was computed as the sum of the mean annual GHGs emissions ($GHG$) of all dams ($d$) included in the portfolio ($P$):

$$J_3(P) = \sum_{d \in P} GHG(d) \tag{3.9}$$

## 3.5 Borg Multi-Objective Evolutionary Algorithm

In this work of thesis, the strategic dam planning approach is applied by formulating the optimization problem presented in Section 3.4 (Eq. 3.3). Solving this decision problem allows finding the Pareto-Optimal portfolios, i.e., the combinations of dam sites that show the best trade-offs between the three objectives. Since the decision vector $u$ of this case study is composed of 123 Boolean variables, an exhaustive search of the optimal solutions through the entire set of feasible decisions ($U$) would require an enormous amount of time. The total number of possible combinations of dam sites (i.e., the total number of possible portfolios) can be computed as

$$C_{tot} = \sum_{k=1}^{n_{sites}} \frac{n_{sites}!}{k! \times (n_{sites} - k)!} \tag{3.10}$$

where $n_{sites}$ is the number of dam sites. In this case study, since $n_{sites}$ is equal to 123, a complete exploration of all possible solutions ($u \in U$) would require running the model a number of times in the order of $10^{37}$. For this reason, an optimization algorithm was implemented to significantly speed up the computations. This type of algorithm is able to find the optimal solutions ($u^*$) through the exploration of only a portion of the set of all feasible decisions ($U$).

Considering the context of this case study, we chose a Multi-Objective Evolutionary Algorithm (MOEA) to solve the optimization problem (Eq. 3.3). MOEAs are a class of random search optimization algorithms inspired by the processes of natural evolution (e.g., selection based on fitness to the environment, crossover of genes to produce new offspring, random mutation of genes) (*Hadka and Reed*, 2013). They belong to the category of heuristic methods, designed to explore the decision space using some smart strategy that allows to solve the optimization problem more quickly when classic methods are too slow or to find an approximate solution when classic methods fail to achieve any exact solution. This is done by trading optimality, completeness, accuracy, and precision to considerably cut computational times (*Pearl*, 1984). According to *Maier et al.* (2014), MOEAs are the most well-established class of heuristics for solving water resources problems. Hence, considering the framework of the optimization problem and the large set of decisions of this case study, it is easy to understand the reasons behind the choice of this type of algorithm.

Fig. 3.4 presents a general example of two-objectives optimization by means of an MOEA. Note that both the objective indicators ($J$) are to be minimized. Every point in the decision space is an "individual" (i.e., a decision vector $u$), and the components of $u$ represent its "genes". A set of individuals is called

"population". The first step of the procedure consists in selecting a random group of individuals as the initial population, and, by running the model, computing the respective performances in the objective space (Fig. 3.4.A). In this way, the objective vector $J$ measures the "fitness" of the corresponding individual. Then, a subset of solutions with the best performance is selected (green points) and "survives" to the next generation (becoming "parents"), the others are instead discarded (Fig. 3.4.B). At this point, crossover, mutation, and replacement are randomly applied to "parents" to generate the "offspring" (Fig. 3.4.C), i.e., the respective points in the decision space (red points). This procedure is repeated iteratively for every new population (Fig. 3.4.D), until a certain termination condition is reached (Fig. 3.4.E). In the end, the algorithm returns the population that minimizes the objective indicators, i.e., the set of Pareto-Optimal solutions.

The decision problem was solved by using the Borg Multi-Objective Evolutionary Algorithm (MOEA), developed by *Hadka and Reed* (2013). This optimization problem is an "a-posteriori" optimization problem, in which search precedes the decision-making process. As any iterative algorithm, the Pareto front is not completely explored. The aim of the Borg MOEA is to obtain the most accurate approximation of the Pareto front, which allows the decision-makers to explore the various trade-offs and select the best solution (or solutions) according to their preferences. Borg assimilates several design principles from existing MOEAs and introduces some novel components, such as an $\epsilon$-dominance archive with auto-adaptive operators that detect search stagnation, randomized restarts exploitation to escape local minima, and recombination operators selection based on their success in generating high-quality solutions.

One of the problems encountered when using MOEAs in real-world contexts is the inability to know "a-priori" which recombination operator performs best on a given problem. Borg implements a feedback loop in which recombination operators that produce more successful offspring are rewarded by increasing the number of offspring produced by that operator. This auto-adaptive multi-operator recombination makes Borg not a single algorithm, but a class of algorithms whose operators are adaptively selected based on the problem (*Hadka and Reed*, 2013).

Fig. 3.5 displays the flowchart of the Borg main loop. The auto-adaptive multi-operator procedure is used to choose one of the recombination operators. For a recombination operator requiring $k$ parents, one parent is randomly selected from the archive. The remaining $k$ - 1 parents are selected from the population using tournament selection. The resulting offspring are evaluated and then considered for inclusion in the population and archive. If the offspring

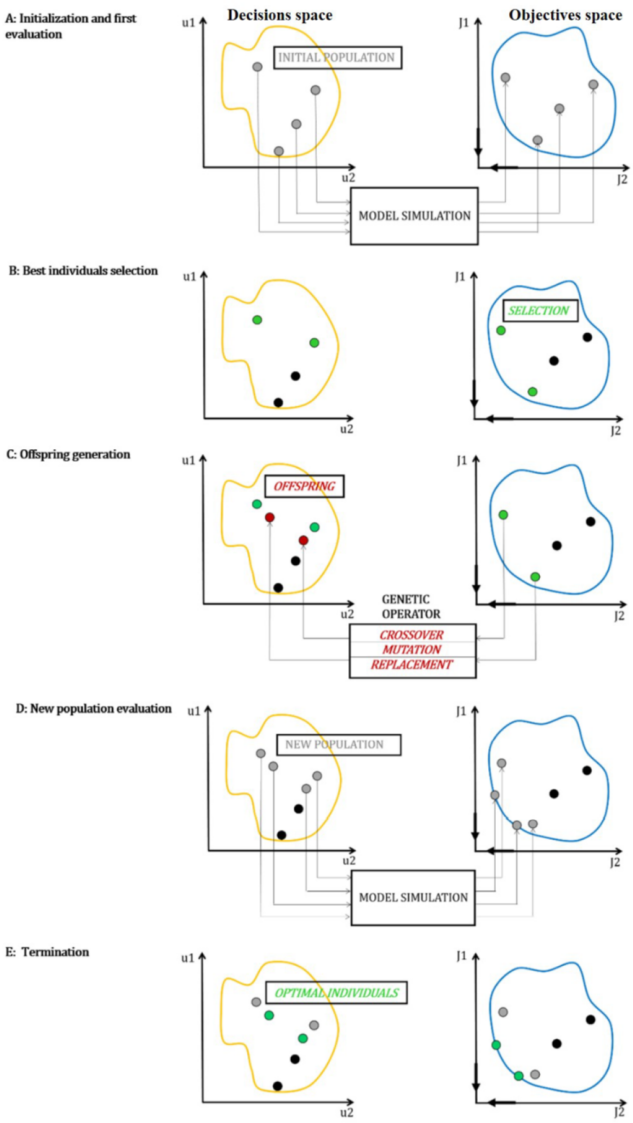


**Figure 3.4:** *General example of optimization by means of an MOEA. (A) A random group of individuals is selected as the initial population and the respective performances in the objective space are computed. (B) Solutions with the best performance are selected (green points). (C) Genetic operators are applied to the best solutions to generate "offspring" in the decision space (red points). (D) The procedure is repeated starting from the new population. (E) When a certain termination condition occurs, the algorithm returns the Pareto-Optimal solutions.*

dominates one or more population members, the offspring randomly replaces one of these dominated members. If the offspring is dominated by at least one population member, the offspring is not added to the population. Otherwise, the offspring is non-dominated and replaces a randomly-selected member of the population. Each iteration of this main loop produces one offspring.

"Deterioration" is a fundamental issue encountered by MOEAs. It occurs whenever the solution set discovered by an MOEA at time $i$ contains one or

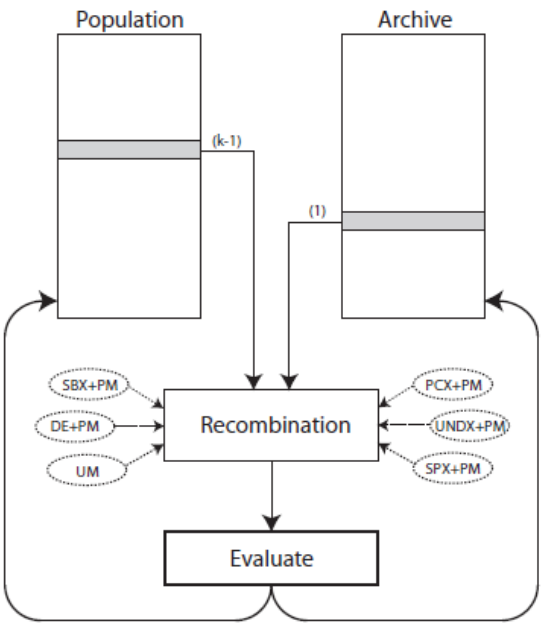


**Figure 3.5:** *Flowchart of the Borg main loop. The auto-adaptive multi-operator procedure is used to choose one of the recombination operators. For a recombination operator requiring k parents, 1 parent is randomly selected from the archive. The remaining k - 1 parents are selected from the population using tournament selection. The resulting offspring are evaluated and then considered for inclusion in the population and archive. (Hadka and Reed, 2013)*

more solutions dominated by a solution discovered at some earlier point in time $j < i$. In the extreme, deterioration can cause an MOEA to diverge away from the Pareto front. To counter this phenomenon, *Laumanns et al.* (2002) developed the "$\epsilon$-dominance archive", which guarantees simultaneous convergence and diversity in MOEAs. In the specific case of Borg, a variant called the "$\epsilon$-box dominance archive" is used. The latter divides the objective space into hyper-boxes with side-length $\epsilon$, called "$\epsilon$-boxes". Search stagnation due to pre-convergence to local minima is avoided by introducing the concept of "$\epsilon$-progress". $\epsilon$-progress defines $\epsilon$ as the minimum threshold for the improvement. An MOEA must periodically produce at least one solution whose improvement exceeds this threshold. If stagnation is detected, appropriate action can be taken to either revive the search or terminate the algorithm. Figure 3.6 displays a 2D example of how $\epsilon$-progress is measured. Existing archive members are indicated by "•", and the $\epsilon$-boxes dominated by these members are shaded in gray. New solutions are indicated by "×". Cases (1) and (2) show occurrences of $\epsilon$-progress: the new solutions reside in previously unoccupied $\epsilon$-boxes. Instead, case (3) shows the situation in which the new solution is accepted into the archive, but, since it resides in an already occupied $\epsilon$-box, it does not count towards $\epsilon$-progress (i.e., the improvement is below the threshold $\epsilon$).

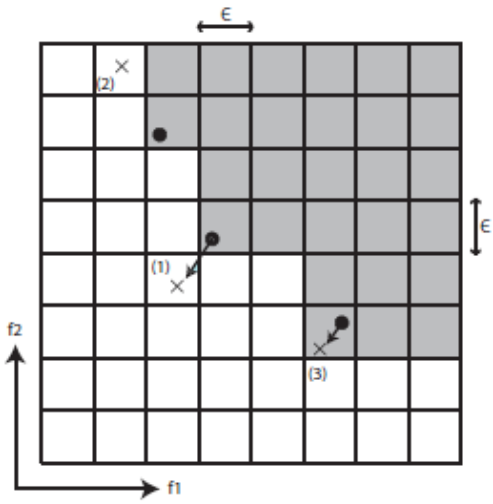


**Figure 3.6:** *2D example showing how $\epsilon$-progress is measured. Existing archive members are indicated by "•", and the $\epsilon$-boxes dominated by these members are shaded in gray. New solutions are indicated by "×". Cases (1) and (2) show occurrences of $\epsilon$-progress since the improvement is above the threshold $\epsilon$. On the contrary, the new solution of case (3) resides in an already occupied $\epsilon$-box, and therefore it does not count towards $\epsilon$-progress. (Hadka and Reed, 2013)*

"Restarts" are a mechanism for reviving search after stagnation is detected using $\epsilon$-dominance. Fig. 3.6 displays the flowchart of the Borg restart logic, which can be summarized in three main steps:

1. the search population size is adapted to remain proportional to the archive size;

2. the tournament selection size is adapted to maintain elitist selection;

3. the population is emptied and repopulated with solutions from the archive, with any remaining slots filled by mutated archive solutions ("injection").

The population-to-archive ratio ($\gamma$), which specifies the ratio of the population size to the archive size, is computed as follows:

$$\gamma = \frac{\text{population size}}{\text{archive size}} \geq 1 \tag{3.11}$$

At any point during the execution of the algorithm, if the population-to-archive ratio differs from $\gamma$ by more than 25%, the population size is adapted. Moreover, Borg is designed such that it maintains tournament sizes to be a fixed percentage of the population size. The population-to-archive ratio, together with $\epsilon$-progress, is checked periodically after a certain number of iterations of this main loop.

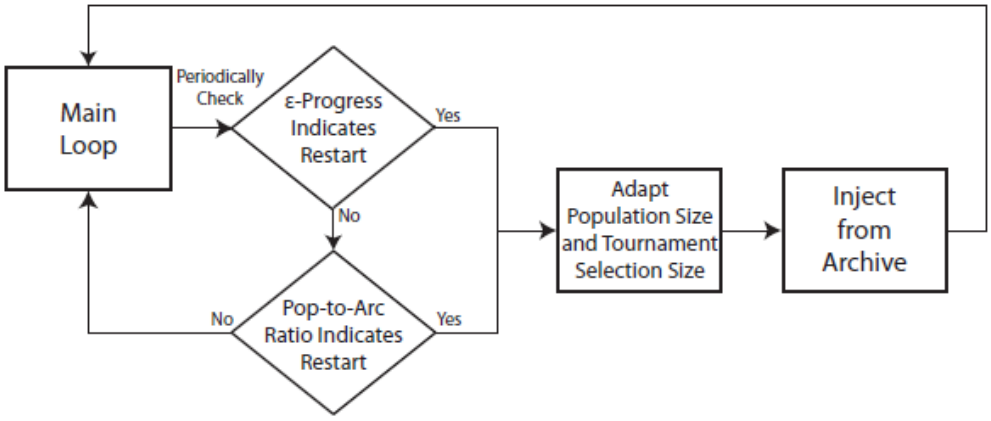


**Figure 3.7:** *Flowchart of the Borg restart logic. After a certain number of evaluations, Borg breaks out of its main loop to check if $\epsilon$-progress or the population-to-archive ratio indicate a restart is required. If so, the population is resized and filled with all members of the archive. Any remaining population slots are filled with solutions selected randomly from the archive and mutated. In addition, the tournament selection size is adjusted to account for the new population size. Finally, Borg's main loop is resumed. (Hadka and Reed, 2013)*

### 3.5.1 Borg parameters setting

In this section, we will describe how the Borg MOEA parameters were set. The principle for the selection of parameters values is based on finding the best trade-off between the computational times and the quantity and quality of optimal solutions. For the present study, we set the majority of the parameters as recommended by the creators of the algorithm ((*Hadka and Reed*, 2013)) and followed the procedure presented in the study made by *Schmitt et al.* (2019).

$NFE$, i.e., the Number of Function Evaluations, defines how many times the Borg MOEA can invoke the objective function in each optimization. It represents the termination condition: once the $NFE$ limit is reached, the algorithm terminates and returns the result. In general, the higher is the NFE, the more in-depth is the search. This translates into a higher number and density of optimal solutions, but also higher computational costs. In this case study, the best trade-off was found by choosing $NFE$ equal to 100,000 ($10^5$).

As anticipated, $\epsilon$ (side-length of $\epsilon$-boxes) controls the "resolution" of solutions discovered by the Borg MOEA. Smaller values result in fine-grained Pareto sets, while larger values in coarse-grained sets (see Fig. 3.6). Since this is a three-objective problem, there will be one $\epsilon$ value for each of the dimensions of the objective space, i.e., one for each objective. Hence, $\epsilon$ is defined as a vector whose cells contain the minimum threshold for improvement of each objective

during the optimization, calculated as follows:

$$\epsilon_i = \frac{\Delta J_i}{x} \quad , \qquad i = 1, 2, 3 \tag{3.12}$$

where $\Delta J_i$ is the maximum variation in the value of the correspondent objective, $x$ is a parameter to set depending on the particular case study, and $i$ is the index denoting each objective of the optimization. In this case study, in the absence of information about the shape of the Pareto front or the variation ranges of the objectives values, we chose $x$ equal to 100 as suggested by *Hadka and Reed* (2013). $\Delta J_i$ is computed as the difference between the maximum and the minimum value of the objective $i$, which correspond respectively to the scenarios where all dams are built ($J_{i,all_dams}$) or none ($J_{i,no_dams}$). Note that this is true if the indicator is to be maximized, i.e., $J_1$ and $J_2$. For $J_3$, since it is to be minimized, it is vice versa. In general, whatever is the criterion, $\Delta J_i$ can be calculated as

$$\Delta J_i = |J_{i,all_dams} - J_{i,no_dams}| \tag{3.13}$$

Table 3.2 reports the computed values of $J_{i,all_dams}$, $J_{i,no_dams}$, and $\epsilon_i$ for each objective.

| | $J_1$ | $J_2$ | $J_3$ |
|---|---|---|---|
| $J_{all_dams}$ | $9.26 \times 10^6$ $t/year$ | $2.67 \times 10^5$ $GWh/year$ | $2.55 \times 10^{10}$ $kg\,CO_2\,eq/year$ |
| $J_{no_dams}$ | $1.60 \times 10^8$ $t/year$ | - | - |
| $\epsilon$ | $1.51 \times 10^6$ $t/year$ | $2.67 \times 10^3$ $GWh/year$ | $2.55 \times 10^8$ $kg\,CO_2\,eq/year$ |

**Table 3.2:** *$\epsilon$ values and objectives values for all-dams and no-dams scenarios, for each indicator.*

The parameters set up to this point are enough to run a single Borg optimization and find an approximation of the Pareto front in the objective space.

### 3.5.2 Borg simulation modes

As anticipated in Section 1.4, every optimization can consider two different hydropower development scenarios:

- "pristine" situation, in which no dam is built within the basin;
- "actual" situation, in which the current hydropower development is taken into account.

We implemented the Borg MOEA in MATLAB environment and, according to the type of optimization, it was possible to choose whether to run the algorithm in the "pristine" or "actual" simulation mode.

Since the "pristine" simulation mode considers an ideal empty basin, all the 123 dams are decision variables and therefore included in the decision vector $u$. This means that even the dams that are existent and already operating ("E") or under construction ("C") could be excluded by Borg from a Pareto-Optimal portfolio.

When selecting the "actual" simulation mode, instead, Borg is forced to include in every Pareto-Optimal portfolio all the dams that are existent and already operating ("E") or under construction ("C"). This implies that only planned ("P") dams are included in the decision vector $u$, which is shortened from 123 to 68 elements (see Section 3.1). In this way, the "operating space" of Borg is reduced, which results in a fewer number of optimal solutions and worst objective values in terms of sediment delivery to the delta and GHGs emissions from reservoirs.

## 3.6 Sensitivity Analysis on GHGs emissions and sediment connectivity parameters

In this section, we will explain the principles and the procedures behind the Sensitivity Analysis approach anticipated in Section 1.4.

Sensitivity Analysis can be defined as the study of how the impact of uncertainties of one or more input variables of a model can lead to uncertainties on the output variables (*Pichery*, 2014). This is done by recomputing the outcomes under alternative assumptions, i.e., by varying the value of one or multiple input variables and evaluating how this perturbation induces a change in the outputs (*Saltelli et al.*, 2004). As described in Section 3.1, the Mekong River Basin case study is characterized by low data availability and deep uncertainty. Sensitivity Analysis allowed us to test the robustness of the results of the optimization performed with the standard inputs values and to better understand the relationships between them.

The main steps of a Sensitivity Analysis are the following:

1. sampling the inputs domain;
2. evaluating the model against the sampled inputs;
3. post-processing input/output samples.

The first step defines the criterion behind each Sensibility Analysis, i.e. how input variables are perturbed. In this work of thesis, we firstly performed a Sensitivity Analysis perturbing GHGs emissions values of each dam (Section 4.2).

After that, we repeated the procedure simultaneously perturbing the values related to GHGs emissions, river sediment supply, and dams' trapping efficiency (Section 4.3).

In Section 3.5 we described how we implemented the Borg MOEA to solve the optimization problem defined in Eq. 3.3. In order to perform the Sensitivity Analyses, Borg needs to be run for a large number of separate optimizations. In this case, to each Sensitivity Analysis correspond 1,024 separate optimizations. Unless otherwise specified, the initial population of solutions is randomly generated at the beginning of every separate optimization. To coherently compare the results coming from the different optimizations of the same Sensitivity Analysis, the initial population should be identical for every different simulation. To do so, Borg allows the user to set a "seed" as an additional parameter, and avoid this problem.

### 3.6.1 Perturbing GHGs emissions

Performing a Sensitivity Analysis on GHGs emissions from dam reservoirs means solving the decision problem for a high number of separate optimizations, each time with a different combination of Carbon Intensity values, and seeing the effect of this perturbation on the Pareto-Optimal solutions.

In Section 3.2 and Section 3.4.3 we described how we computed the values of GHGs emissions for each dam. We also pointed out that these estimates are subjected to high uncertainty due to the large natural variability of the phenomenon and the extreme difficulties in the assessments. The value that we initially assigned to each dam, expressed in the form of Carbon Intensity ($kg\,CO_2\,eq/MWh$), was the average of 10,000 values computed through a bootstrapping re-sampling procedure starting from published data. For the Sensitivity Analysis, we assumed that the "true" value is likely to be between the 2.5th percentile and the 97.5th percentile of the bootstrapping-generated series.

A complete and exhaustive exploration of every combination of GHGs emissions values between all the dams would clearly be unfeasible due to the extremely high computational costs. Hence, we also assumed that dams with similar characteristics in terms of GHGs emissions could present a correlated uncertainty, and, as a consequence, for each separate optimization, similar values of Carbon Intensity were perturbed in the same way. This allowed to efficiently explore the input domain across the different simulations.

To do so, we subdivided the "GHGs emissions per MWh" values of each dam into different classes according to the "Jenks natural breaks" clustering method, designed by *Jenks* (1967). This classification technique determines the best ar-

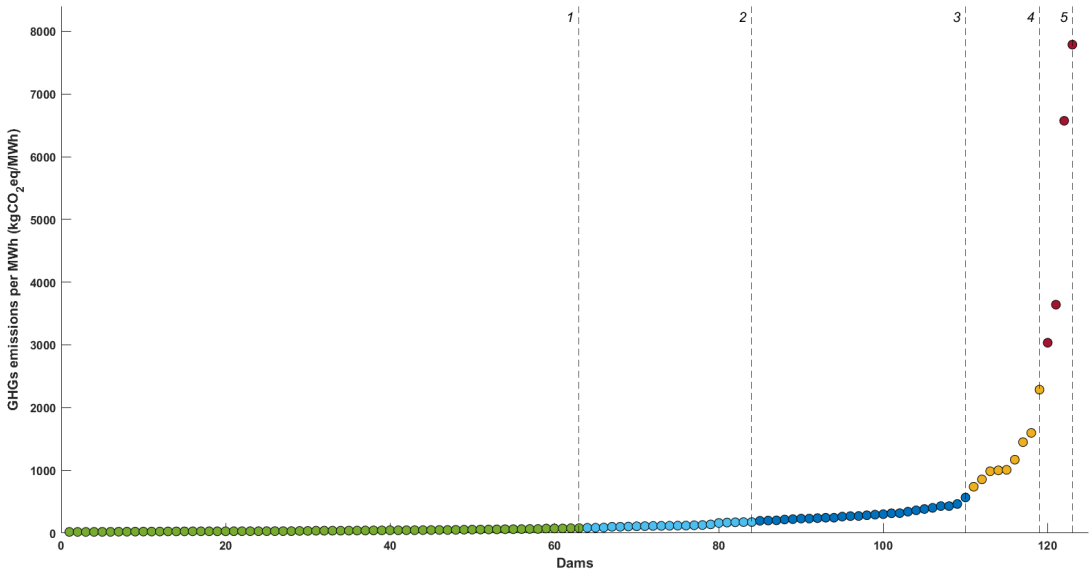


**Figure 3.8:** *"Jenks natural breaks" clustering for GHGs emissions values. "Cluster 1" refers to the lowest values, while "Cluster 5" to the highest.*

rangement of values into different classes by seeking to minimize each cluster's average deviation from the cluster mean, while maximizing each cluster's deviation from the means of the other clusters. In simpler words, this method seeks to reduce the variance within clusters and maximize the variance between clusters. By analyzing the distribution of GHGs emissions values, we considered the subdivision into 5 clusters the best classification for this case study. Fig. 3.8 shows how the "GHGs emissions per MWh" values of each dam were sorted in ascending order and split into 5 clusters according to the "Jenks natural breaks" method. Note that "Cluster 1" refers to the lowest values, while "Cluster 5" to the highest.

At this point, we can define a cluster-specific multiplier ($\mu_{CI}$) for the Carbon Intensity ($CI$) of dams ($d$) in each $cluster$. Thus, for each separate optimization of the Sensitivity Analysis, the Carbon Intensity of a dam is determined by

$$CI'(d) = \mu_{CI}(cluster) \times CI(d) \tag{3.14}$$

The different scenarios of GHGs emissions were generated by sampling the 5-dimensional parameter space (one dimension for each $cluster$) using a 5-dimensional Sobol sequence. Firstly introduced by *Sobol'* (1967), Sobol sequences are an example of quasi-random low-discrepancy sequences. The discrepancy ($D_N$) of a sequence $\{s_1, \ldots, s_N\}$ with respect to the interval $[a, b]$ can

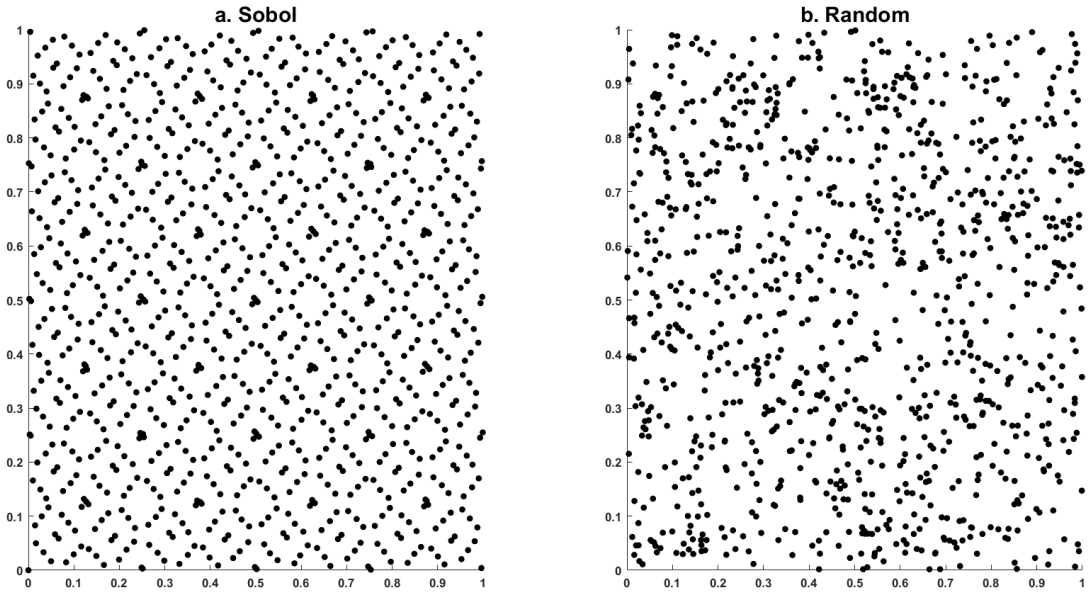


**Figure 3.9:** *2D comparison between the first 1,024 elements of a Sobol sequence (a) and a random sequence (b), both generated with MATLAB. Sobol sampling ensures a more homogeneous coverage of the domain.*

be defined as follows:

$$D_N = \sup_{a \leq c \leq d \leq b} \left| \frac{\{s_1, \ldots, s_N\} \cap [c, d]}{N} - \frac{d - c}{b - a} \right| \tag{3.15}$$

In other words, the discrepancy $D_N$ is computed as the absolute maximum difference between the fraction of elements belonging to the subset $[c, d]$ with respect to the total number of elements of the sequences and the ratio between the corresponding hyper-volumes. When $D_N$ tends to zero as $N$ tends to infinity, the sequence is equidistributed. Low-discrepancy sequences have the property that as the sequence length gets very large, the discrepancy shrinks much more quickly than one computed for a random sequence. Fig. 3.9 displays a 2D comparison between a Sobol sequence ($a$) and a random sequence ($b$). The algorithm that generates low-discrepancy sequences is biased on the selection of new points to "keep them away" from the points already sampled. As a consequence, Sobol sampling ensured a more homogeneous coverage of the multi-dimensional parameter domain.

For the Sensitivity Analysis, we selected the first 1,024 elements of the 5-dimensional Sobol sequence, and, assuming a uniform probability distribution within the range of feasible GHGs emissions values, we created 1,024 different scenarios in which the Carbon Intensity value of each dam is perturbed according to which *cluster* it belongs to (Eq. 3.14). Obviously, a higher number

of scenarios could have allowed a better exploration of the parameter domain, but we evaluated this amount as the best trade-off between the quality of the results and the computational times.

### 3.6.2 Perturbing sediment connectivity parameters

In order to perform the second Sensitivity Analysis, we perturbed two sediment connectivity parameters. In particular, taking inspiration from the study made by *Schmitt et al.* (2021), the two sediment-related variables are the Trapping Efficiency ($TE$) of each dam and the sediment yield ($\Theta$) at each node of the river network (see section 3.4.1). These values were perturbed following a procedure analogous to the one of Section 3.6.1.

We defined a country-specific multiplier ($\mu_{TE}$) for the Trapping Efficiency ($TE$) of dams ($d$) in each *country* (see Fig. 3.1.b). This is based on the assumption that environmental regulations for dam design and operation, and the requirements for sediment passage, would potentially be established on a national level. In addition, we evaluated the possibility to implement a drawdown sediment flushing strategy whenever the characteristics of a dam would make it sufficiently effective. To do this, we perturbed Trapping Efficiency values only for dams for which this approach could be efficiently implemented (see Section 1.2.2 and Fig. 1.7).

According to *Kondolf et al.* (2014a), for flushing to be technically successful, the condition that should be verified is based on this empirical formula:

$$\frac{\textit{Reservoir gross storage } [m^3]}{\textit{Mean annual inflow to the reservoir } [m^3/year]} < 4\% \tag{3.16}$$

This is because drawdown sediment flushing involves the complete emptying of the reservoir through low-level gates and reservoirs with large storage cannot be easily drawn down. Fig. 3.10 shows the 65 dams for which sediment flushing would be effective in the Mekong River Basin.

Thus, for each separate optimization of the Sensitivity Analysis, the Trapping Efficiency of a dam is determined by

$$\begin{cases} TE'(d) = \mu_{TE}(country) \times TE(d) \ , & \textit{if flushing is effective} \\ TE'(d) = TE(d) \ , & \textit{if flushing is not effective} \end{cases} \tag{3.17}$$

Regarding the sediment yield ($\Theta$), we defined a multiplier ($\mu_{\Theta}$) that is specific to the Geomorphic Province ($GP$) where each source node ($\varsigma$) is located (see Fig. 3.3). Differently from what we reported in Section 3.3.2, in this phase

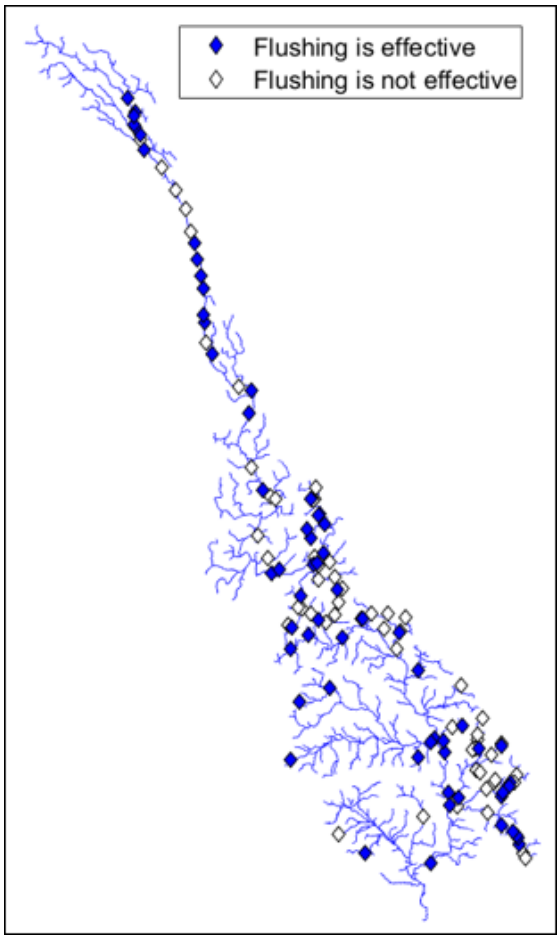


**Figure 3.10:** *Map of the dams for which sediment flushing would be effective in the Mekong River Basin.*

the number of Geomorphic Provinces taken into account is seven instead of nine, since two of them (the ones related to the Tonle Sap Basin and the Mekong Delta) present a sediment yield equal to zero (see Table 3.1). Thus, for each separate optimization of the Sensitivity Analysis, the sediment yield of a source node is determined by

$$\Theta'(\varsigma) = \mu_{\Theta}(GP) \times \Theta(\varsigma) \tag{3.18}$$

As anticipated in Section 3.6, the Sensitivity Analysis on sediment connectivity parameters was performed by simultaneously perturbing also GHGs emissions values. Hence, for this procedure, we had to sample a 17-dimensional parameter space (5 Carbon Intensity clusters, 5 countries, and 7 Geomorphic Provinces). GHGs emissions values were perturbed as described in Section 3.6.1. For what concerns sediment-related parameters, we considered again 1,024 different scenarios determined using the Sobol sampling method. We set the range of $\mu_{TE}$ to 0.1 to 1, and the range of $\mu_{\Theta}$ to 0.2 to 2. Note that we capped

$\mu_{TE}$ at 1, implying that, in the worst case, the drawdown sediment flushing strategy is completely ineffective, and thus the Trapping Efficiency of the dam would remain unchanged. In every other case, sediment trapping would be lower than the estimates derived from the Brune curve (Fig. 1.4), up to 10% of the initial value.

### 3.6.3 Statistics to elaborate Sensitivity Analysis outcomes

We already mentioned in previous sections that we performed the Sensitivity Analyses in two ways: initially, by perturbing the values related to GHGs emissions from each dam reservoir (Section 4.2), and then by simultaneously perturbing GHGs emissions, sediment supply, and Trapping Efficiency values (Section 4.3). In both cases, the Sensitivity Analyses were performed considering 1,024 different scenarios of input data perturbation (see Section 3.6.1 and Section 3.6.2). This means that, for each Sensitivity Analysis, the optimization problem presented in Section 3.4 was solved for 1,024 separate simulations, obtaining for each of them an approximation of the Pareto front. Each point of the Pareto front represents a Pareto-Optimal solution, i.e., a Pareto-Optimal portfolio of dams. To elaborate the results of the Sensitivity Analyses, we calculated some statistics that will be useful in Chapter 4.

Consider now a single Sensitivity Analysis and the corresponding 1,024 separate optimizations. Firstly, for each of the latter, we computed the (experimental) probability of each dam ($d$) to be included in a Pareto-Optimal (PO) portfolio, named Probability of Inclusion ($PoI$), as

$$PoI(d) = \frac{\textit{Occurrences (i.e., number of times the dam is included in a PO portfolio)}}{\textit{Total number of PO portfolios}} \tag{3.19}$$

Note that the *total number of PO portfolios* is not a constant value, since it depends on the amount of solution that Borg is able to find in each scenario. Then, we computed the Mean Probability of Inclusion ($MPoI$) of each dam ($d$) in PO portfolios across the different scenarios simply as

$$MPoI(d) = \frac{1}{n_{opt}} \sum_{n=1}^{n_{opt}} \Big( PoI(d) \Big)_n \tag{3.20}$$

where $n_{opt}$ is the number of separate optimizations, in this case always constant and equal to 1,024.

Lastly, in order to evaluate the uncertainty associated with each dam ($d$), we considered the Interquartile Range ($IQR$) of Probability of Inclusion across the

different scenarios, calculated as

$$IQR(d) = Q_3(PoI(d)) - Q_1(PoI(d)) \tag{3.21}$$

where $Q_3(PoI(d))$ and $Q_1(PoI(d))$ are respectively the 75th percentile (also called "upper quartile") and the 25th percentile (also called "lower quartile") of the $PoI$ values of each dam ($d$) in each separate optimization. The Interquartile Range is a measure of statistical dispersion, i.e., the spread of a sample of numerical data. It is an example of a trimmed estimator, as it excludes all the extreme values outside the range between the lower and the upper quartile to obtain a more robust statistic (*Kaltenbach*, 2011). Note that high values of $IQR$ indicate a high dispersion of $PoI$ values, to which high uncertainty is associated. On the contrary, low values of $IQR$ correspond to low uncertainty.

# 4

# Results

## 4.1 Pareto-Optimal dam portfolios

In this section, we will present the results of the optimization executed with the initial input values as defined in Section 3.1, Section 3.2, and Section 3.3.2. The goal of this optimization consists in trying to answer the following question: *which combinations of dams would have given the best trade-offs between sediment supply, hydropower production, and GHGs emissions in a pristine Mekong River Basin?* To do this, we solved the decision problem defined in Eq. 3.3 with the Borg MOEA (see Section 3.5), finding 363 Pareto-Optimal (PO) portfolios (i.e., combinations of dam sites). Note that, even with the same inputs and Borg parameters, the number of solutions is not constant because of the intrinsic nature of evolutionary algorithms.

Fig. 4.1 displays the shape of the Pareto front in the objective space, where all the optimal solutions are plotted according to the corresponding values of three objective indicators. The coordinates of each point represent the values of the objective indicators $J_1$ (sediment supply to the delta) and $J_2$ (hydropower production); the corresponding value of the objective indicator $J_3$ (GHGs emissions from reservoirs) is instead indicated by the color of each point, with a gradient from yellow (lowest values) to dark red (highest values). Black arrows near axes labels point towards the preferred direction of each objective; in particular, since sediment supply and hydropower production are both to be maximized, the corresponding black arrows point towards the highest values; on the contrary, black arrow related to GHGs emissions points towards the

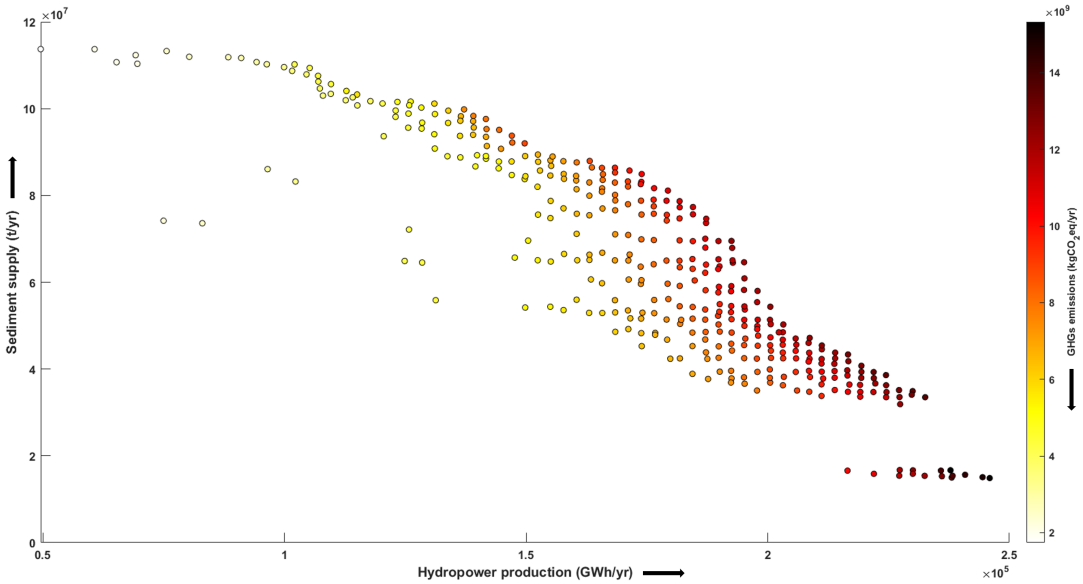


**Figure 4.1:** *Objective space in which Pareto-Optimal solutions of the decision problem are displayed. The coordinates of each point represent the values of the objective indicators $J_1$ (sediment supply to the delta) and $J_2$ (hydropower production), while the color indicates the corresponding value of the objective indicator $J_3$ (GHGs emissions from reservoirs). Black arrows near axes labels point toward the preferred direction of each objective.*

lowest values since this objective is to be minimized.

By looking at the shape of the Pareto front in Fig. 4.1, one can notice a large horizontal gap in the bottom-right corner. A closer examination of the interested portfolios revealed that all the solutions below this gap include the Sambor dam, which is instead always excluded from all the other portfolios. In Figure 4.2 we reported all the dams in the basin colored according to their annual GHGs emissions, highlighting the Sambor dam with a red circle. This dam is one of the largest in the entire basin, characterized by very high hydropower production, but also very high GHGs emissions (dark-colored in Fig 4.2). Moreover, we can observe that it is located in the mainstem just before the delta, which is a critical spot for sediment connectivity within the basin. From this, we can deduce that the large horizontal gap in Fig. 4.1 derives from the massive impact on sediment delivery to the delta caused by the presence of the Sambor dam. This confirms the thesis of a previous study made by *Schmitt et al.* (2019), who claimed that the construction of this large and lowland dam would have caused an abrupt decrease in sediment load reaching the delta.

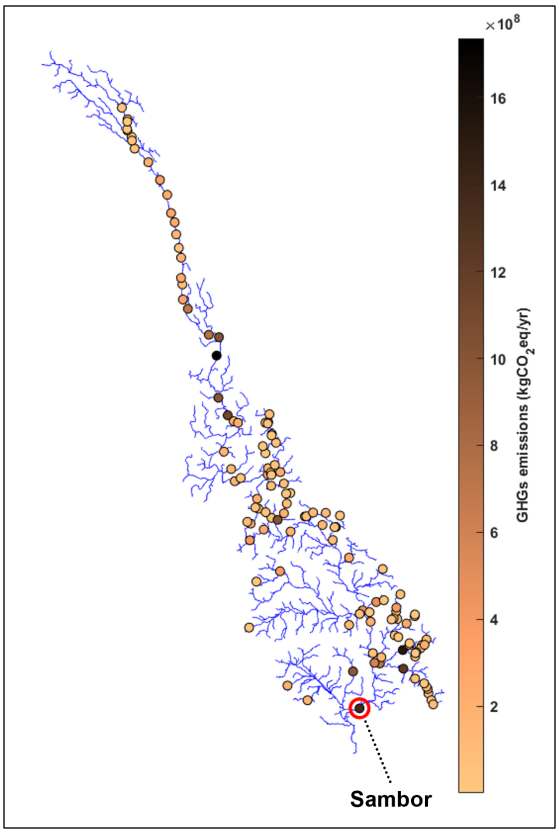


**Figure 4.2:** *Map of all dams colored according to their annual GHGs emissions using a brownish shade (lighter colors correspond to lower emissions, darker colors correspond to higher emissions). The Sambor dam is highlighted with a red circle.*

## 4.2 Sensitivity Analysis on GHGs emissions

This section is dedicated to the presentation of the outcomes of the Sensitivity Analysis on GHGs emissions, performed to answer the following question: *how much the optimization problem results are robust to uncertainty in the estimations of GHGs emissions input data?* Considering the high uncertainty related to GHGs emissions input values (see Section 3.2), *how much and in which way does perturbing these values affects the outcomes?* To interpret the results, we adopted a telescopic approach, starting from the entire basin and then focusing on the most interesting groups of dams.

The outcomes of the 1,024 separate optimizations (see Section 3.6.1) consist of as many approximations of the Pareto front, in which each point represents a PO portfolio. For each of the separate optimizations, we computed the (experimental) probability of each dam to be included in a PO portfolio ($PoI$) using Eq. 3.19. Then, we calculated the Mean Probability of Inclusion ($MPoI$) of each dam in PO portfolios across the different scenarios using Eq. 3.20. Based on this value, we defined two categories of dams: the "Almost Never Included Dams",

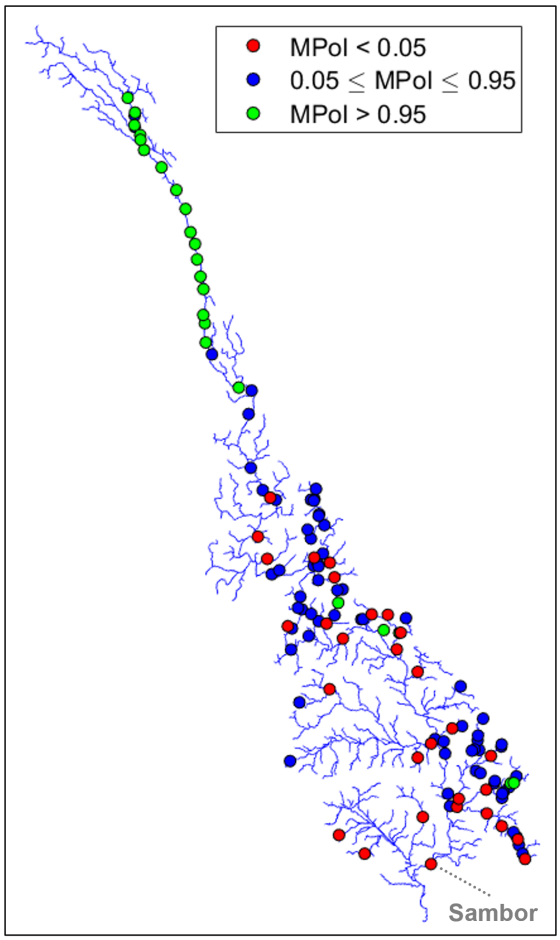


**Figure 4.3:** *Map of all dams subdivided according to their Mean Probability of Inclusion (MPoI). Red points represent the "Almost Never Included Dams" (MPoI < 0.05) and green points represent the "Almost Always Included Dams" (MPoI > 0.95).*

defined as the dams whose $MPoI$ is less than 0.05, and the "Almost Always Included Dams", defined as the dams whose $MPoI$ is greater than 0.95. Note that we could interpret the "Almost Never Included Dams" and the "Almost Always Included Dams" as the dams which are, with a relatively high degree of confidence, "not recommended" and "highly recommended" by the algorithm, respectively.

In all of the Mekong River Basin, we identified 31 "Almost Never Included Dams" (about 25% of all 123 dams) and 24 "Almost Always Included Dams" (about 20% of all 123 dams). Fig. 4.3 shows the map of all dams in the basin subdivided according to their $MPoI$ value as explained above. We can notice that most of the "Almost Always Included Dams" correspond to most of the dams located in the Upper MRB, along the Lancang River mainstem. On the contrary, all the "Almost Never Included Dams" are distributed in the entire Lower MRB, generally on tributaries. Moreover, note that the Sambor dam highlighted in

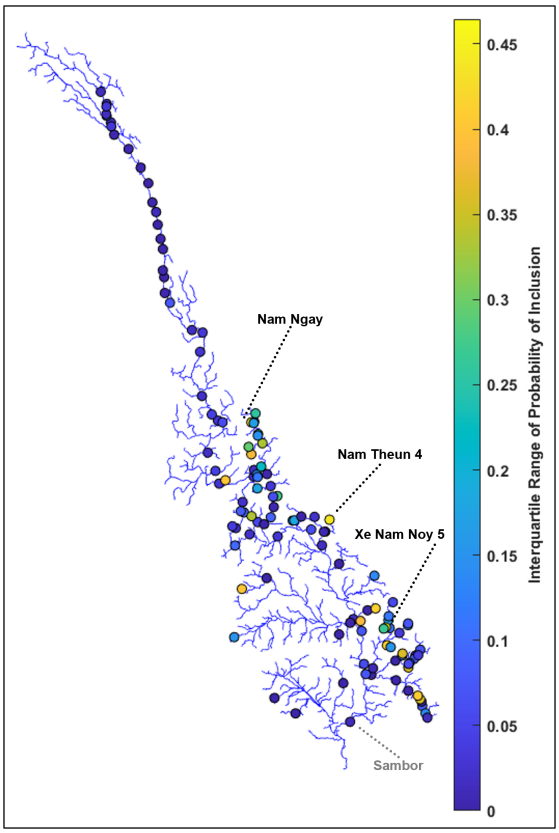


**Figure 4.4:** *Map of all dams with the associated value of IQR (blue points indicate low IQR, while yellow points indicate high IQR). The Sambor dam and the three dams with the highest values of IQR are indicated with their respective names.*

the previous section belongs to the "Almost Never Included Dams".

In order to evaluate the uncertainty associated with each dam, we used Eq. 3.21 to compute the Interquartile Range ($IQR$) of Probability of Inclusion across the different scenarios. High values of $IQR$ indicate a high dispersion of $PoI$ values, to which high uncertainty is associated, while low values of $IQR$ correspond to low uncertainty (see Section 3.6.3). Fig. 4.4 shows the map of all dams with the associated value of $IQR$ (blue points indicate low $IQR$, while yellow points indicate high $IQR$). From this map, we can derive that, as one could expect, the dams in the Lancang River Basin are also the ones that present the lowest uncertainty. The highest $IQR$ values are instead spread across all the Lower MRB.

To further analyze the uncertainty associated with each dam, we plotted, for each dam, the corresponding values of $MPoI$ and $IQR$ (Fig. 4.5). We can notice how the points are arranged in a "triangular pattern", where "Almost Never Included Dams" and "Almost Always Included Dams" present the lowest $IQR$ values, while the highest uncertainty is associated with mid values of $MPoI$.

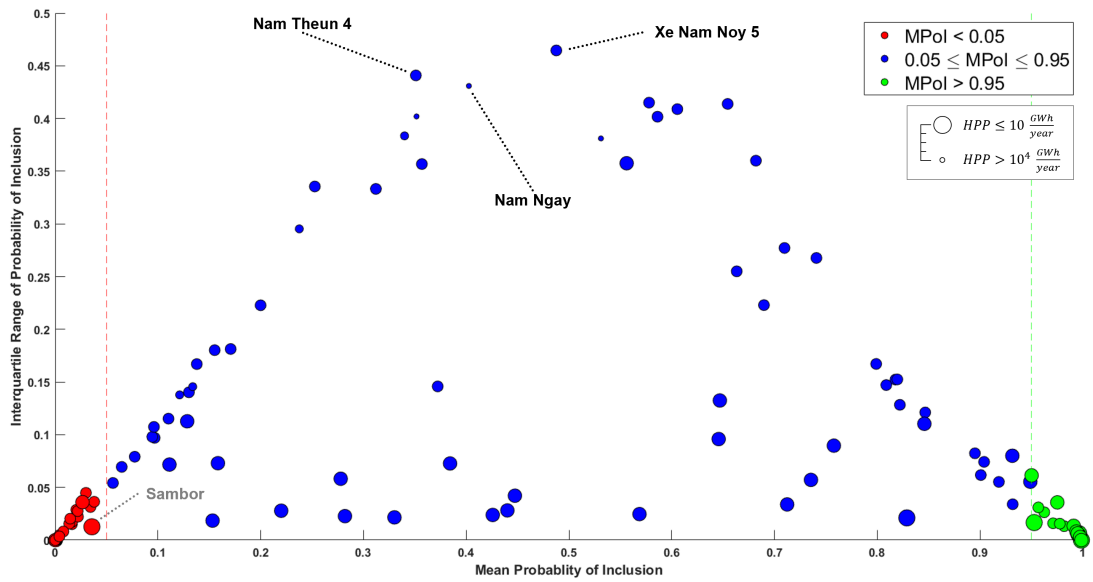


**Figure 4.5:** *The "triangular pattern" of uncertainty. "Almost Never Included Dams" and "Almost Always Included Dams" present the lowest IQR values, while the highest uncertainty is associated with mid values of MPoI. The Sambor dam and the three dams with the highest values of IQR are indicated with their respective names. Point size is proportional to the Mean Annual Hydropower Production (GWh/year).*

The latter correspond to dams with medium "performance" (in terms of the three objectives) and similar characteristics to each other, and thus they can be included or not in PO portfolios depending on the way GHGs emissions values are perturbed in one scenario or in another. This highlights the major influence of uncertainty on these dams.

In order to see how uncertainty could be linked to GHGs emissions of each dam reservoir, we added the information related to "Annual GHGs emissions" values ($kg\,CO_2\,eq/year$) to the plot of Fig. 4.5. Moreover, for the same reason, we repeated this approach by considering also the "Mean Annual Hydropower production" values ($GWh/year$). The two resulting plots are respectively shown in Fig. 4.6 and Fig. 4.7, where the lowest values of $IQR$ are indicated in blue and the highest in yellow. We can notice that, in general, the highest uncertainty is obviously associated with mid values of $MPoI$ (like already shown in Fig. 4.5) and mid-low values of both "Annual GHGs emissions" and "Mean Annual Hydropower production" values. The similar pattern observed in these two plots highlights a correlation between GHGs emissions and hydropower production (as one could expect from Eq. 3.8).

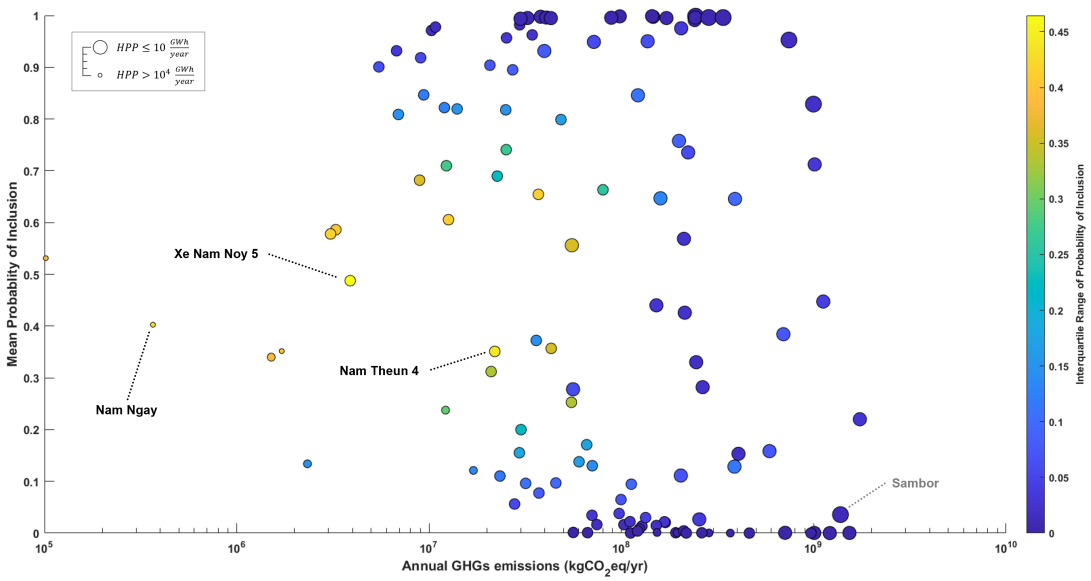


**Figure 4.6:** *The link between uncertainty and GHGs emissions. For each dam, the MPoI, IQR, and "Annual GHGs emissions" (kg $CO_2$ eq/year) values are reported. Blue points are associated with the lowest values of IQR, while yellow with the highest. The Sambor dam and the three dams with the highest values of IQR are indicated with their respective names. Point size is proportional to the Mean Annual Hydropower Production (GWh/year).*

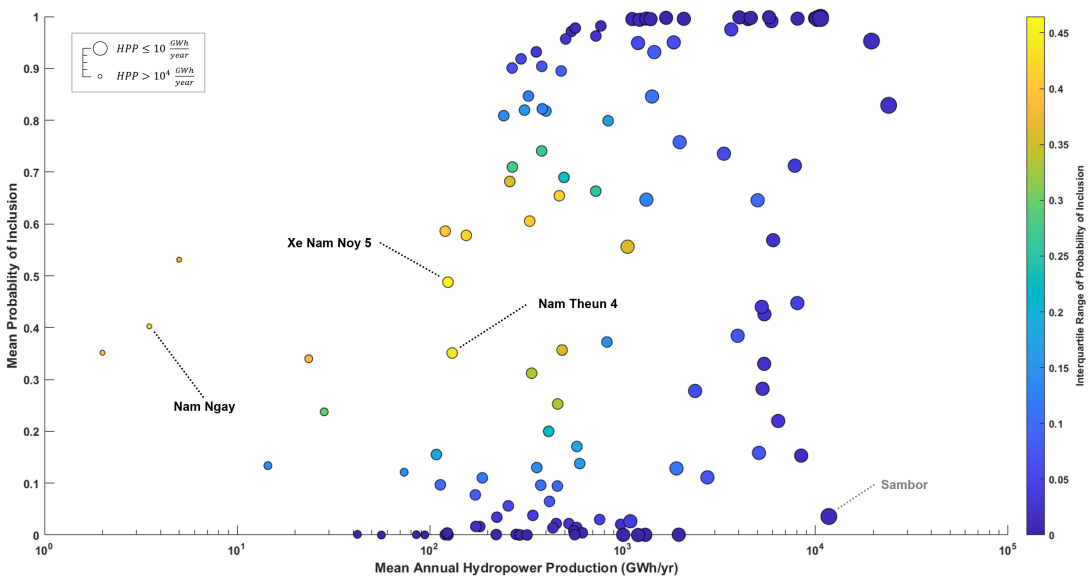


**Figure 4.7:** *The link between uncertainty and hydropower production. For each dam, the MPoI, IQR, and "Mean Annual Hydropower production" (GWh/year) values are reported. Blue points are associated with the lowest values of IQR, while yellow with the highest. The Sambor dam and the three dams with the highest values of IQR are indicated with their respective names. Point size is proportional to the Mean Annual Hydropower Production (GWh/year).*

### 4.2.1 "Dams with High Uncertainty"

So far, we just have a general idea of how the dams in the basin are affected by uncertainty. Let's now have a closer look at the dams associated with the highest values of $IQR$. To do this, we defined the "Dams with High Uncertainty" as the dams whose $IQR$ is greater than 0.2. Fig. 4.8 shows the map of the basin (*a*) and the "$IQR$ vs $MPoI$" plot (*b*), in which the "Dams with High Uncertainty" are highlighted in magenta. Note that, as might have been expected from the general analysis in Section 4.2, all these dams belong to the interval "$0.05 \leq MPoI \leq 0.95$". In fact, none of the "Almost Never Included Dams" and "Almost Always Included Dams" present a $IQR$ greater than 0.2.

In all of the Mekong River Basin, we identified 21 "Dams with High Uncertainty", corresponding to around 17% of the total number of dams. Nearly half of them (10 dams out of 21, about 48%) are planned dams, while the rest are either existent and already operating or under construction (11 dams out of 21, about 52%). We evaluated which "GHGs emissions per MWh" cluster each "Dam with High Uncertainty" belongs to (see Section 3.6.1. Remember that "Cluster 1" refers to the lowest values, while "Cluster 5" to the highest. We identified 14 dams included in "Cluster 1" (about 66%), 5 in "Cluster 2" (about 24%), 1 in "Cluster 3" (about 5%), and 1 in "Cluster 4" (about 5%). This means that most of the uncertainty is associated with dams characterized by low GHGs emissions, confirming what was anticipated by describing Fig. 4.6. This is even more evident by comparing the "Dams with High Uncertainty" with respect to the dams of the entire basin. Table 4.1 reports the mean "GHGs emissions per year" ($kg\,CO_2\,eq/year$) and the mean "annual hydropower production" ($GWh/year$) calculated for all the dams in the basin and then only for the "Dams with High Uncertainty". We can notice that both the statistics regarding the "Dams with High Uncertainty" are approximately one order of magnitude smaller than the ones computed for all the dams.

| | **All dams in the MRB** | **"Dams with High Uncertainty"** |
|---|---|---|
| **Mean "GHGs emissions per year"** | $2.08 \times 10^8\ kg\,CO_2\,eq/year$ | $2.15 \times 10^7\ kg\,CO_2\,eq/year$ |
| **Mean "annual hydropower production"** | $2.17 \times 10^3\ GWh/year$ | $2.99 \times 10^2\ GWh/year$ |

**Table 4.1:** *Mean "GHGs emissions per year" ($kg\,CO_2\,eq/year$) and mean "annual hydropower production" ($GWh/year$) calculated for all the dams in the basin and only for the "Dams with High Uncertainty".*

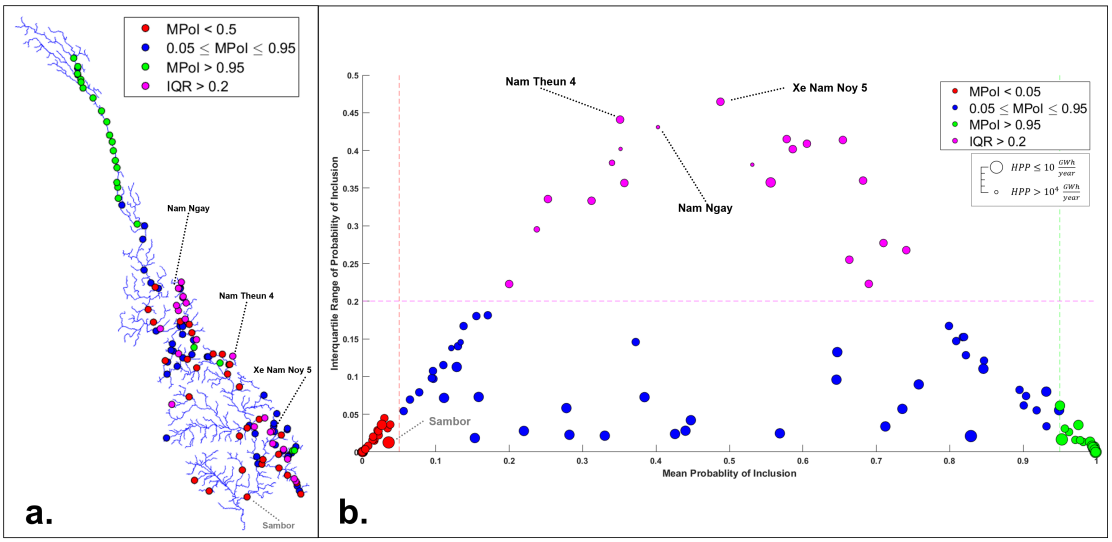


**Figure 4.8:** *Map of the basin (a) and the "IQR vs MPoI" plot (b), in which the "Dams with High Uncertainty" (IQR > 0.2) are highlighted in magenta. The Sambor dam and the three dams with the highest values of IQR are indicated with their respective names. Point size in the "IQR vs MPoI" plot is proportional to the Mean Annual Hydropower Production (GWh/year).*

## 4.3 Sensitivity Analysis on GHGs emissions and sediment connectivity parameters

In this section, we will try to answer the following question: *how do the outcomes of the Sensitivity Analysis change if now we perturb simultaneously the input values related to GHGs emissions and sediment connectivity parameters?* Specifically, in addition to the Carbon Intensity of each dam, we perturbed the values of the sediment yield into each reach and the Trapping Efficiency of each dam, resulting in a three-degrees-of-freedom Sensitivity Analysis (see Section 3.6.1 and Section 3.6.2). To analyze the outcomes of the 1,024 separate optimizations, we followed the same procedure of Section 4.2. In general, we obtained very similar results. For example, the amount and the spatial distribution of "Almost Never Included Dams" and "Almost Always Included Dams" remained nearly unchanged, except for two former "Almost Always Included Dams" and one former "Almost Never Included Dams" that, in this case, belong to the interval "$0.05 \leq MPoI \leq 0.95$". Thus, we will focus only on the most relevant changes.

Fig. 4.9 shows a comparison between the "Dams with High Uncertainty" on the "IQR vs MPoI" plot for the Sensitivity Analysis on GHGs emissions (*a*) and for the Sensitivity Analysis on GHGs emissions and sediment connectivity parameters (*b*). In general, by looking at the $IQR$ values associated with each dam, we can notice an overall increase in uncertainty, also highlighted by the total number of "Dams with High Uncertainty", which increases from 21 to 30

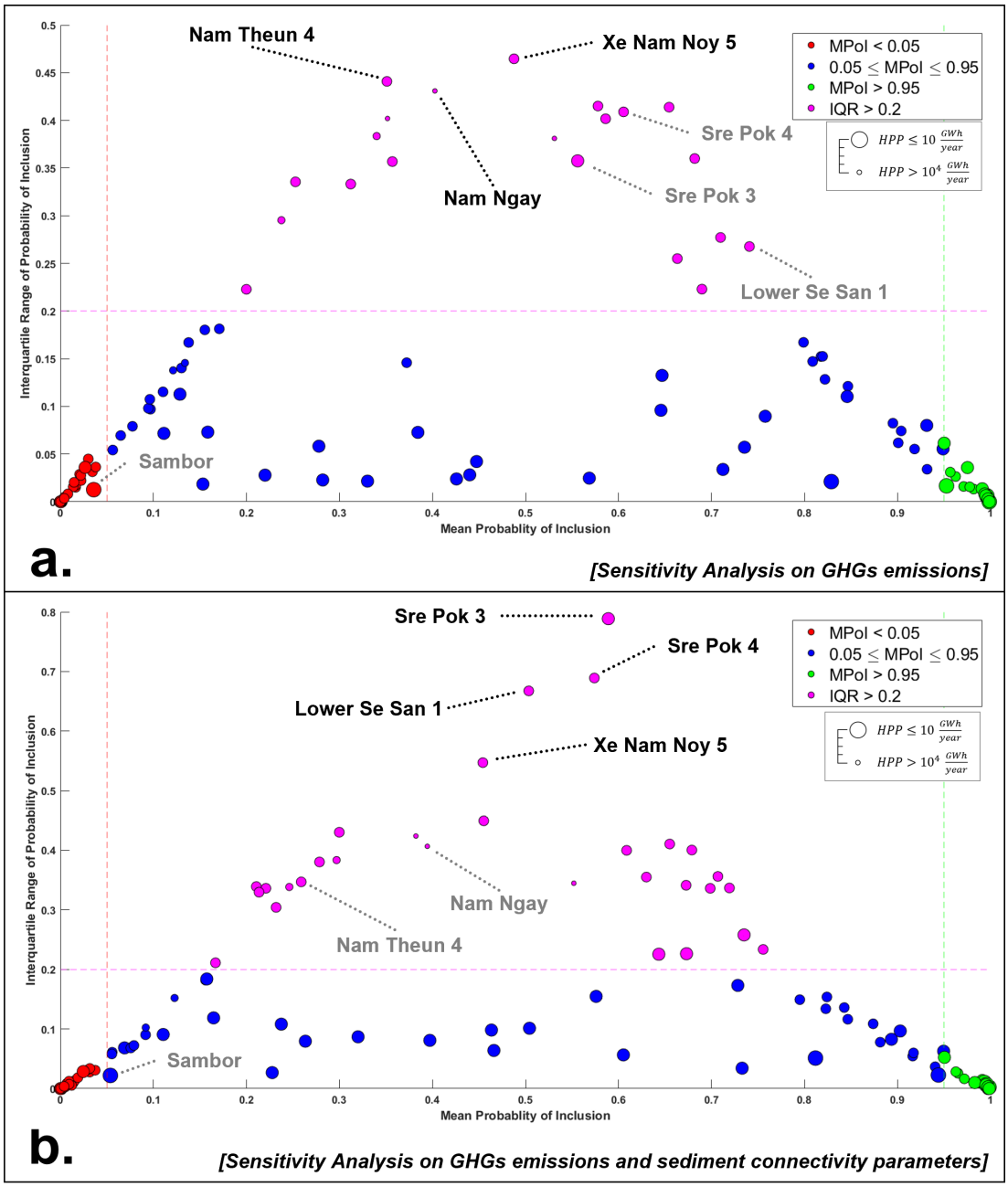


**Figure 4.9:** *Comparison between the "Dams with High Uncertainty" on the "IQR vs MPoI" plot for the Sensitivity Analysis on GHGs emissions (a) and for the Sensitivity Analysis on GHGs emissions and sediment connectivity parameters (b). The Sambor dam and some "Dams with High Uncertainty" (magenta points) are indicated with their respective names. Point size is proportional to the Mean Annual Hydropower Production (GWh/year).*

(+43%). In particular, four dams (Sre Pok 3, Sre Pok 4, Lower Se San 1, and Xe Nam Noy 5) present extremely high values of $IQR$. We named them "Dams with Very High Uncertainty", defined as the dams whose $IQR$ is greater than 0.5. *Where are these dams located and what are their characteristics?* We will answer

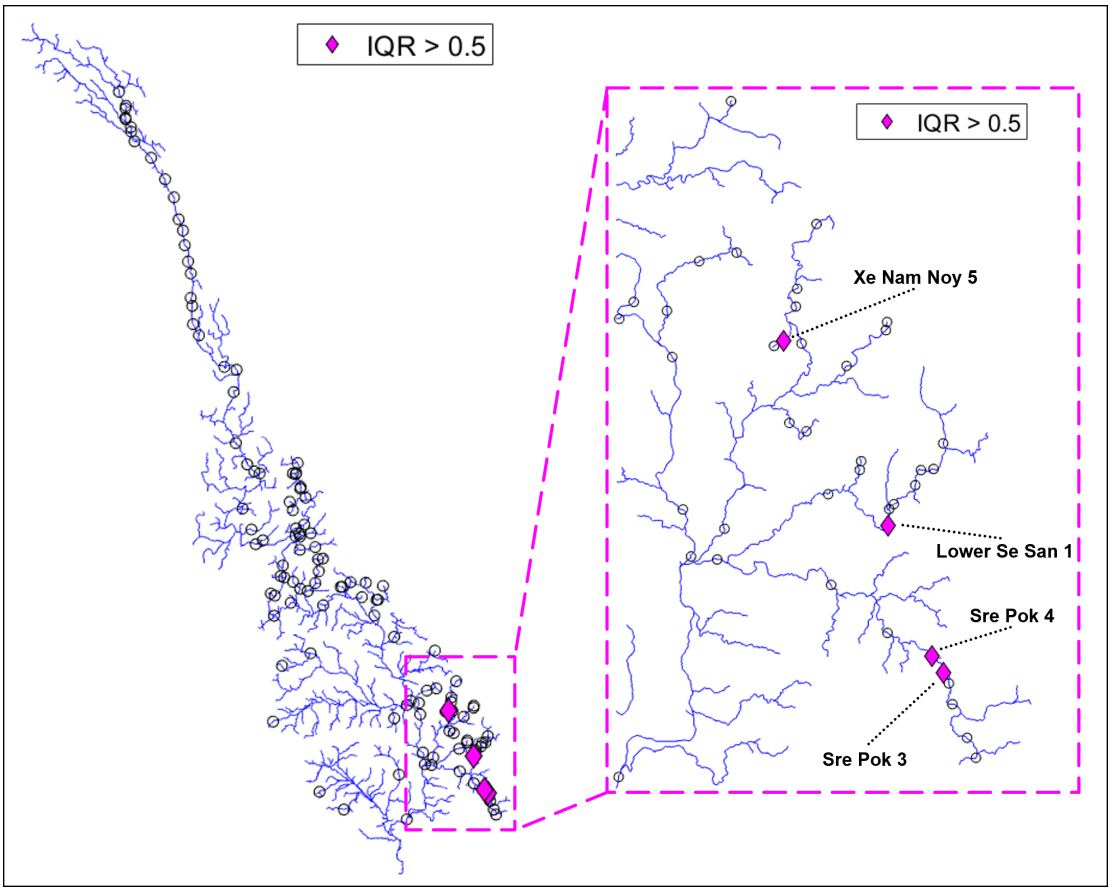


**Figure 4.10:** *"Dams with Very High Uncertainty" (IQR > 0.5) in the 3S Basin, indicated with magenta diamonds and the respective names. All other dams in the basin are represented by black empty circles.*

this question in the next section.

From Fig. 4.9, we can also notice a slightly increase of the $MPoI$ value related to the Sambor dam, that now belongs to the interval "$0.05 \leq MPoI \leq 0.95$". Although this value remains very low, around the 0.05 threshold, this change underlines the need to pay particular attention to the Sambor dam.

### 4.3.1 "Dams with Very High Uncertainty"

In the previous section, we named "Dams with Very High Uncertainty" the four dams with a value of $IQR$ greater than 0.5 resulting from the Sensitivity Analysis on GHGs emissions and sediment connectivity parameters. By looking at Fig. 4.10, we can notice how they are all located in the 3S Basin (Fig. 2.3). In particular, as suggested by their names, Sre Pok 3 and Sre Pok 4 dams are situated along the Sre Pok River mainstem (more precisely, in Vietnamese highlands, before the Cambodian border), the Lower Se San 1 dam along the Se San

River mainstem (in Cambodia), and the Xe Nam Noy 5 dam in the Se Kong River subbasin (in Laos). The first two dams present very similar features: in addition to the very close location, they are both existent and already operating ("E"), and, regarding GHGs emissions, they both belong to "Cluster 1". The Lower Se San 1 dam and the Xe Nam Noy 5 dam are instead planned ("P") and belong respectively to "Cluster 2" and "Cluster 1". Therefore, all four dams present relatively low GHGs emissions. It is also interesting to observe that all four dams are located in the same Geomorphic Province, the "Tertiary Volcanic Plateau". Furthermore, all these dams (except for the Xe Nam Noy 5 dam) share the possibility to efficiently implement the sediment flushing strategy.

## 4.4 "Lost Opportunities"

Sensitivity Analyses performed by considering a pristine basin offered the possibility to discover how hydropower could have developed by applying a strategic dam planning approach. This is, of course, just a Utopian scenario, and we already described in Section 2.4 how different reality is. So, *what is, in detail, the consequence of the project-by-project planning approach often applied in the past in the Mekong River Basin?* To answer this question, we defined a new category of dams, named "Lost Opportunities", as all the "Almost Never Included Dams" which are either existent and already operating ("E") or under construction ("C"). "Almost Never Included Dams" are, by definition, those dams which are almost always excluded from the Pareto-Optimal portfolios due to their bad "performance" with respect to the three objectives of the optimization problem. In Section 4.2, we already pointed out that they could be interpreted as the dams "not recommended" by the algorithm. "Lost Opportunities" represent all the dams that, contrary to the actual basin situation, should have not been constructed (according to the algorithm).

We identified 12 "Lost Opportunities" in the Mekong River Basin, displayed in Fig. 4.11. They are generally characterized by high GHGs emissions, as evidenced by their classification according to the "GHGs emissions per MWh" clusters: 1 dam included in "Cluster 2" (about 8%), 5 in "Cluster 3" (about 42%), 4 in "Cluster 4" (about 33%), and 2 in "Cluster 5" (about 17%). The bad performance of "Lost Opportunities" with respect to the three objectives is even more evident from the comparison of these dams with the dams of the entire basin. Table 4.2 reports the mean "GHGs emissions per year" ($kg\,CO_2\,eq/year$) and the mean "annual hydropower production" ($GWh/year$) calculated for all the dams in the basin and then only for the "Lost Opportunities". We can notice that, despite the statistic related to GHGs emissions being of the same order of

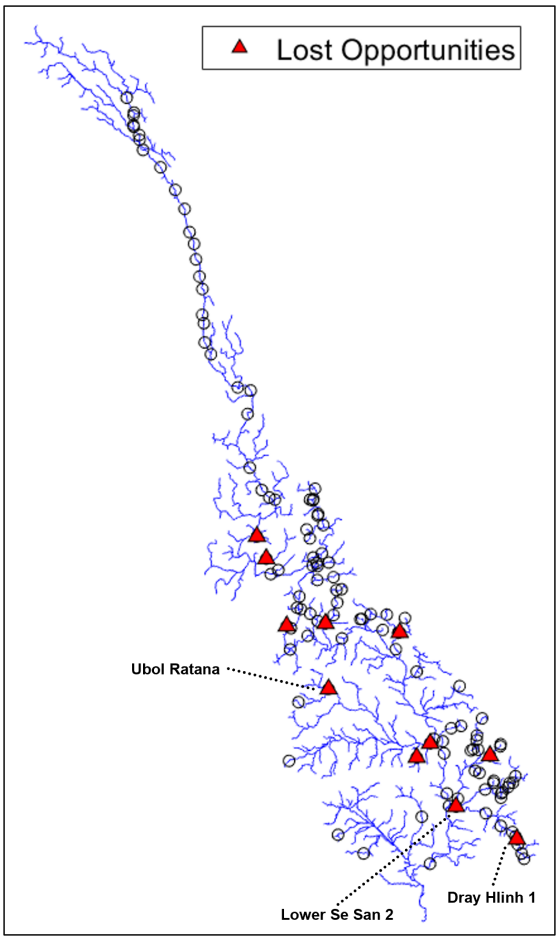


**Figure 4.11:** *Map of the "Lost Opportunities" in the Mekong River Basin, indicated with red triangles. All other dams in the basin are represented by black empty circles. Three "Lost Opportunities" are highlighted with their respective names.*

magnitude, the mean "annual hydropower production" corresponding to "Lost Opportunities" is approximately one order of magnitude smaller than the one computed for all the dams.

Lastly, note than we did not specified if these results come from the Sensitivity Analysis on GHGs emissions or the one performed simultaneously on GHGs emissions and sediment connectivity parameters. This is because both of them provided the same outcome.

| | All dams in the MRB | "Lost Opportunities" |
|---|---|---|
| **Mean "GHGs emissions per year"** | $2.08 \times 10^8$ $kg\,CO_2\,eq/year$ | $3.00 \times 10^8$ $kg\,CO_2\,eq/year$ |
| **Mean "annual hydropower production"** | $2.17 \times 10^3$ $GWh/year$ | $5.56 \times 10^2$ $GWh/year$ |

**Table 4.2:** *Mean "GHGs emissions per year" ($kg\,CO_2\,eq/year$) and mean "annual hydropower production" ($GWh/year$) calculated for all the dams in the basin and only for "Lost Opportunities".*

## 4.5 Current basin dam portfolio and the actual planning possibilities

So far, we have based all our optimizations on the hypothesis of a pristine basin, where no dam has yet been constructed. As already explained, this Utopian scenario was useful to evaluate the consequence of project-by-project hydropower development and how strategic dam planning could have helped to achieve better results. But now, considering the current dam portfolio, *what are the actual planning possibilities?* We tried to answer this question by repeating every procedure discussed until now considering the actual hydropower development in the basin as the starting point for solving the decision problem. This means that we forced the algorithm to include all the dams classified as "existent and already operating" ("E") or "under construction" ("C") in each Pareto-Optimal portfolio resulting from every separate optimization. We performed the Sensitivity Analyses in both ways, but, since the outcomes were very similar, we decided to present only the ones related to the Sensitivity Analysis performed by perturbing simultaneously GHGs emissions and sediment connectivity parameters values.

Fig. 4.12 shows the map of the 68 "planned" ("P") dams subdivided according to their Mean Probability of Inclusion (MPoI). Once again, "Almost Never Included Dams" are represented in red, while "Almost Always Included Dams" in green. At first glance, we can immediately notice how their distribution across the basin is very similar to that in the analogous map of the "pristine" scenario (Fig. 4.3), with green points mostly concentrated in the Lancang River Basin and red points distributed along tributaries of the Lower MRB. In particular, we identified 23 "Almost Never Included Dams" and 9 "Almost Always Included Dams". In relative terms, since the total number of dams included in the respective optimizations changed from 123 ("pristine" scenario) to 68 ("actual" scenario"), "Almost Never Included Dams" went from representing 25%

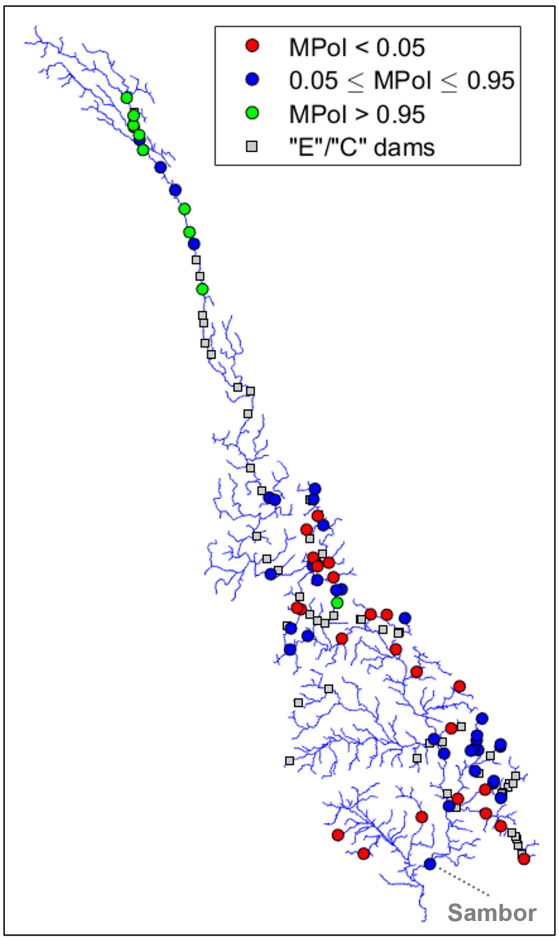


**Figure 4.12:** *"Actual" hydropower development scenario: map of all planned dams subdivided according to their Mean Probability of Inclusion (MPoI). Red points represent the "Almost Never Included Dams" (MPoI < 0.05) and green points represent the "Almost Always Included Dams" (MPoI > 0.95). All the dams classified as "existent and already operating" ("E") or "under construction" ("C") are indicated with gray squares.*

of the total number of included dams to 34%, while "Almost Always Included Dams" from 18% to 13%. In Fig. 4.12 we also indicated with gray squares the 55 dams classified as "existent and already operating" ("E") or "under construction" ("C"). Note that, for the "actual" scenario, these dams can be considered, by definition, as "Always Included Dams".

The most significant differences between the outcomes of the optimizations related to the two hydropower development scenarios emerge by considering the "Dams with High Uncertainty" ($IQR > 0.2$). Fig. 4.13 shows a comparison between the "Dams with High Uncertainty" on the "IQR vs MPoI" plot for the "pristine" scenario (*a*) and the "actual" scenario (*b*). Note that, in Fig. 4.13 we displayed only the "planned" ("P") dams, since all other dams are characterized, by definition, by $MPoI$ equal to 1 and $IQR$ equal to 0 for the "actual"

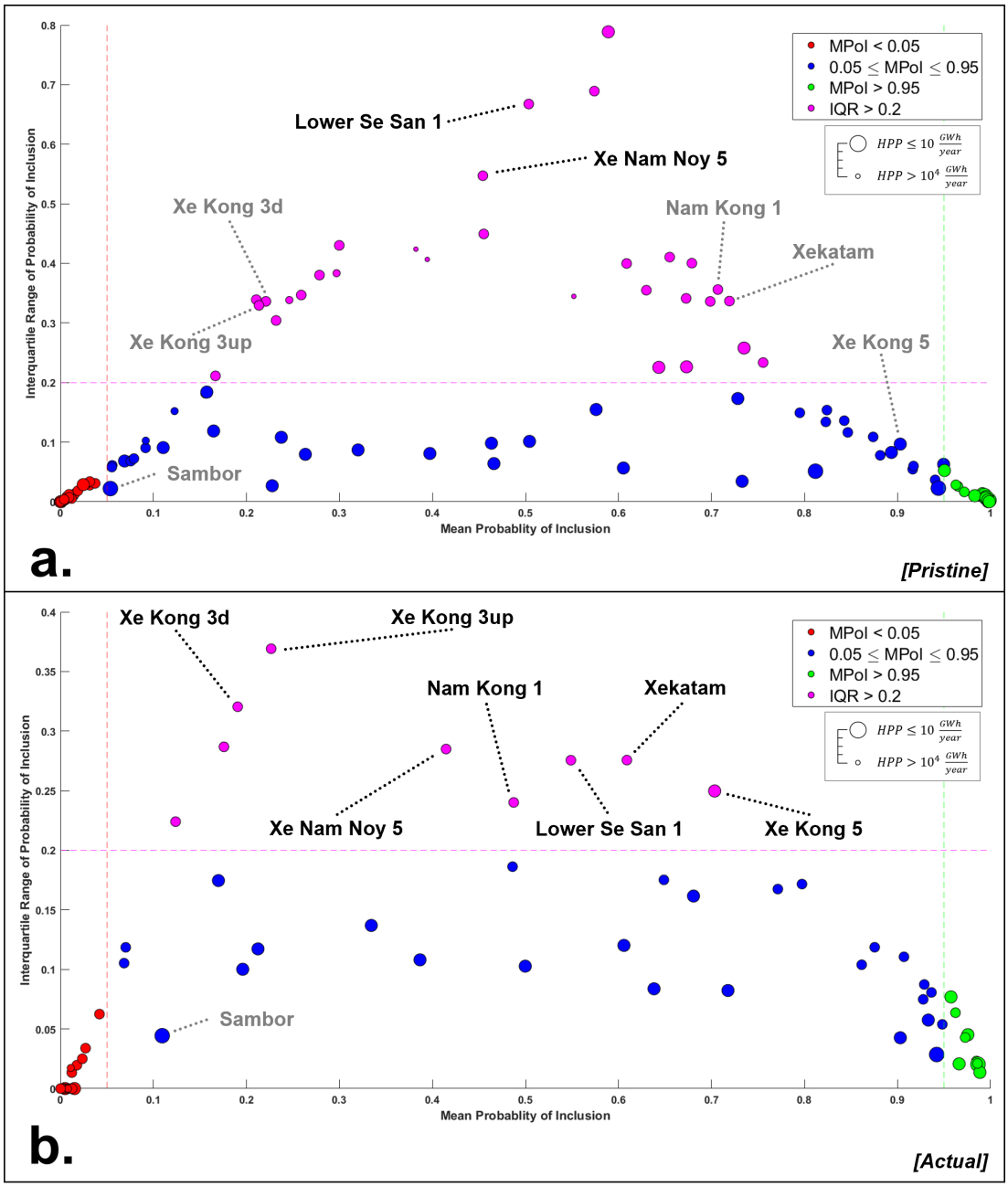


**Figure 4.13:** *Comparison between the "Dams with High Uncertainty" on the "IQR vs MPoI" plot for the "pristine" scenario (a) and the "actual" scenario (b). For the latter, only "planned" ("P") dams are displayed. The Sambor dam and some "Dams with High Uncertainty" (magenta points) are indicated with their respective names. Point size is proportional to the Mean Annual Hydropower Production (GWh/year).*

scenario. We can observe an overall decrease of uncertainty: the "triangular pattern", despite still visible, has "flattened", and, in general, the dams present lower values of $IQR$. This is also evident by comparing the total number of "Dams with High Uncertainty" resulting in the two scenarios: for the "pristine"

scenario, we identified 30 "Dams with High Uncertainty", which represented 24% of the total number of dams included in the optimization; for the "actual" scenario, we identified 9 "Dams with High Uncertainty", corresponding to 13%.

It is also interesting to notice that the $MPoI$ value related to the Sambor dam, which was around 0.05 for both the Sensitivity Analyses of the "pristine" scenario (Fig. 4.9), is now higher than 0.1. The reasons may be found in the shape of the Pareto fronts associated with the two scenarios. We noticed that the total number of Pareto-Optimal solutions found by the algorithm for the "actual" scenario is much lower than the corresponding number for the "pristine" scenario (due to the smaller decision space). Nevertheless, we also found that the region of the objective space characterized by the optimal portfolios that always include the Sambor dam (see Section 4.1) had usually a higher density of solutions. Consequently, by looking at Eq. 3.19, we can understand why the $MPoI$ value related to the Sambor dam, although remaining relatively low, increased in such a way.

In Fig. 4.13.b we highlighted seven "Dams with High Uncertainty" by indicating their names on the plot. These dams are among the ones associated with the highest uncertainty for the "actual" hydropower development scenario. By analyzing them in detail, we discovered that they present several common features. Fig. 4.14 shows that these dams are all planned in the 3S Basin (Fig. 2.3). We can also notice that six of them are all planned in the Se Kong River subbasin, while the Lower Se San 1 dam is located along the Se San River mainstem. We already described the Lower Se San 1 dam and its characteristics in Section 4.3.1, thus we will now focus on the six dams in the Se Kong River subbasin. They are all located in Laos and are characterized by low GHGs emissions. In fact, considering the classification explained in Section 3.6.1 and displayed in Fig. 3.8, 4 of them belong to "Cluster 1" and 2 to "Cluster 2". Except for the Xe Kong 5 dam which is located in the "Kon Tum Massif" Geomorphic Province, all other dams belong to the "Tertiary Volcanic Plateau" Geomorphic Province. Moreover, only the Xe Kong 3d dam could efficiently implement the sediment flushing strategy.

Lastly, we compared all the seven "Dams with High Uncertainty" located in the 3S Basin with respect to the dams of the entire basin by calculating the corresponding values of mean "GHGs emissions per year" ($kg\ CO_2\ eq/year$) and mean "annual hydropower production" ($GWh/year$). As we can see from Table 4.3, we can notice that both the statistics regarding the seven "Dams with High Uncertainty" in the 3S Basin are approximately one order of magnitude smaller than the ones computed for all the dams.

| | All dams in the MRB | "Dams with High Uncertainty" in the 3S Basin |
|---|---|---|
| **Mean "GHGs emissions per year"** | $1.91 \times 10^8\ kg\,CO_2\,eq/year$ | $3.90 \times 10^7\ kg\,CO_2\,eq/year$ |
| **Mean "annual hydropower production"** | $1.91 \times 10^3\ GWh/year$ | $5.19 \times 10^2\ GWh/year$ |

**Table 4.3:** *Mean "GHGs emissions per year" (kg $CO_2$ eq/year) and mean "annual hydropower production" (GWh/year) calculated for all the dams in the basin and only for the seven "Dams with High Uncertainty" in the 3S Basin.*

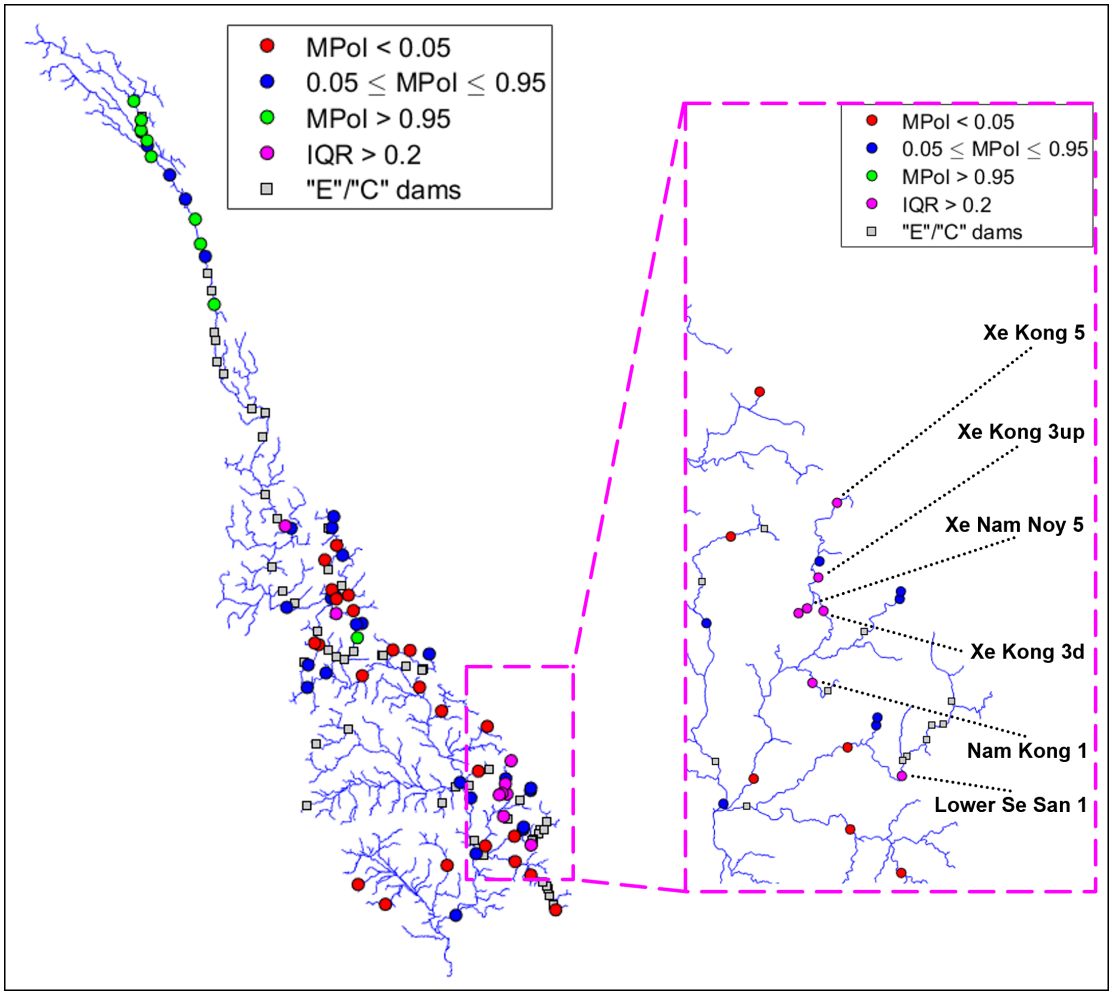


**Figure 4.14:** *"Dams with High Uncertainty" (IQR > 0.2) in the 3S Basin for the "actual" hydropower development scenario, indicated with magenta points and the respective names.*

# 5

# Discussion and conclusions

## 5.1 Main findings

In a global context in which the need for contrasting Climate Change is increasingly evident and underlined by scientific research, hydropower represents one of the most important renewable energy sources and alternatives to electricity generation by fossil fuels. This technology has experienced rapid growth over the last century, during which many countries all over the world tried to find the best trade-offs between electricity generation and several impacts on the environment caused by dam construction. Among them, the alteration of the river system equilibrium and the natural flow regime, the interruption of longitudinal connectivity (including both fish migration, and sediment and nutrient transport), and the displacement of the local population have been the subject of scientific research for many years. Nevertheless, our knowledge of these subjects is still far from being complete. For example, hydropower was, until quite recently, considered a close-to-zero-emission technology. Recent findings have instead shown how large amounts of GHGs could be emitted during the creation and the life of a reservoir-based hydropower plant (see Section 1.2). Considering the high uncertainty that still characterizes research and assessments on this topic, it is certainly clear that further in-depth analyses are more than needed. This work of thesis aims to give a contribution to the scientific literature in this regard. In particular, the novelty of our approach consists in considering simultaneously hydropower production, river sediment connectivity, and GHGs emissions, in order to better understand the cumulative impacts of

dam construction at a basin scale.

The present study has its roots in the works of *Schmitt et al.* (2019) and *Almeida et al.* (2019), who highlighted the importance of strategic dam planning for sustainable hydropower development. We analyzed the case study of the Mekong River Basin, denominated the "Battery of South-East Asia" for its large hydropower potential. To date, as described in Chapter 2, a project-by-project approach has led to a sub-optimal situation, in which the cumulative impacts of dam construction at the scale of the entire basin were underestimated (*Schmitt et al.*, 2019). Hence, we started by considering a pristine basin, where none of the 123 dams has yet been constructed, to investigate the full spectrum of possibilities that the basin could have offered before being altered by the current hydropower layout.

We developed a framework for strategic dam planning based on the optimization of three objectives: maximize hydropower production, maximize sediment supply to the delta, and minimize GHGs emissions from reservoirs (see Section 3.4). We took available data regarding hydropower production and river sediment connectivity from published dam databases as done by *Schmitt et al.* (2019), and estimated GHGs emissions from reservoirs following the procedure described by *Almeida et al.* (2019). To simulate sediment delivery from the uplands to the delta, we adopted the CASCADE model and framework introduced by *Schmitt et al.* (2016). We used the Borg Multi-Objective Evolutionary Algorithm to solve the optimization problem accounting for different scenarios (see Section 3.5). Initially, considering the available data, we obtained a set of 363 Pareto-Optimal portfolios, i.e., combinations of dam sites associated with the best trade-offs between the three objectives. Since the initial data were affected by high uncertainty, we tested the robustness of these outcomes by performing a Sensitivity Analysis on GHGs emissions and sediment connectivity parameters input values.

Sensitivity Analysis was applied following two approaches: at first, by perturbing the GHGS emissions input data, and then by perturbing simultaneously GHGs emissions and river sediment connectivity parameters input data. In both cases, the optimization problem was solved for 1,024 different scenarios. To sum up the outcomes of all the separate optimizations, we calculated the mean (experimental) probability of each dam to be included in a Pareto-Optimal portfolio, i.e., the Mean Probability of Inclusion ($MPoI$). Using this definition, we could define two categories of dams: the "Almost Never Included Dams" (MPoI < 0.05) and the "Almost Always Included Dams" (MPoI > 0.95), that can be respectively interpreted as the dams "not recommended" and "highly recommended" by the algorithm (see Section 3.6.3).

We started by considering only the results coming from the Sensitivity Analysis on GHGs emissions values. Fig. 4.3 shows the spatial distribution of all dams within the basin subdivided according to their $MPoI$ value. We can notice how dams sites in the Lancang River Basin (Upper Mekong River Basin, China) and the "Almost Always Included Dams" nearly coincide. This could derive from the very steep topology of this region that makes it particularly suitable for hydropower production. In fact, as explained in Section 2.1, dams in the Upper MRB are characterized by high installed capacity and small reservoir areas, which results in high energy densities and low carbon intensities (see Section 1.2.3). In reality, the situation is much more complex. For example, it has been estimated that about 50% of the sediment supply of the Mekong River comes from the Lancang River Basin and China has been strongly criticized by downstream countries for its hydropower expansion in this region. The difficult socio-political situation and China's strategic upstream position are among the main drivers of the project-by-project hydropower development in the Mekong River Basin (see Section 2.4). In order to be efficiently applied, strategic dam planning would require increased coordination between Lower MRB countries and China. This could be achieved if existing coordination such as the Mekong River Commission (MRC) and emerging whole-basin organizations such as the Lancang-Mekong Cooperation were strengthened. A higher effort in data collection and sharing between countries would represent an important step in the direction of sustainable hydropower development (*Schmitt et al.*, 2019).

As regards the "Almost Never Included Dams", Fig. 4.3 shows how they are distributed between the countries of the Lower Mekong River Basin. This is in accordance with what we said above about the characteristics of the Upper MRB. Differently from the latter, lowland dams are typically characterized by large reservoir areas, and consequently by lower energy densities and higher carbon intensities (see Section 1.2.3). A striking example is the Sambor dam, located in the mainstem of the Mekong River just before the delta. The Mekong River Delta latter is particularly vulnerable to the cumulative impacts of dam construction on sediment delivery, which could lead to serious subsidence and erosion phenomena (*Kondolf et al.*, 2018). The Sambor dam, both for its location and its characteristics, represents a perfect example of the potentially devastating effects on sediment supply to the delta (see Section 4.1). In addition, of particular interest is the fact that no dams are "recommended" by the algorithm in the Tonle Sap Basin (Fig. 2.2), which is one of the most important ecosystems in terms of biodiversity and productivity not only in the Mekong River Basin, but in the entire planet (*Kuenzer et al.*, 2013).

We already mentioned that data, estimates, and research regarding hydropower development in the Mekong River Basin are affected by high uncertainty, especially those regarding GHGs. We tried to quantitatively express the uncertainty associated with each dam by computing the Interquartile Range ($IQR$) of Probability of Inclusion, a measure of statistical dispersion (see Section 3.6.3). In Fig. 4.5 we plotted these values against the corresponding values of Mean Probability of Inclusion ($MPoI$), obtaining a "triangular pattern". In fact, both the "Almost Never Included Dams" and the "Almost Always Included Dams" are associated with low uncertainty. On the contrary, the highest values of $IQR$ correspond to mid values of $MPoI$.

We decided to further investigate the highest $IQR$ values by defining the "Dams with High Uncertainty" ($IQR > 0.2$), highlighted in Fig. 4.8. We compared these dams with respect to all the dams in the Mekong River Basin by calculating two representative statistics: the mean "GHGs emissions per year" ($kg\,CO_2\,eq/year$) and the mean "annual hydropower production" ($GWh/year$). The results, reported in Table 4.1, show that both the statistics regarding the "Dams with High Uncertainty" are about one order of magnitude lower than the respective statistics computed for all the dams in the basin. We can conclude that, in general, the dams affected by high uncertainty are the ones characterized by low GHGs emissions, but also low hydroelectric generation. Hence, they are most likely dams with medium "performance" in terms of the three objectives of the optimization problem and similar characteristics to each other, and, consequently, they can be included or not in a Pareto-Optimal portfolio depending on the way GHGs emissions values are perturbed in one scenario or in another.

Then, we repeated these procedures by perturbing simultaneously GHGs emissions and sediment connectivity parameters (in particular, trapping efficiency of each dam and sediment yield of each river reach), resulting in a three-degrees-of-freedom Sensitivity Analysis (see Section 3.6.2). We noticed that this addition introduced more uncertainty in the results, as visible in Fig. 4.9. Of particular interest are the four dams associated with extremely high values of $IQR$ in Fig. 4.9.b, that we denominated "Dams with Very High Uncertainty" ($IQR > 0.5$). These dams were still classified as "Dams with High Uncertainty" in the previous case (Fig. 4.9.a), but $IQR$ values this high indicate that they are particularly sensitive to sediment-related input data perturbation. As displayed in Fig. 4.10, we also discovered that all these four dams are located in the 3S Basin (Fig. 2.3), which plays a crucial role in the sediment balance of all the Mekong River Basin (see Section 2.5). The importance of the 3S Basin, associated with the extremely high uncertainty that characterizes these three

dams, highlights the urgent need to increase the efforts on data collection and in-depth research regarding this region.

Sensitivity Analyses performed by considering a pristine basin offered the possibility to become aware of the consequence of the project-by-project planning approach often applied in the Mekong River Basin. We classified as "Lost Opportunities" all the "Almost Never Included Dams" which are "existent and already operating" or "under construction". By definition, the "Almost Never Included Dams" are the ones "not recommended" by the algorithm due to their bad "performance" in terms of trade-offs between the three objectives of the optimization problem. "Lost Opportunities" represent all the dams that, contrary to the actual basin situation, should have not been constructed according to the outcomes found by the algorithm. Fig. 4.11 shows their spatial distribution. As expected from the previous results, they are all located in the Lower MRB, since no dam classified as "Almost Never Included Dams" is present in the Upper MRB. The bad "performance" of "Lost Opportunities" is well highlighted by the comparison with all the other dams in the basin. We repeated the approach followed for the "Dams with High Uncertainty", re-computing the same two statistics in an analogous way. Unsurprisingly, we discovered that, despite a mean "GHGs emissions per year" value of the same order of magnitude, the mean "annual hydropower production" corresponding to "Lost Opportunities" is approximately one order of magnitude smaller than the one computed for all the dams. In simple terms, "Lost Opportunities" emit like the average dam in the basin, while generating much less hydroelectric energy.

Lastly, we repeated every procedure described so far considering instead the current basin dam portfolio, in order to evaluate what are the actual planning possibilities. This means that the optimizations were performed only on "planned" dams (68 out of 123). The most significant differences between the two scenarios are visible in Fig. 4.13, which shows the "Dams with High Uncertainty" on the "IQR vs MPoI" plot. We can observe an overall decrease of uncertainty: the "triangular pattern", despite still visible, has "flattened", and, in general, the dams present lower values of $IQR$. One of the reasons may be found in the lower number of dams included in the optimization for the "actual" scenario, which results in a lower "competition" between these dams. In addition, by analyzing in detail the "Dams with High Uncertainty" for the "actual" scenario, we discovered that seven of them (on a total of 9) are located in the 3S Basin (Fig. 2.3), adding even more uncertainty to the dams located in this region. For this reason, we underline once again the necessity to deepen the studies regarding dam development in this crucial area of the Mekong River Basin.

It is now clear how strategic dam planning could and should be applied for sustainable hydropower development, in which sediment connectivity and GHGs emissions must be taken into account simultaneously. Moreover, we demonstrated how Sensitivity Analysis can be used to distinguish between robust results and the ones affected by high uncertainty. This is extremely important, especially for a river basin such as the Mekong's, for which data and researches on these topics are often very scarce. In conclusion, we would like to point out that the framework and the methodology adopted in this work of thesis are quite universal, and, with the right precautions, they could be extended to other case studies all over the world.

## 5.2 Limitations and future developments

As stated in Section 1.4, the goal of this work of thesis consists in giving a contribution to the scientific literature regarding the topic of strategic dam planning at a basin-wide scale. Although we made some steps forward with respect to the past studies by considering simultaneously sediment connectivity and GHGs emissions, and by dealing with uncertainty through Sensitivity Analyses, our work is far from being exhaustive and presents some important limitations. Solving these problems will let any possible future development based on this study make further progress in this direction. For this reason, we will now describe the main limitations in the following lines.

First of all, we explained in Section 3.1 that our case study, i.e., the Mekong River Basin, due to its relatively recent hydropower development, is characterized by a general problem of data availability. The dam database used for this work of thesis comes from published databases (*Mekong River Commission and others*, 2014; *International Rivers*, 2014; *Open Development Mekong*, 2014), in which some values are uncertain or totally missing. GHGs emissions data were almost completely estimated following the procedure illustrated by *Almeida et al.* (2019), since, to date, there exist published GHGs emissions measurements only for three reservoirs in Laos (*Räsänen et al.*, 2018). The high uncertainty of these data was the main reason why we decided to perform a Sensitivity Analysis, in order to decrease as much as possible the importance of their initial values. Needless to say that this is not enough, and more efforts on measurements, data sharing, and in-depth research are much needed. This is especially true for those regions that, according to our findings, are severely affected by uncertainty, e.g., the 3S Basin (see Section 5.1).

In a multi-objective optimization problem, the choice of each objective and the relative indicator strongly influences the solutions. Based on the stud-

ies made by *Schmitt et al.* (2019) and *Almeida et al.* (2019), we formulated our 3-objective optimization problem considering hydropower production, river sediment supply to the delta, and GHGs emissions. This means that we completely neglected other potential dam impacts, such as alteration of river system equilibrium, change in natural flow regime, worsening of water quality, interruption of longitudinal and lateral fish migration, and displacement of the local population due to dam construction (see Section 1.2.1). Thus, further optimizations may be performed by adding one or more objectives related to other dam impacts to the decision problem. In addition, even considering the same three objectives, changing the corresponding indicators could represent a valid alternative. For instance, one could compute a hydropower production indicator for each country, to highlight the conflicts between them and the sub-optimal solutions derived by a non-cooperative approach. In addition, we only considered the sediment supply to the delta as the indicator for the corresponding objective. This means that we totally ignored the impact of sediment disruption along the river course, which can be considered by adding more indicators related to sediment connectivity.

Moreover, we claim that excluding one of the three objectives accounted for this work of thesis from future analyses will represent a huge step backward, since we consider them of fundamental importance. This, together with a basin-wide approach, should represent the starting point of every future study regarding strategic dam planning.

*Schmitt et al.* (2019) claimed that strategic dam planning should not be applied only to find the optimal combination of dams in space, but also in time. In fact, considering the temporal sequence to follow for dams construction allows to better quantify the marginal impacts on sediment trapping of each dam within a portfolio. Starting from the results of this study, one should repeat these elaborations by integrating the impacts related to GHGs emissions in the optimizations.

The decision vector of our optimization problem consisted of binary decision variables, indicating only whether a dam is included in a portfolio or not. Further optimizations could include some dam characteristics as additional decision variables, e.g., the size of the hydropower plant or its installed capacity. In addition, in this work of thesis we accounted for just the drawdown sediment flushing as a possible reservoir sediment management strategy (in an extremely simplified way). A more in-depth study could also consider other sediment trapping mitigation approaches (see Section 1.2.2).

Furthermore, our approach consisted of a planning problem, which did not consider how the management of dams could be used to mitigate the impacts

on GHGs emissions and sediment connectivity, e.g., by synchronizing sediment flushing (see Section 1.2.2), or by paying particular attention to drawdown emissions caused by fluctuation of water levels (see Section 1.2.3). Future studies could try to solve a strategic dam planning and management problem, in which optimal solutions are computed considering both dams sites and their management over time.

As described in Section 2.3, one of the main reasons that led to a sub-optimal current dam portfolio in the Mekong River Basin is the project-by-project approach deriving from the complex geopolitical and social situation between the six riparian countries (Fig. 2.1). To date, despite some attempts at cooperation, several disputes remain unresolved, especially considering China. This work of thesis has underlined many times the need of changing this approach in favor of strategic dam planning at the whole-basin scale. This implies complete cooperation between the six countries, which is far from being realistic. For example, the optimal solutions found by the algorithm indicate that the most "recommended" dams are the ones in Chinese territory. In reality, these dams have been strongly criticized by downstream countries due to their potential impacts on the entire Lower Mekong River Basin.

In order to solve the optimization problem, we used the Borg Multi-Objective Evolutionary Algorithm. We explained in Section 3.5 how the choice of the values of some parameters can strongly affect the final results. For example, a lower value of $\epsilon$ and a higher value of $NFE$ would have resulted in a higher quantity and quality of optimal solutions. Since the Sensitivity Analyses required to solve the optimization problem for a high number of different scenarios, one of the major limitations consisted in the high computational costs. We tried several other settings for these parameters to improve the outcomes, but they mostly resulted in prohibitive computational times. We thus had to limit ourselves according to the available computational power, but future studies with the possibility to access better resources could try to repeat our procedure with more advantageous parameters values.

We mainly based the evaluation of the outcomes of the Sensitivity Analyses on the computation of two statistics: the Mean Probability of Inclusion ($MPoI$) and the Interquartile Range ($IQR$) of Probability of Inclusion. These are the ones that, according to our opinion, were the best to analyze this type of results, but the choice was wide. For example, in the beginning, to measure uncertainty, we also took into account the Delta Probability of Inclusion (difference between the maximum and the minimum value) and the Coefficient of Variation of Probability of Inclusion. Unlike the Interquartile Range, both these statics consider the full interval of the outcomes, resulting in a higher sensibil-

ity to extreme values. However, we finally decided to use only Interquartile Range for the reasons explained in Section 3.6.3.

As anticipated in Section 3.2.1, since the computation of the GHGs emissions is based on the definition of Global Warming Potential (GWP), the choice of the time horizon of the analysis could significantly affect the results. In this work of thesis, we decided to consider a 100-year time horizon, which is the most widely used for large infrastructures, such as dams. However, recent studies showed that GHGs emissions from reservoirs have a peak in the first decade after dam construction, and then fall exponentially over time (*Prairie et al.*, 2018). Moreover, $CH_4$ has a relatively short residence time (around 12 years), but also a very strong radiative forcing effect. For example, the GWP of methane on a 20-year time horizon (84 $kg\,CO_2\,eq/kg\,CH_4$) is much higher than the corresponding 100-year value, which is about equal to 34 $kg\,CO_2\,eq/kg\,CH_4$ (*Myhre*, 2013). Hence, given the importance of $CH_4$ emissions in the total balance, the 100-year time horizon does not necessarily represent the best choice.

In the end, we wanted to highlight that hydropower is certainly one of the most important sources of renewable energy, but, obviously, not the only one. For example, photovoltaic and wind energy represent as well valid alternatives to fossil fuels. If a hypothetical decision-maker wants to choose a Pareto-Optimal portfolio characterized by low hydropower production and high environment-related indicators, the introduction of an integrated energy plan which considers the full spectrum of renewable technologies could compensate for the lower contribution of hydroelectric energy (*Schmitt et al.*, 2019).

# Bibliography


Abadie, L. M., J. M. Chamorro, S. Huclin, and D.-J. van de Ven (2020), On flexible hydropower and security of supply: Spain beyond 2020, *Energy*, *203*, 117,869.

Abril, G., et al. (2005), Carbon dioxide and methane emissions and the carbon budget of a 10-year old tropical reservoir (petit saut, french guiana), *Global biogeochemical cycles*, *19*(4).

Almeida, R. M., et al. (2019), Reducing greenhouse gas emissions of amazon hydropower with strategic dam planning, *Nature Communications*, *10*(1), 1–9.

Anderson, E. P., et al. (2018), Fragmentation of andes-to-amazon connectivity by hydropower dams, *Science advances*, *4*(1), eaao1642.

Baran, E., and C. Myschowoda (2009), Dams and fisheries in the mekong basin, *Aquatic Ecosystem Health & Management*, *12*(3), 227–234.

Barros, N., J. J. Cole, L. J. Tranvik, Y. T. Prairie, D. Bastviken, V. L. Huszar, P. Del Giorgio, and F. Roland (2011), Carbon emission from hydroelectric reservoirs linked to reservoir age and latitude, *Nature geoscience*, *4*(9), 593–596.

Bouckaert, S., A. F. Pales, C. McGlade, U. Remme, B. Wanner, L. Varro, D. D'Ambrosio, and T. Spencer (2021), Net zero by 2050: A roadmap for the global energy sector.

Bravard, J.-P., M. Goichot, and S. Gaillot (2013), Geography of sand and gravel mining in the lower mekong river. first survey and impact assessment, *EchoGéo*, (26).

Brismar, A. (2002), River systems as providers of goods and services: a basis for comparing desired and undesired effects of large dam projects, *Environmental management*, *29*(5), 598–609.

Brune, G. M. (1953), Trap efficiency of reservoirs, *Eos, Transactions American Geophysical Union*, *34*(3), 407–418.

CGIAR Consortium for Spatial Information (CSI) (2008), Srtm 90m digital elevation database v4.1, https://cgiarcsi.community/data/srtm-90m-digital-elevation-database-v4-1/.

CGIAR Research Program on Water, Land and Ecosystems (WLE) (2022), https://wle-mekong.cgiar.org/.

De Faria, F. A., P. Jaramillo, H. O. Sawakuchi, J. E. Richey, and N. Barros (2015), Estimating greenhouse gas emissions from future amazonian hydroelectric reservoirs, *Environmental Research Letters*, *10*(12), 124,019.

Deemer, B. R., et al. (2016), Greenhouse gas emissions from reservoir water surfaces: a new global synthesis, *BioScience*, *66*(11), 949–964.

DelSontro, T., D. F. McGinnis, S. Sobek, I. Ostrovsky, and B. Wehrli (2010), Extreme methane emissions from a swiss hydropower reservoir: contribution from bubbling sediments, *Environmental science & technology*, *44*(7), 2419–2425.

DelSontro, T., M. J. Kunz, T. Kempter, A. WuÃàest, B. Wehrli, and D. B. Senn (2011), Spatial heterogeneity of methane ebullition in a large tropical reservoir, *Environmental science & technology*, *45*(23), 9866–9873.

Demarty, M., and J. Bastien (2011), Ghg emissions from hydroelectric reservoirs in tropical and equatorial regions: Review of 20 years of ch4 emission measurements, *Energy Policy*, *39*(7), 4197–4206.

Edenhofer, O. (2015), *Climate change 2014: mitigation of climate change*, vol. 3, Cambridge University Press.

Edenhofer, O., et al. (2011), *Renewable Energy Sources and Climate Change Mitigation: Special Report of the Intergovernmental Panel on Climate Change*, Cambridge University Press.

European Environmental Agency (EEA) (2022), https://www.eea.europa.eu/themes/climate.

Forsberg, B. R., J. M. Melack, T. Dunne, R. B. Barthem, M. Goulding, R. C. Paiva, M. V. Sorribas, U. L. Silva Jr, and S. Weisser (2017), The potential impact of new andean dams on amazon fluvial ecosystems, *PloS one*, *12*(8), e0182,254.

Giuliani, M., A. Castelletti, and R. Soncini-Sessa (2012), Multi-agent water resources management: Centralized vs decentralized approach, in *10th International Conference on Hydroinformatics (HIC), Hamburg, Germany*.

Hadka, D., and P. Reed (2013), Borg: An auto-adaptive many-objective evolutionary computing framework, *Evolutionary computation*, *21*(2), 231–259.

Hay, M., J. Skinner, and A. Norton (2019), Dam-induced displacement and resettlement: a literature review, *Available at SSRN 3538211*.

Hertwich, E. G. (2013), Addressing biogenic greenhouse gas emissions from hydropower in lca, *Environmental science & technology*, *47*(17), 9604–9611.

International Centre for Environmental Managenment (ICEM) (2016), https://icem.com.au/3s-river-basins-study-set-to-begin/news/.

International Hydropower Association (IHA) (2019), https://www.hydropower.org/blog/blog-hydropower-growth-and-development-through-the-decades.

International Hydropower Association (IHA) (2021), 2021 hydropower status report, https://www.hydropower.org/.

International Rivers (2014), Spreadsheet of major dams in china, https://archive.internationalrivers.org/resources/spreadsheet-of-major-dams-in-china-7743.

Jadoon, T. R., M. K. Ali, S. Hussain, A. Wasim, and M. Jahanzaib (2020), Sustaining power production in hydropower stations of developing countries, *Sustainable Energy Technologies and Assessments*, *37*, 100,637.

Jager, H. I., R. A. Efroymson, J. J. Opperman, and M. R. Kelly (2015), Spatial design principles for sustainable hydropower development in river basins, *Renewable and Sustainable Energy Reviews*, *45*, 808–816.

Jenks, G. F. (1967), The data model concept in statistical mapping, *International yearbook of cartography*, *7*, 186–190.

Kaltenbach, H.-M. (2011), *A concise guide to statistics*, Springer Science & Business Media.

Koehnken, L. (2014), Discharge sediment monitoring project (dsmp) 2009,Äî2013: Summary & analysis of results: Final report, *Mekong River Commission (MRC) and Deutsche Gesellschaft für Internationale Zusammenarbeit (GIZ), Phnom Penh, Cambodia*.

Kondolf, G. M. (1997), Profile: hungry water: effects of dams and gravel mining on river channels, *Environmental management*, *21*(4), 533–551.

Kondolf, G. M., et al. (2014a), Sustainable sediment management in reservoirs and regulated rivers: Experiences from five continents, *Earth's Future*, *2*(5), 256–280.

Kondolf, G. M., Z. K. Rubin, and J. Minear (2014b), Dams on the mekong: Cumulative sediment starvation, *Water Resources Research*, *50*(6), 5158–5169.

Kondolf, G. M., et al. (2018), Changing sediment budget of the mekong: Cumulative threats and management strategies for a large river basin, *Science of the total environment*, *625*, 114–134.

Kuby, M. J., W. F. Fagan, C. S. ReVelle, and W. L. Graf (2005), A multiobjective optimization model for dam removal: an example trading off salmon passage with hydropower and water storage in the willamette basin, *Advances in Water Resources*, *28*(8), 845–855.

Kuenzer, C., I. Campbell, M. Roch, P. Leinenkugel, V. Q. Tuan, and S. Dech (2013), Understanding the impact of hydropower developments in the context of upstream–downstream relations in the mekong river basin, *Sustainability science*, *8*(4), 565–584.

Laumanns, M., L. Thiele, K. Deb, and E. Zitzler (2002), Combining convergence and diversity in evolutionary multiobjective optimization, *Evolutionary computation*, *10*(3), 263–282.

Lehner, B., et al. (2011), High-resolution mapping of the world's reservoirs and dams for sustainable river-flow management, *Frontiers in Ecology and the Environment*, *9*(9), 494–502.

Lohrberg, A., O. Schmale, I. Ostrovsky, H. Niemann, P. Held, and J. Schneider von Deimling (2020), Discovery and quantification of a widespread methane ebullition event in a coastal inlet (baltic sea) using a novel sonar strategy, *Scientific reports*, *10*(1), 1–13.

Maeck, A., T. DelSontro, D. F. McGinnis, H. Fischer, S. Flury, M. Schmidt, P. Fietzek, and A. Lorke (2013), Sediment trapping by dams creates methane emission hot spots, *Environmental science & technology*, *47*(15), 8130–8137.

Maier, H. R., et al. (2014), Evolutionary algorithms and other metaheuristics in water resources: Current status, research challenges and future directions, *Environmental Modelling & Software*, *62*, 271–299.

McCartney, M., C. Sullivan, M. C. Acreman, and D. McAllister (2001), Ecosystem impacts of large dams, *Background paper*, *2*.

Mekong River Commission and others (2014), Hydropower project database, *Basin development plan programme. Mekong River Commission, Vientiane, Lao PDR*.

Mekong River Commission (MRC) (2020a), Piloting a joint environmental monitoring programme on two mekong mainstream dams ,Äòdon sahong hydropower project and xayaburi hydropower project,Äô: An inception report, *Tech. rep.*, Vientiane: MRC Secretariat.

Mekong River Commission (MRC) (2020b), https://www.mrcmekong.org/our-work/topics/hydropower/.

Mekong River Commission (MRC) (2022), https://www.mrcmekong.org/.

Myhre, G. (2013), Anthropogenic and natural radiative forcing. cambridge united kingdom and new york ny usa: Climate change, *The physical science basis. Contribution of working group I to the fifth assessment report of the intergovernmental panel on climate change*, pp. 129–234.

Nilsson, C., C. A. Reidy, M. Dynesius, and C. Revenga (2005), Fragmentation and flow regulation of the world's large river systems, *science*, *308*(5720), 405–408.

O'Hanley, J. R., J. Wright, M. Diebel, M. A. Fedora, and C. L. Soucy (2013), Restoring stream habitat connectivity: a proposed method for prioritizing the removal of resident fish passage barriers, *Journal of environmental management*, *125*, 19–27.

Open Development Mekong (2014), Greater mekong subregion hydropower dams, https://data.opendevelopmentmekong.net/en/dataset/greater-mekong-subregion-hydropower-dams.

Owusu, P. A., and S. Asumadu-Sarkodie (2016), A review of renewable energy sources, sustainability issues and climate change mitigation, *Cogent Engineering*, *3*(1), 1167,990.

Pachauri, R. K., et al. (2014), *Climate change 2014: synthesis report. Contribution of Working Groups I, II and III to the fifth assessment report of the Intergovernmental Panel on Climate Change*, Ipcc.

Paul, T. (2019), Looking at comparable deltas: Experiences from mekong, *Tech. rep.*, The World Bank.

Pearl, J. (1984), Heuristics: Intelligent search strategies for computer problem solving.

Pichery, C. (2014), Sensitivity analysis, in *Encyclopedia of Toxicology (Third Edition)*, edited by P. Wexler, third edition ed., pp. 236–237, Academic Press, Oxford, doi: https://doi.org/10.1016/B978-0-12-386454-3.00431-0.

Poulsen, A., P. Penh, O. Poeu, S. Viravong, U. Suntornratana, N. T. Tung, M. R. Commission, et al. (2002), Fish migrations of the lower mekong river basin: implications for development, planning and environmental management.

Prairie, Y. T., et al. (2018), Greenhouse gas emissions from freshwater reservoirs: what does the atmosphere see?, *Ecosystems*, *21*(5), 1058–1071.

Qazi, A., F. Hussain, N. A. Rahim, G. Hardaker, D. Alghazzawi, K. Shaban, and K. Haruna (2019), Towards sustainable energy: A systematic review of renewable energy sources, technologies, and public opinions, *IEEE Access*, *7*, 63,837–63,851, doi: 10.1109/ACCESS.2019.2906402.

Räsänen, T. A., O. Varis, L. Scherer, and M. Kummu (2018), Greenhouse gas emissions of hydropower in the mekong river basin, *Environmental Research Letters*, *13*(3), 034,030.

Richter, B. D., S. Postel, C. Revenga, T. Scudder, B. Lehner, A. Churchill, and M. Chow (2010), Lost in development's shadow: The downstream human consequences of dams, *Water Alternatives*, *3*(2), 14.

Saltelli, A., S. Tarantola, F. Campolongo, and M. Ratto (2004), *Sensitivity analysis in practice: a guide to assessing scientific models*, vol. 1, Wiley Online Library.

Schmitt, R., M. Giuliani, S. Bizzi, G. Kondolf, G. Daily, and A. Castelletti (2021), Strategic basin and delta planning increases the resilience of the mekong delta under future uncertainty, *Proceedings of the National Academy of Sciences*, *118*(36).

Schmitt, R. J., S. Bizzi, and A. Castelletti (2016), Tracking multiple sediment cascades at the river network scale identifies controls and emerging patterns of sediment connectivity, *Water Resources Research*, *52*(5), 3941–3965.

Schmitt, R. J., S. Bizzi, A. Castelletti, and G. Kondolf (2018a), Improved trade-offs of hydropower and sand connectivity by strategic dam planning in the mekong, *Nature Sustainability*, *1*(2), 96–104.

Schmitt, R. J., S. Bizzi, A. F. Castelletti, and G. Kondolf (2018b), Stochastic modeling of sediment connectivity for reconstructing sand fluxes and origins in the unmonitored se kong, se san, and sre pok tributaries of the mekong river, *Journal of Geophysical Research: Earth Surface*, *123*(1), 2–25.

Schmitt, R. J., S. Bizzi, A. Castelletti, J. Opperman, and G. M. Kondolf (2019), Planning dam portfolios for low sediment trapping shows limits for sustainable hydropower in the mekong, *Science advances*, *5*(10), eaaw2175.

Schmutz, S., and J. Sendzimir (2018), *Riverine ecosystem management: Science for governing towards a sustainable future*, Springer Nature.

Schulz, C., and W. M. Adams (2019), Debating dams: the world commission on dams 20 years on, *Wiley Interdisciplinary Reviews: Water*, *6*(5), e1396.

Sobek, S., T. DelSontro, N. Wongfun, and B. Wehrli (2012), Extreme organic carbon burial fuels intense methane bubbling in a temperate reservoir, *Geophysical Research Letters*, *39*(1).

Sobol', I. M. (1967), On the distribution of points in a cube and the approximate evaluation of integrals, *Zhurnal Vychislitel'noi Matematiki i Matematicheskoi Fiziki*, *7*(4), 784–802.

Soncini-Sessa, R., E. Weber, and A. Castelletti (2007), *Integrated and participatory water resources management-theory*, Elsevier.

Song, C., K. H. Gardner, S. J. Klein, S. P. Souza, and W. Mo (2018), Cradle-to-grave greenhouse gas emissions from dams in the united states of america, *Renewable and Sustainable Energy Reviews*, *90*, 945–956.

St. Louis, V. L., C. A. Kelly, É. Duchemin, J. W. Rudd, and D. M. Rosenberg (2000), Reservoir surfaces as sources of greenhouse gases to the atmosphere: A global estimate: Reservoirs are sources of greenhouse gases to the atmosphere, and their surface areas have increased to the point where they should be included in global inventories of anthropogenic emissions of greenhouse gases, *BioScience*, *50*(9), 766–775.

Suhardiman, D., M. Giordano, and F. Molle (2015), Between interests and worldviews: The narrow path of the mekong river commission, *Environment and Planning C: Government and Policy*, *33*(1), 199–217.

Sun, X., X. Wang, L. Liu, and R. Fu (2019), Development and present situation of hydropower in china, *Water Policy*, *21*(3), 565–581.

Syvitski, J. P., C. J. Vorosmarty, A. J. Kettner, and P. Green (2005), Impact of humans on the flux of terrestrial sediment to the global coastal ocean, *science*, *308*(5720), 376–380.

Tangi, M., R. Schmitt, S. Bizzi, and A. Castelletti (2019), The cascade toolbox for analyzing river sediment connectivity and management, *Environmental Modelling & Software*, *119*, 400–406.

Teodoru, C. R., Y. T. Prairie, and P. A. Del Giorgio (2011), Spatial heterogeneity of surface co2 fluxes in a newly created eastmain-1 reservoir in northern quebec, canada, *Ecosystems*, *14*(1), 28–46.

Tilt, B., Y. Braun, and D. He (2009), Social impacts of large dam projects: A comparison of international case studies and implications for best practice, *Journal of environmental management*, *90*, S249–S257.

Turowski, J. M., D. Rickenmann, and S. J. Dadson (2010), The partitioning of the total sediment load of a river into suspended load and bedload: a review of empirical data, *Sedimentology*, *57*(4), 1126–1146.

United Nations (UN) (2015), https://sdgs.un.org/goals.

Vörösmarty, C. J., M. Meybeck, B. Fekete, K. Sharma, P. Green, and J. P. Syvitski (2003), Anthropogenic sediment retention: major global impact from registered river impoundments, *Global and planetary change*, *39*(1-2), 169–190.

Weissenberger, S., M. Lucotte, S. Houel, N. Soumis, É. Duchemin, and R. Canuel (2010), Modeling the carbon dynamics of the la grande hydroelectric complex in northern quebec, *Ecological Modelling*, *221*(4), 610–620.

Winemiller, K. O., et al. (2016), Balancing hydropower and biodiversity in the amazon, congo, and mekong, *Science*, *351*(6269), 128–129.

World Commission on Dams (WCD) (2000), *Dams and development: A new framework for decision-making: The report of the world commission on dams*, Earthscan.

Zarfl, C., A. E. Lumsdon, J. Berlekamp, L. Tydecks, and K. Tockner (2015), A global boom in hydropower dam construction, *Aquatic Sciences*, *77*(1), 161–170.

Zheng, P. Q., B. F. Hobbs, and J. F. Koonce (2009), Optimizing multiple dam removals under multiple objectives: linking tributary habitat and the lake erie ecosystem, *Water Resources Research*, *45*(12).

Ziv, G., E. Baran, S. Nam, I. Rodríguez-Iturbe, and S. A. Levin (2012), Trading-off fish biodiversity, food security, and hydropower in the mekong river basin, *Proceedings of the National Academy of Sciences*, *109*(15), 5609–5614.